JSCSEN 74(4)359–476(2009)

Journal of the Serbian Chemical Society

VOLUME 74

No 4

BELGRADE 2009

Available on line at

www.shd.org.rs/JSCS

Journal of the Serbian Chemical Society
JSCS@tmf.bg.ac.rs • www.shd.org.rs/JSCS

J. Serb. Chem. Soc. Vol. 74, No. 4 (2009)

CONTENTS

Published by the Serbian Chemical Society
Karnegijeva 4/III, 11000 Belgrade, Serbia
Printed by the Faculty of Technology and Metallurgy
Karnegijeva 4, P.O. Box 35-03, 11120 Belgrade, Serbia

Journal of the Serbian Chemical Society
JSCS@tmf.bg.ac.rs • www.shd.org.rs/JSCS

J. Serb. Chem. Soc. 74 (4) 359–366 (2009)
JSCS–3837

UDC 582.998.2:57.083.32:66.095.11:66.02
Original scientific paper

Chemical modification of Art v 1, a major mugwort pollen allergen, by *cis*-aconitylation and citraconylation

DRAGANA STANIĆ[1*#], LIDIJA BURAZER[2], MARIJA GAVROVIĆ-JANKULOVIĆ[3#], RATKO M. JANKOV[3#] and TANJA ĆIRKOVIĆ VELIČKOVIĆ[3#]

[1]Institute for Chemistry, Technology and Metallurgy – Center for Chemistry, Njegoševa 12, P.O. Box 473, 11001 Belgrade, [2]Institute of Virology, Vaccines and Sera – Torlak, Vojvode Stepe 458, P.O. Box 1, 11221 Belgrade and [3]Faculty of Chemistry, University of Belgrade, Studentski trg 16, P.O. Box 158, 11001 Belgrade, Serbia

(Received 19 September, revised 6 November 2008)

Abstract: Art v 1 is the major allergen of mugwort (*Artemisia vulgaris*) pollen, a significant cause of hay fever all over Europe. Specific immunotherapy is the only treatment modality for allergic disease. Application of modified allergens makes the treatment safer and more efficient. In this work, two out of three (citraconic anhydride, *cis*-aconitic anhydride, 2,3-dimethylmaleic anhydride) tested anhydrides were proven to be suitable for chemical modifications of allergens. Art v 1 was modified by *cis*-aconitylation and citraconylation in order to obtain derivatives of Art v 1 that may be suitable for further immunological testing. Acylation of Art v 1 gave derivatives (caaArt v 1 and citArt v 1) with about 80 % modified amino groups. The derivatives were in the monomeric form and had dramatically reduced pI values. Both derivatives were relatively stable at neutral pH values, while the acyl groups undergo hydrolysis under acidic conditions. Modification of allergens by *cis*-aconitylation and citraconylation could be a new tool for obtaining allergoids.

Keywords: allergoid; mugwort pollen; Art v 1; chemical modification; allergen-specific immunotherapy.

INTRODUCTION

IgE-mediated allergy is a global problem affecting more then 40 % of the population in industrialized countries.[1] In contrast to symptomatic treatments, specific immunotherapy (SIT) is the only prophylactic desensitizing therapy for allergy.[2,3] SIT modifies cellular and humoral responses to allergens by driving the immune response from the T helper 2 (Th 2) towards the T helper 1 (Th 1) type and generating allergen-specific regulatory T cells that can suppress the

* Corresponding author. E-mail: dstanic@chem.bg.ac.rs
# Serbian Chemical Society member.
doi: 10.2298/JSC0904359S

responses of effector T cells, accompanied with an increase in allergen-specific antibodies of the IgG class (blocking antibodies).[4] On the other hand, the potential for local and systemic reactions has forced improvements to the traditional use of allergen extracts. The main approaches involve the generation of hypoallergenic derivatives, by chemical modification[5,6] or protein engineering of recombinant allergens,[7,8] which are aimed at reducing potentially fatal reactions to allergen administration during immunotherapy. On the other hand, altered allergens have to retain their immunogenicity, *i.e.*, recognition of the modified allergen by T cells. Finally, it would be useful to have immunogens with an inherent strong Th 1-skewing potential, which is usually obtained by the usage of an adjuvant (*e.g.*, a monophosphoryl lipid).[9]

Scavenger receptors (SR) expressed on antigen presenting cells (APC) bind a variety of polyanionic ligands, thus delivering them into the endolysosomal pathway.[10] Many proteins are known to become SR ligands when chemically modified to enhance their negative charge by alteration of the ε-amino groups of their lysine residues with acetic or maleic anhydride.[11] It was shown that maleylating protein immunogens, so that they become SR ligands, leads to a more efficient antigen presentation to T cell receptors and to a greater immunogenicity with a dominantly Th 1 type of immune response.[12,13] The main problem with usage of modified immunogens is a reduced immunogenicity as consequence of affinity loss of T cell receptors for the modified epitopes. Shakushiro *et al.*[14] showed that ovalbumin (OVA) modified to become more acidic by succinylation (Suc-OVA), maleylation (Mal-OVA) or *cis*-aconitylation (Aco-OVA) was efficiently taken up by dendritic cells (DC) *via* SR. Mal-OVA and Aco-OVA were efficiently cross--presented by DC, while cross-presentation of Suc-OVA was hardly observed. In contrast to Mal-OVA and Aco-OVA, which are prone to deacylatation in lisosomes, Suc-OVA is chemically stable under acidic conditions. As a consequence, succinyl groups inhibit ubiquitin conjugation on the lysine residues, which is important in proteasomal degradation,[15] leading to the lack of recognition by T cells through T cell receptors (TCR).

Although a clear reduction in immunogenicity was observed for many allergoids,[5,6] hitherto the approach of reversible modification of allergens with the aim of preserving immunogenicity and recognition of T-cell receptors has not been reported.

Mugwort (*Artemisia vulgaris*) pollen is an important cause of allergy in Europe. Ninety-five percent of patients with mugwort allergy are sensitized to Art v 1, the sole major allergen in mugwort pollen.[16,17]

The aim of this work was to modify chemically Art v 1 with new modifying agents with specific features, *i.e.*, the introduction of highly negative charges that may enable them to react with scavenger receptors on antigen presenting cells and their reversible modification that may improve their immunogenicity when

compared to the traditionally used chemically modified allergens. In this study, three new chemical agents were tested and the obtained allergoids were biochemically characterized. Purified Art v 1 was modified by citraconic, *cis*-aconitic and 2,3-dimethylmaleic anhydride. *cis*-Aconitylation and citraconylation of Art v 1 gave derivatives (caaArt v 1 and citArt v 1), with about 80 % modified amino groups and dramatically reduced pI values, which could make them good candidate allergoids. The stability of the bond formed enables further animal testing of these derivatives.

EXPERIMENTAL

Citraconic anhydride, *cis*-aconitic anhydride, 2,3-dimethylmaleic anhydride and 2,4,6-trinitrobenzensulfonic acid (TNBS) were purchased from Sigma-Aldrich (Steinheim, Germany). All other chemicals used in this work were of analytical grade.

Acylation of Art v 1

Art v 1 was isolated from pollen extract of *Artemisia vulgaris* and purified by ion-exchange HPLC.[18] Art v 1 (1.5 mg/ml) in 4 % $NaHCO_3$ was treated with the bolus addition of 15 portions of *cis*-aconitic or dimethylmaleic or citraconic anhydride during 30 min with extensive mixing at 4 °C. The final anhydride concentration was 400 mM. After every bolus addition, the pH was adjusted to 9.0 with solid Na_2CO_3. The mixture was extensively dialyzed against phosphate buffered saline (PBS) for 20 h at 4 °C. All samples were stored at –20 °C until use.

Determination of the free amino groups

The free amino groups were determined using the TNBS method.[19] The results are expressed as the means of three different determinations for modified Art v 1 as a percentage of the number of amino groups determined for the native Art v 1 (expressed as 100 %).

Sodium dodecyl sulfate polyacrylamide gel electrophoresis (SDS PAGE), native PAGE and isoelectric focusing (IEF)

Native and modified Art v 1 were analyzed by SDS PAGE (12 % polyacrylamide gels) under reducing condition using the Laemmli method.[20] Molecular weight standards were run simultaneously. Native PAGE was realized as for the SDS PAGE but under native conditions, without the addition of SDS in the sample buffer and in the electrophoresis buffer. The protein bands were stained with Coomassie Brilliant Blue R-250.

High-performance gel filtration liquid chromatography (HPLC)

Size exclusion HPLC was performed using an Akta HPLC system equipped with a Superdex 75 PC 3.2/30 (3.2 mm×300 mm) column (Amersham Pharmacia Biotech, Sweden). Before analysis, the samples were centrifuged (20 min, 12000 g) and 10 μl of the supernatant was injected onto the column. The components were eluted with 50 mM Tris buffer pH 8.2 containing 0.2 M NaCl and 1 mM EDTA at a flow rate of 0.05 ml/min and detected at 215 and 280 nm.

Protein concentration determination

The protein concentrations of the native and modified proteins were determined spectrophotometrically at 280 nm using an extinction coefficient 640 ml mg^{-1} cm^{-1}, calculated for Art v 1 as described previously.[18]

pH stability

The pH stability of the Art v 1 derivatives was estimated by determination of the free amino groups remaining after exposure of the derivatives to PBS (pH 7.2), 100 mM acetate buffer (pH 4.5) or 100 mM phosphate buffer (pH 2.0) at 37 °C for 1, 4 and 18 h. The results are expressed as means of two different determinations for modified Art v 1 as a percentage of the number of amino groups determined for the native Art v1 (expressed as 100 %).

RESULTS AND DISCUSSION

In present study, Art v 1 was modified by adding negative charges, which should, in principle, facilitate SR-mediated uptake and presentation of this allergen by APC and increase its immunogenicity. After treatment of Art v 1 with *cis*--aconitic and citraconic anhydrides, Art v 1 derivatives, caaArt v 1 and citArt v1, respectively, were obtained with 80 % of the amino groups modified. In the 2,3-dimethylmaleic anhydride-treated Art v 1, number of amino groups was similar to that in unmodified Art v 1 (Table I). As dimethylmaleyl groups easily hydrolyze at neutral pH,[21] it is supposed that Art v 1 was actually modified with 2,3-dimethylmaleic anhydride but that this derivative (dmaArt v 1) was hydrolyzed during the 20 h dialysis against PBS. All derivatives were completely soluble over a wide range of pH values (2.0–10).

TABLE I. Percent of remaining amino groups after Art v 1 treatment with citraconic, *cis*-aconitic and 2,3-dimethylmaleic anhydride, estimated by the TNBS method

Derivative	Amino groups, %
Art v 1	100±2.7
citArt v 1	23.1±1.8
caaArt v 1	22.2±1.5
dmaArt v 1	96.6±3.8

SDS PAGE demonstrated that caaArt v 1 and citArt v 1 were monomers with molar masses virtually indiscernible from that of unmodified Art v 1 (Fig. 1a). The size exclusion chromatograms (Fig. 2) show that, according to the retention times of the derivatives, citArt v 1 (t_r = 22.35 min) and caaArt v 1 (t_r = 21.83 min) had slightly increased molecular masses compared to unmodified Art v 1 (t_r = = 23.69 min). Retention of the monomeric structure, with molar masses similar to that of native Art v 1, as well as their complete solubility, makes these derivatives promising candidates as immunogens for allergen immunotherapy.

The native PAGE results show that the derivatives were very acidic in contrast to native Art v 1 (pI around 8), which did not even enter into the running gel (Fig 1b). caaArt v 1 was more acidic than cit Art v 1 because it has one carboxyl group more per introduced acyl group. By IEF, it was observed that the pI value of the derivatives was lower then 3.5 (results not shown). These results suggest that these derivatives with a very high negative charge density could be good SR ligands. Also with a so significantly altered structure, it is expected that the IgE binding would be dramatically reduced.

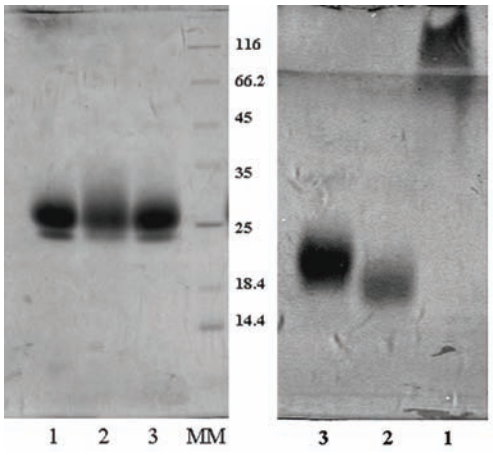

(a) (b)

Fig. 1. a) SDS PAGE of unmodified Art v 1 (lane 1), caaArt v 1 (lane 2) and citArt v 1 (lane3); b) native PAGE.

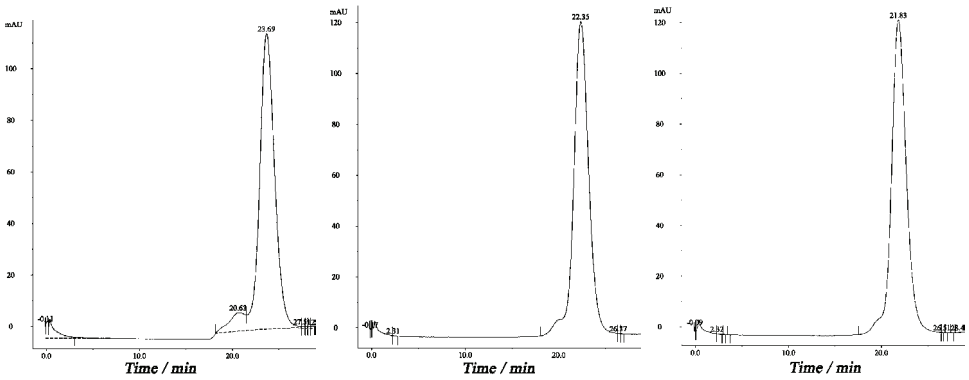

Panel A Panel B Panel C

Fig. 2. Size exclusion chromatograms of native Art v 1 (panel A), citArt v 1 (panel B) and caaArt v 1 (panel C).

The pH stability test of the Art v 1 modifications showed that at physiological pH (pH 7.4), the half life is 30 and 25 h for caaArt v 1 and citArt v 1, respectively. At pH 4.5 (pH in the lysosomal compartment), the half-life of caaArt v 1 and citArt v 1 was 6 and 2 h, respectively. Finally, at pH 2.0, the half-life of both derivatives was about 2 h (Fig. 3). The stability of the derivatives at pH 7.0 should enable their relatively long half-life in circulation. On the other hand, their short half-life in an acidic environment, such as lysosomes during antigen processing, should enable these modified allergens to retain immunogenicity, *i.e.* to stimulate allergen specific T cells in a similar manner to native allergens.

In order for a protein to act as a good SR-ligand, it must have a certain negative charge density. On the other hand, a too high level of acetylation or succi-

nylation (which could provide this property) might decrease immunogenicity and T cell recognition. In contrast, a high degree citraconylation and *cis*-aconitylation generates two and three times greater negative charge density compared to acetylation (and, consequently, giving much better ligands for SR). A further potential advantage of the studied chemical modifications is the expected hydrolysis of acyl groups during antigen processing, which should allow the generation by an APC of the same set of peptides as the native allergen. This could be especially important because it was shown that T cell response to Art v 1 is characterized by one strong immunodominant epitope of 15 amino acids, containing up to three lysine residues.[22]

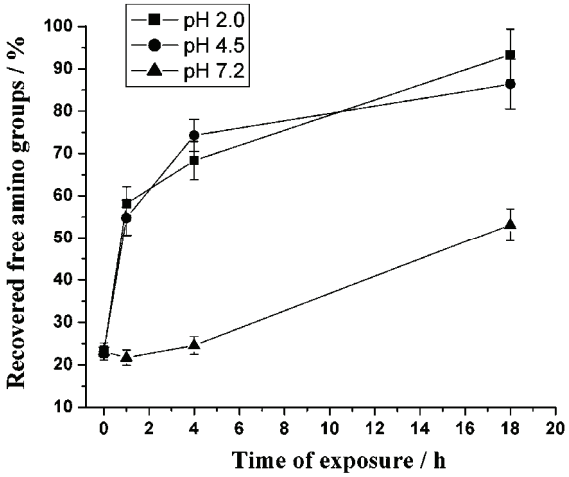

(a)

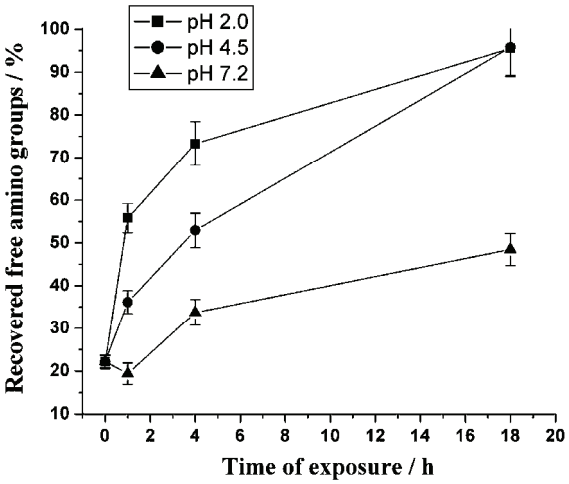

(b)

Fig. 3. pH stability of a) citArt v 1 and b) caaArt v 1. The results are presented as percent of the remaining amino groups of the modified Art v 1, taking the number of native Art v 1 amino groups as 100 %.

CONCLUSIONS

In this work, the preparation of reversibly modified Art v 1, the major mugwort allergen, by treatment with citraconic, *cis*-aconitic anhydride and 2,3-dimethylmaleic anhydridesis described. Acylation of Art v 1 by treatment with citraconic and *cis*-aconitic anhydride gave highly negatively charged derivatives (caaArt v 1 and citArt v 1). As 2,3-dimethylmaleyl derivative was hydrolyzed rapidly even at neutral pH values, this derivative was too unstable to be studied further and thereby was dismissed as a potential allergoid candidate. Additionally, the low stability of caaArt v 1 and citArt v 1 in an acidic environment would enable the complete retention of the specificity of the unmodified allergen. Modification of allergens by *cis*-aconitylation and citraconylation could be a new strategy for safer and more efficient allergen-specific immunotherapy. The derivatives obtained by citraconic and *cis*-aconitic anhydride treatment are suitable for further immunological testing.

Acknowledgment. The work of the authors was supported by the Ministry of Science of the Republic of Serbia (Grant No. 142020).

И З В О Д

ХЕМИЈСКЕ МОДИФИКАЦИЈЕ Art v 1, ГЛАВНОГ АЛЕРГЕНА *Artemisia vulgaris*, *cis*-АКОНИТИЛОВАЊЕМ И ЦИТРАКОНИЛОВАЊЕМ

ДРАГАНА СТАНИЋ[1], ЛИДИЈА БУРАЗЕР[2], МАРИЈА ГАВРОВИЋ-ЈАНКУЛОВИЋ[3], РАТКО М. ЈАНКОВ[3] и ТАЊА ЋИРКОВИЋ ВЕЛИЧКОВИЋ[3]

[1]*Институт за хемију, технологију и металургију – Центар за хемију, Његошева 12, 11001 Београд,*
[2]*Институт за вирологију, вакцине и серуме – Торлак, Војводе Степе 458, 11221 Београд и*
[3]*Хемијски факултет, Универзитет у Београду, Студентски трг 16, 11001 Београд*

Art v1 је главни алерген полена црног пелина (*Artemisia vulgaris*), значајног узрочника поленске грознице широм Европе. Алерген-специфична имунотерапија је за сада једини делотворан начин за третирање алергија, при чему примена модификованих алергена чини овакав третман безбеднијим и ефикаснијим. У овом раду, два од три (анхидрид *cis*-аконитне, цитраконске и 2,3-диметилмалеинске киселине) испитивана анхидрида су се показала погодним за хемијске модификације алергена. Art v 1 је модификован *cis*-аконитиловањем и цитракониловањем у циљу добијања деривата Art v 1 погодних за даље имунолошке тестове. Ацеловањем Art v 1 добијени су деривати (caaArt v 1 и citArt v 1) са око 80 % измодификованих амино група. Добијени деривати су мономерни, са молекулском масом сличном нативном Art v 1, али са драматично смањеним pI вредностима. Оба деривата су релативно стабилна у неутралној, док се у киселој средини ацил групе хидролизују. Модификација алергена *cis*-аконитиловањем и цитракониловањем може бити нови начин за добијање алергоида.

(Примљено 19. септембра, ревидирано 6. новембра 2008)

REFERENCES

1. ISAAC Steering Committee, *Lancet* **351** (1998) 1225
2. J. Bousquet, R. Lockey, H. J. Malling, *J. Allergy Clin. Immunol.* **102** (1998) 558

3. S. R. Durham, S. M. Walker, E. M. Varga, M. R. Jacobson, F. O'Brien, W. Noble, S. J. Till, Q. A. Hamid, K. T. Nouri-Aria, *N. Engl. J. Med.* **341** (1999) 468
4. M. Larche, C. A. Akdis, R. Valenta, *Nat. Rev. Immunol.* **6** (2006) 761
5. H. Kahler, H. Stuwe, O. Cromwell, H. Fiebig, *Int. Arch. Allergy Immunol.* **120** (1999) 146
6. L. Lund, H. Henmar, P. A. Wurtzen, G. Lund, N. Hjortskov, J. N. Larsen, *Clin. Exp. Allergy* **37** (2007) 564
7. M. Jutel, L. Jaeger, R. Suck, H. Meyer, H. Fiebig, O. Cromwell, *J. Allergy Clin. Immunol.* **116** (2005) 608
8. V. Niederberger, F. Horak, S. Vrtala, S. Spitzauer, M. T. Krauth, P. Valent, J. Reisinger, M. Pelzmann, B. Hayek, M. Kronqvist, G. Gafvelin, H. Gronlund, A. Purohit, R. Suck, H. Fiebig, O. Cromwell, G. Pauli, M. van Hage-Hamsten, R. Valenta, *Proc. Natl. Acad. Sci. USA* **101 Suppl. 2** (2004) 14677
9. P. Patel, A. M. Salapatek, *Expert Rev. Vaccines* **5** (2006) 617
10. H. Zhang, Y. Yang, U. P. Steinbrecher, *J. Biol. Chem.* **268** (1993) 5535
11. M. E. Haberland, A. M. Fogelman, *Proc. Natl. Acad. Sci. USA* **82** (1985) 2693
12. R. Abraham, N. Singh, A. Mukhopadhyay, S. K. Basu, V. Bal, S. Rath, *J. Immunol.* **154** (1995) 1
13. D. Rajagopal, K. A. Ganesh, P. V. Subba Rao, *Int. Arch. Allergy Immunol.* **121** (2000) 308
14. K. Shakushiro, Y. Yamasaki, M. Nishikawa, Y. Takakura, *Immunology* **112** (2004) 211
15. E. P. Grant, M. T. Michalek, A. L. Goldberg, K. L. Rock, *J. Immunol.* **155** (1995) 3750
16. V. M. Leb, B. Jahn-Schmid, K. G. Schmetterer, H. J. Kueng, D. Haiderer, A. Neunkirchner, G. F. Fischer, K. Nissler, A. Hartl, J. Thalhamer, B. Bohle, B. Seed, W. F. Pickl, *J. Allergy Clin. Immunol.* **121** (2008) 64
17. Y. Yamasaki, T. Ikenaga, T. Otsuki, M. Nishikawa, Y. Takakura, *Vaccine* **25** (2007) 85
18. M. Blanuša, I. Perović, M. Popović, N. Polović, L. Burazer, M. Milovanović, M. Gavrović-Jankulović, R. Jankov, T. Ćirković Veličković, *J. Chromatogr., B: Anal. Technol. Biomed. Life Sci.* **857** (2007) 188
19. T. W. Willis, A. T. Tu, *Biochemistry* **27** (1988) 4769
20. U. K. Laemmli, *Nature* **227** (1970) 680
21. J. Pavel, C. Harter, F. T. Wieland, *Proc. Natl. Acad. Sci. USA* **95** (1998) 2140
22. B. Jahn-Schmid, P. Kelemen, M. Himly, B. Bohle, G. Fischer, F. Ferreira, C. Ebner, *J. Immunol.* **169** (2002) 6005.

Journal of the Serbian Chemical Society
JSCS@tmf.bg.ac.rs • www.shd.org.rs/JSCS
J. Serb. Chem. Soc. *74* (4) 367–377 (2009)
JSCS–3838
UDC 616.33:615.37:633.852.73:633.879.1
Original scientific paper

Phytochemical analysis and gastroprotective activity of an olive leaf extract

DRAGANA DEKANSKI[1]*, SNEŽANA JANIĆIJEVIĆ-HUDOMAL[2], VANJA TADIĆ[3], GORAN MARKOVIĆ[3], IVANA ARSIĆ[3] and DUŠAN M. MITROVIĆ[4]

[1]Biomedical Research, R & D Institute, Galenika a.d., Pasterova 2, 11000 Belgrade, [2]Pharmacology Department, School of Medicine, University of Priština (Kosovska Mitrovica), [3]Institute for Medicinal Plant Research "Dr Josif Pančić", Tadeuša Košćuška 1, 11000 Belgrade and [4]Institute of Medical Physiology, School of Medicine, University of Belgrade, Višegradska 26, 11000 Belgrade, Serbia

(Received 8 September, revised 7 November 2008)

Abstract: Some medicinal features of olive leaf have been known for centuries. It has been traditionally used as an antimicrobial and to prevent and treat diabetes mellitus and heart disease. Whether olive leaf, a natural antioxidant, influences the gastric defense mechanism and exhibits gastroprotection against experimentally-induced gastric lesions remains unknown. In this study, the content of total phenols, total flavonoids and tannins in olive leaf extract (OLE) were determined. Seven phenolic compounds were identified and quantified (oleuropein, caffeic acid, luteolin, luteolin-7-*O*-glucoside, apigenine-7-*O*-glucoside, quercetin, and chryseriol). Furthermore, the protective activity of the OLE in gastric mucosal injury induced by a corrosive concentration of ethanol was investigated. In relation to the control group, pretreatment with OLE (40, 80 and 120 mg kg^{-1}) significantly ($p < 0.001$) attenuated the gastric lesions induced by absolute ethanol. The protective effect of the OLE was similar to that obtained with a reference drug, ranitidine. The results obtained indicate that OLE possesses significant gastroprotective activity, and that the presence of compounds with antioxidative properties would probably explain this effect.

Keywords: olive leaf extract; phenols; flavonoids; tannins; gastroprotection.

INTRODUCTION

Research on flavonoids and other polyphenols, their antioxidant properties, biological activities and their effects in disease prevention truly began in the last decade. There is an increasing interest in medicinal plant extracts, the greatest value of which may be due to constituents that contribute to the modulation of the oxidative balance *in vivo*. Benefits of the olive (*Olea europaea* L.) leaf have been

* Corresponding author. E-mail: ddekan@sezampro.rs
doi: 10.2298/JSC0904367D

known for centuries and it has been traditionally used to prevent and treat different diseases.

Olive leaf is used to enhance the immune system, as an antimicrobial and in heart disease. Folk medicine uses also include hypertonia, arteriosclerosis, rheumatism, gout, diabetes mellitus, and fever.[1] Recently, experimental animal studies have demonstrated hypoglycemic,[2,3] hypotensive,[4] anti-arrhythmic,[5] anti-atherosclerotic,[6] and vasodilator effects,[7] as well as a stimulatory effect on the activity of the thyroid.[8] Antimicrobial,[9–12] antiviral,[13,14] anti-tumor,[15,16] and anti--inflammatory activity[17] were also reported.

Despite the number of papers published on olive leaf and the effects of its constituents, none has focused on its influence on the gastric defense mechanism and gastroprotective activity.

It is well known that oleuropein, one of the iridoide monoterpenes, is the main phenolic constituent of olive leaves, which is thought to be responsible for their pharmacological effects. Furthermore, olive leaves contain triterpenes, flavonoids, and chalcones.[1,18] Its chemical content makes olive leaf one of the most potent natural antioxidant.

The gastric mucosa plays the role of a barrier that limits exposure of the gastric mucosal cells to numerous injurious luminal agents and irritants of exogenous and endogenous origin. Pretreatment with different substances could effectively prevent the gastric mucosa from the development of erosions and ulceration. This action, called gastro- or cyto-protection is not related to the inhibition of gastric acid secretion and is known to account for gastroprotection by various irritants. The role of oxygen-derived free radicals in the generation of gastric injury is also well-known. Effects of reactive oxygen species (ROS) on the gastric mucosa in various experimental models of stress-induced mucosal injury were proven. Previous studies demonstrated that the damaging action of absolute ethanol could be attributed to the enhancement of the ROS and the ROS-dependent increase in lipid peroxidation and inhibition of antioxidative enzyme activity.[19]

In light of the above considerations, the chemical composition and the protective effect of an olive leaf extract (OLE) on ethanol-induced gastric mucosal damage in rats were investigated, since in this experimental model the pathogenesis of the lesions has been related with production of reactive oxygen species. This study represents the first step in the recognition of the gastroprotective properties of the olive leaf.

EXPERIMENTAL

Materials

Standardized dry olive leaf extract, EFLA® 943, was purchased from Frutarom Industry Ltd. (Wädenswil, Switzerland). Ranitidine tablets were obtained from Galenika a.d. (Belgrade, Serbia). Sodium bicarbonate (analytical grade) was purchased from Sigma-Aldrich (Schnelldorf, Germany). Analytical grade reagents ethyl acetate, acetone, hydrochloric acid (HCl) and

absolute ethanol were purchased from Merck (Darmstadt, Germany). HPLC grade acetonitrile (MeCN) and methanol were also purchased from Merck (Darmstadt, Germany). Reference HPLC standards were purchased from Carl Roth (Karlsruhe, Germany).

Determination of total phenols content

The total content of phenols was determined by the Folin–Ciocalteu method.[20] A total of 100 µl of a methanolic solution of dry extract (17.5, 13.1, and 8.8 µg ml^{-1} final quantity) was mixed with 0.75 ml of Folin–Ciocalteu reagent (previously diluted 10-fold with distilled water) and allowed to stand at 22 °C for 5 min; 0.75 ml of sodium bicarbonate (60 g l^{-1}) solution was added to the mixture. After 90 min at 22 °C, the absorbance was measured using a Hewlett Packard 8453 UV–Vis spectrophotometer (Agilent Technologies, Santa Clara, CA) at λ_{max} 725 nm. Results are expressed as gallic acid equivalents (GAE), and presented as mean ± ± standard deviation (*SD*) of three determinations.

The percentage content of tannins was calculated using the method described in the European Pharmacopoeia, Ph. Eur., 6.0.[21] The content of tannins, expressed as pyrogallol percentage, is presented as the mean ± *SD* of three determinations.

Determination of total flavonoids content

The percentage content of flavonoids expressed as hyperoside was calculated using the method described in the Deutsches Arzneibuch, DAB (German Pharmacopoeia) 10.[22] Briefly, the sample was extracted with acetone/HCl under a reflux condenser; the $AlCl_3$ complex of the flavonoid fraction was extracted with ethyl acetate and measured by a UV–Vis spectrophotometer at λ_{max} 425 nm. The content of flavonoid, expressed as the hyperoside percentage, is presented as the mean ± *SD* of three determinations.

High pressure liquid chromatography (HPLC) procedure

A HPLC fingerprint of the extract and quantification of the identified compounds was achieved by HPLC (Agilent Technologies 1200). Detection was performed using a diode array detector (DAD) and the chromatographs were recorded at λ = 260 nm (for flavonoids and oleuropein) and at 325 nm (for caffeic acid). The spectra recorded at 360 nm were used to identify luteolin and chryseriol. HPLC separation of components was achieved using a LiChrospher 100 RP 18e (5 µm), 250 mm×4 mm i.d. column with a mobile phase flow rate of 1.0 ml min^{-1}. The mobile phase A consisted of 500 ml of H_2O plus 9.8 ml of 85 % H_3PO_4 (w/w), while B was MeCN. A combination of gradient modes: 92–75 % A, 0–8 min; 75–60 % A, 35–55 min and 60–50 % A, 55–60 min. The sample was prepared by dissolving 66.4 mg of the extract in 10 ml of methanol, filtered through 0.20 µm PTFE membrane filters. The identification was realized according to retention time and spectra matching. Once spectra matching succeeded, the results were confirmed by spiking with the respective standards to achieve a complete identification by means of the so-called peak purity test. Peaks not fulfilling these requirements were not quantified. Quantification was performed by external calibration with standards.

Gastric lesions induction and evaluation

This study was approved by the Ethical Committee, School of Medicine, University of Belgrade, and run in accordance to the statements of the European Union regarding the handling of experimental animals. Wistar male rats (n = 30), weighing between 200 and 220 g were randomly divided into 5 groups. The animals were placed in individual metabolic cages. Before the experiment, they were fasted overnight, but had free access to water.

The first, control group, received distilled water intragastrically (*i.g.*) 30 min prior to administration of 1.0 ml absolute ethanol. Three different doses of OLE were applied on the next three groups, and finally, the last group (positive control) received 50 mg kg^{-1} of ranitidine, an H_2 receptor antagonist, as a reference drug. For extrapolation of the dosage from humans to rats, the metabolic body size or food intake rather than body weight was used as the criterion.[23,24] Hence, 40 mg kg^{-1} of OLE was administered as the minimum dose but higher doses of 80 and 120 mg kg^{-1} were also given to test for a dose response. Both OLE and ranitidine were suspended in distilled water before administration. One hour after *i.g.* applied ethanol, the animals were sacrificed under the light ether anesthesia, the abdomen was opened by a midline incision, the stomach was removed, opened along the greater curvature, rinsed gently with water and pinned open for macroscopic examination and for photodocumentation by a digital camera (Hewlett Packard PhotoSmart R507). The areas of gastric lesions were measured by planimetry using the NIH ImageJ computer program[25] and the ulcer index (*UI*) were estimated from the formula:

$$UI = (\text{Ulcerated area/Total stomach area}) \times 100$$

Results are expressed as means ± *SD*. Statistical analysis was achieved using the *t*-test. Differences with $p < 0.05$ were considered as significant.

RESULTS AND DISCUSSION

Many different commercial preparations of olive leaf and extracts are available and vary in strength. Various extraction techniques, as well as different origin of the olive leaves, results in some differences in the chemical composition of the extracts. Standardization of commercially available extracts is strictly based on their oleuropein content, although other constituents of olive leaf are not less important in explaining its medicinal features but data are unavailable.

In this study, an olive leaf extract standardized to 18–26 % of oleuropein, with confirmed stability and chemical and microbiological purity, was employed.

Group of active constituents

Quantitative analysis of the contents of total phenols, flavonoids and tannins were performed.

The total phenols content of the OLE, determined by the Folin–Ciocalteu method, was 197.8±11.3 μg GAE *per* g of dry extract. This indicates the expectable high total phenols content (19.8 %) of the OLE. Further phytochemical investigation yielded flavonoids and tannins, 0.29 and 0.52 %, expressed on total dry OLE, respectively.

Flavonoids are a widely distributed group of polyphenolic compounds, identified in recent years as antioxidants in various biological systems. It is well known that one of the important effects of flavonoids is the scavenging of oxygen-derived free radicals, and that flavonoids can prevent injury caused by free radicals, including experimentally induced gastric mucosal injury.[26,27]

Low concentration of tannins are known to “tan” the outermost layer of the gastric mucosa and to render it less permeable and more resistant to chemical and

mechanical injury or irritation.[28,29] The gastroprotective effect of tannins was experimentally confirmed when the administration of tannins was found to significantly lower stomach free radical concentrations in rats.[30]

In order to further elucidate the chemical composition of the OLE, the phenolic compounds were identified and quantified.

Analysis of the OLE by HPLC revealed a complex mixture of phenolic compounds (Fig. 1). It was intended to identify ten components of the OLE and seven of them were found.

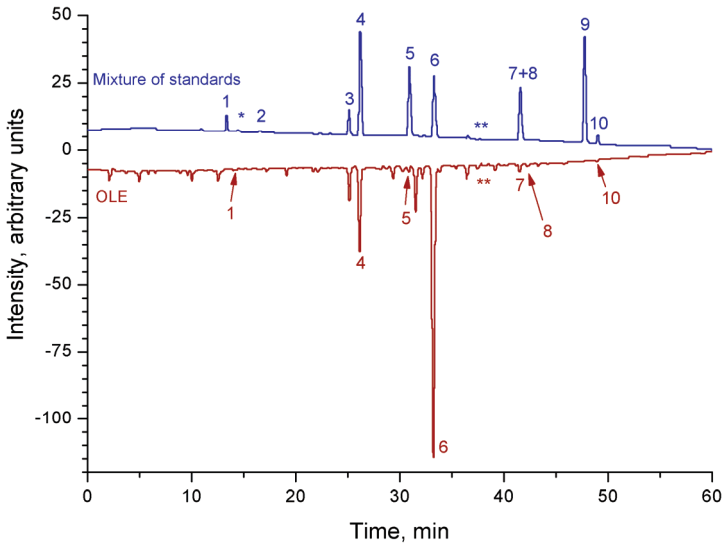

Fig. 1. HPLC chromatogram of the olive leaf extract recorded at 260 nm and compared to the standard mix of identified compounds. The numbers refer to the following: **1**, caffeic acid; **2**, vanillin; **3**, rutin; **4**, luteolin-7-*O*-glucoside; **5**, apigenine-7-*O*-glucoside; **6**, oleuropein; **7**, quercetin; **8**, luteolin; **9**, apigenine; and **10**, chryseriol. *Impurity from caffeic acid; **impurity from the oleuropein standard.

The major constituent of the OLE was oleuropein (Fig. 2), composing 19.8 % of the extract (Table I). The antioxidant properties of oleuropein are well known. It exhibited high antioxidant activity *in vitro*, comparable to a hydrosoluble analog of tocopherol[31] and exhibited strong antioxidant protection in oxidative stress during ischemia-reperfusion in an *in vivo* experimental model.[32]

The other identified components were caffeic acid, luteolin-7-*O*-glucoside, apigenine-7-*O*-glucoside and quercetin (Fig. 2). These constituents of the olive leaf also exert antioxidative properties, which was experimentally confirmed in several studies.[33,34] Moreover, it was shown that a total olive leaf extract had an antioxidant activity higher than that of vitamin C and vitamin E, due to the synergy between the flavonoids, oleuropeosides and substituted phenols.[33]

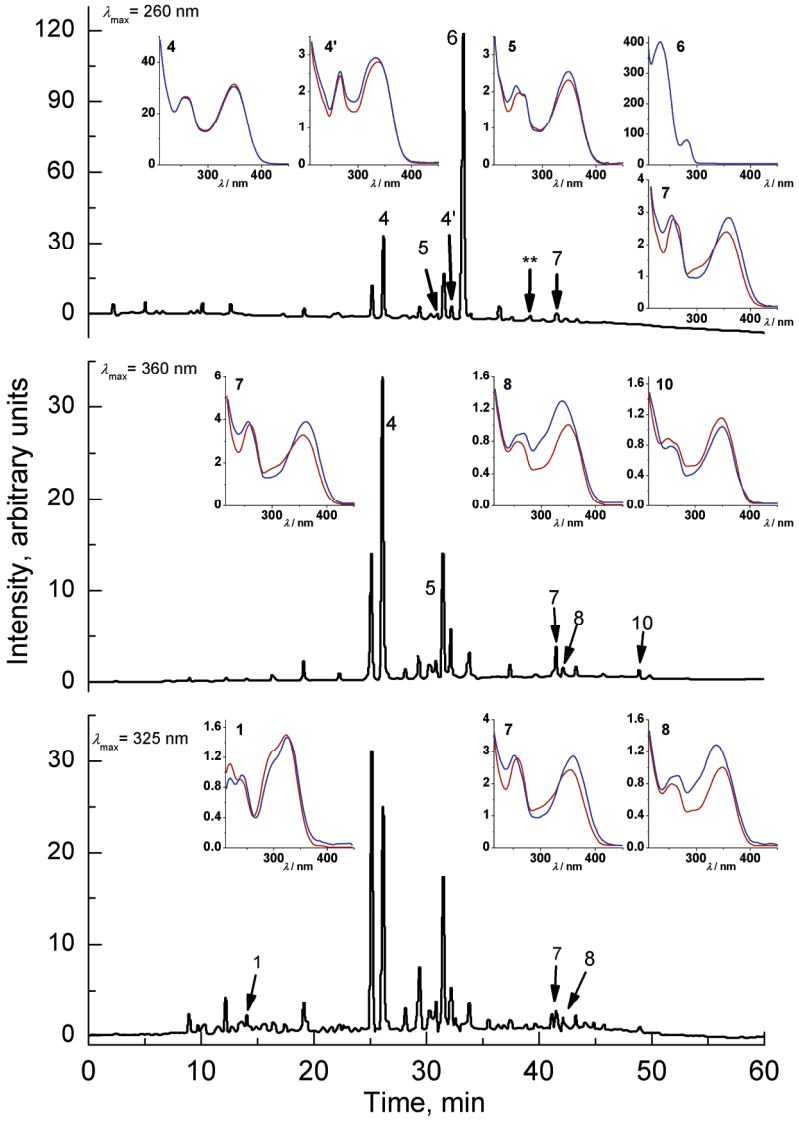

Fig. 2. HPLC chromatogram of the olive leaf extract recorded at 260, 360 and 325 nm with the spectrum of identified compounds and compared to the UV spectra of reference standards. The numbers refer to the following: **1**, caffeic acid; **4**, luteolin-7-*O*-glucoside; **5**, apigenine-7--*O*-glucoside; **6**, oleuropein; **7**, quercetin; **8**, luteolin and **10**, chryseriol (**4**' refers to a derivate of luteolin, taking into account the spectrum of the corresponding peak).
**Impurity from the oleuropein standard.

Luteolin and chryseriol were also isolated from the extract of olive leaves.[17] Since in this study they were present only in the traces (Table I), they did not significantly contribute to the total flavonoid content.

TABLE I. Quantitative determination of flavonoids, phenolcarbonic acids and oleuropein in the studied olive leaf extract

Compound name[a]	Amount	
	mg	%
Caffeic acid (**1**)	0.013	0.02
Vanillin (**2**)	Not found	–
Rutin (**3**)	Not found	–
Luteolin-7-*O*-glucoside (**4**)	0.027	0.04
Apigenine-7-*O*-glucoside (**5**)	0.046	0.07
Oleuropein (**6**)	13.147	19.8
Quercetin (**7**)	0.027	0.04
Luteolin (**8**)	Trace[b]	–
Apigenine (**9**)	Not found	–
Chryseriol (**10**)	Trace[b]	–

[a]The numbers refer to the compounds marked on the HPLC chromatogram (Figs. 1 and 2); [b]determination was not possible – present in the extract under the limit of quantitative analysis

Luteolin-7-*O*-glucoside is widespread in plant species and its anti-radical activity is well-known. Its presence in olive leaf was previously confirmed,[12,35] as well as its anti-ulcer activity.[29] This flavonoid was also identified and quantified in this study, composing 0.04 % of the extract (Table I).

Apigenine, vanillin and rutin were identified in olive leaf in some analytical studies.[12,33,35] Their presence was not confirmed in this investigation, but 0.04 % of quercetin, 0.07 % of apigenine-7-*O*-glucoside and 0.02 % caffeic acid (Table I) were found.

Quercetin is the most abundant of the flavonoid molecules and it is found in many medicinal botanicals. It has been reported to prevent gastric mucosal lesions induced by ethanol.[36] Quercetin increases the amount of neutral glycoproteins in the gastric mucosa[37] and thus participates in the recovery of the mucosal defensive capacity against aggression from absolute ethanol. Other possible mechanisms include inhibition of lipid peroxidation,[36] inhibition of the gastric proton pump,[37] and scavenging of free radicals associated with a significant enhancement in the glutathione peroxidase activity.[38]

Radical scavenging abilities for apigenine-7-*O*-glucoside and for caffeic acid were also reported.[33]

Effect of intragastrically applied OLE on gastric lesions induced by absolute ethanol

There are various plant-originating gastroprotectors with different compositions that have been used in clinical and folk medicine due to their beneficial effects on the gastric mucosa. The documented literature has centered primarily on their pharmacological action in experimental animals. Many studies have demonstrated that substances with antioxidant properties (especially polyphenolic compounds) may protect against the gastric-damaging effects of absolute ethanol.[39–42] The beneficial properties of the polyphenols of olive leaf, the same as in

olive oil, are further enhanced by their good bioavailability. The results obtained for oleuropein and its metabolites, tyrosol and hydroxytyrosol, indicated that they are readily absorbed through the gastrointestinal tract, resulting in significant levels in the circulation.[43,44]

In this study, the protective effect of OLE, a natural antioxidant, on the gastric mucosal damage induced by absolute ethanol in rats was studied.

The administration of absolute ethanol to fasted rats resulted in severe gastric damage, visible from the outside of the stomach as thick reddish-black lines. After opening, gastric lesions were found in the mucosa and consisted of elongated bands, 1–10 mm long, usually parallel to the long axis of the stomach. They were located mostly in the corpus, the portion of the stomach secreting acid and pepsin. No visible lesions developed in the non-secretry part of the stomach.

The effect of absolute ethanol and pretreatment with OLE applied *i.g.* in graded concentrations, as well as ranitidine, on the ulcer index, *UI*, is shown in Fig. 3. Ethanol caused typical widespread gastric lesions on 14.7±5.5 % of total stomach area. Pretreatment with all three doses of OLE significantly ($p < 0.001$) reduced gastric lesions induced by absolute ethanol. The best result was obtained in group pretreated with 80 mg kg^{-1} of OLE, when the ethanol caused gastric lesions on only 2.6±1.4 % of the total stomach area. The gastroprotective effect of OLE was similar to that achieved by pretreatment with the known anti-ulcer drug, ranitidine, when the *UI* was 3.6±0.8 %. Hence, the useful role of gastric anti-sec-

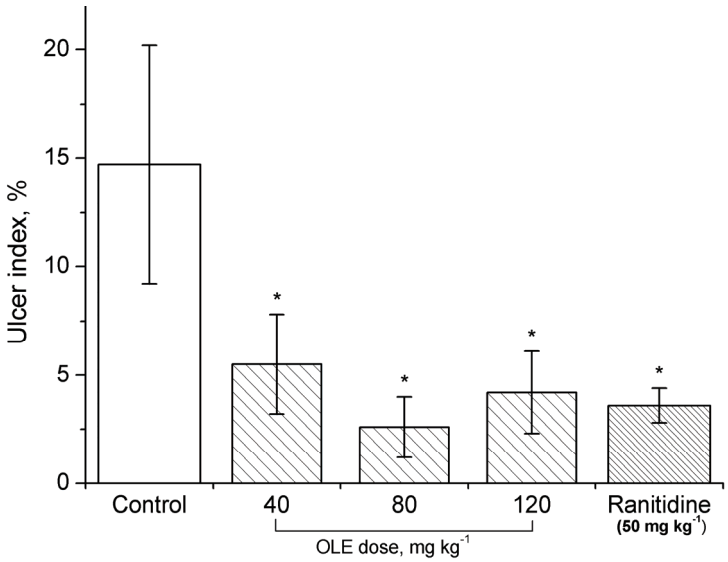

Fig. 3. Effect of intragastric pretreatment with olive leaf extract (OLE) applied in graded doses ranging from 40 up to 120 mg kg^{-1} and ranitidine (50 mg kg^{-1}) on the ulcer index induced by absolute ethanol. The asterisk indicates statistical significance of inhibition ($p < 0.001$), as compared to the control value.

retry medication in the prevention of gastric mucosal damage was also confirmed.

The obtained results indicate that the gastroprotective potential of OLE most probably results from the ability of its constituents to scavenge reactive oxygen species, produced in ethanol-induced gastric injury, which initiate lipid peroxidation. The actual potential is probably related to its ability to maintain the integrity of the cell membrane, by its anti-lipid peroxidative activity and to protect in this way the gastric mucosa against oxidative damage, and by its ability to strengthen the mucosal barrier, the first line of defense against exogenous and endogenous ulcerogenic agents.

CONCLUSIONS

The investigated olive leaf extract caused a significant attenuation of the gastric damage induced by a corrosive concentration of ethanol, suggesting a respectable gastroprotective activity. This activity could be related to its antioxidative properties, since phytochemical analysis of OLE showed a high content of phenolic compounds, well-known antioxidants. However, in order to elucidate the mechanism of OLE gastroprotective effect, and to understand better the actual potential, further investigation will be focused on the determination of lipid peroxidation and antioxidative enzyme activity in the gastric mucosa.

Acknowledgement. The authors thank Ministry of Science and Technological Development, Republic of Serbia, for financial support (project No. 20137).

ИЗВОД

ФИТОХЕМИЈСКА АНАЛИЗА И ГАСТРОПРОТЕКТИВНО ДЕЈСТВО ЕКСТРАКТА ЛИСТА МАСЛИНЕ

ДРАГАНА ДЕКАНСКИ[1], СНЕЖАНА ЈАНИЋИЈЕВИЋ-ХУДОМАЛ[2], ВАЊА ТАДИЋ[3], ГОРАН МАРКОВИЋ[3], ИВАНА АРСИЋ[3] и ДУШАН М. МИТРОВИЋ[4]

[1]Биомедицинска истраживања, Институт за истраживање и развој, Галеника а.д., Пастерова 2, 11000 Београд, [2]Катедра за фармакологију, Медицински факултет, Универзитет у Приштини (Косовска Митровица), [3]Институт за проучавање лековитог биља "Др Јосиф Панчић", Тадеуша Кошћушка 1, 11000 Београд и [4]Институт за медицинску физиологију, Медицински факултет, Универзитет у Београду, Вишеградска 26, 11000 Београд

Нека лековита својства листа маслине су позната вековима. Он се традиционално користи као антимикробни агенс и за превенцију и лечење шећерне болести и срчаних обољења. Остало је непознато да ли примена листа маслине утиче на одбрамбене механизме слузнице желуца и да ли показује гастропротективно дејство код експериментално индукованих лезија желуца. У екстракту листа маслине прво је одређен садржај укупних фенола, флавоноида и танина, а потом идентификовано и квантификовано 7 фенолних једињења (олеуропеин, кафена киселина, лутеолин, лутеолин-7-*O*-глукозид, апигенин-7-*O*-глукозид, кверцетин и хризериол). Испитано је и протективно дејство екстракта листа маслине код оштећења желудачне мукозе корозивном концентрацијом етанола. Претретман екстрактом листа маслине у дозама од 40, 80 и 120 mg kg^{-1} значајно је смањио оштећење желуца у односу на контролну групу ($p < 0,001$). Ово дејство је било слично дејству референтног лека, ранитидина. Добијени резултати указују да екстракт листа маслине поседује значајно гастро-

протективно дејство, које би се донекле могло објаснити присуством антиоксиданаса у његовом хемијском саставу.

(Примљено 8. септембра, ревидирано 7. новембра 2008)

REFERENCES

1. *Physician's Desk References for Herbal Medicine*, Medical Economics Company, Montvale, NJ, 2000, p. 556
2. M. Gonzales, A. Zarzuelo, M. J. Gamez, M. P. Utrilla, J. Jimenez, I. Osuna, *Planta Med.* **58** (1992) 513
3. H. F. Al-Azzawie, M. S. Alhamdani, *Life Sci.* **78** (2006) 1371
4. M. T. Khayyal, M. A. el-Ghazaly, D. M. Abdallah, N. N. Nassar, S. N. Okpanyi, M. H. Kreuter, *Arzneim.-Forsch.* **52** (2002) 797
5. L. I. Somova, F. O. Shode, M. Mipando, *Phytomedicine* **11** (2004) 121
6. L. Wang, C. Geng, L. Jiang, G. Gong, D. Liu, H. Yoshimura, L. Zhong, *Eur. J. Nutr.* **47** (2008) 235
7. A. Zarzuelo, J. Duarte, J. Jimenez, M. Gonzales, M. P. Utrilla, *Planta Med.* **57** (1991) 417
8. A. A. Al-Quarawi, M. A. Al-Damegh, S. A. El-Mougy, *Phytother. Res.* **16** (2002) 286
9. G. Bisignano, A. Tomaino, R. Lo Cascio, G. Crisafi, N. Uccella, A. Saija, *J. Pharm. Pharmacol.* **51** (1999) 971
10. P. M. Furneri, A. Marino, A. Saija, N. Ucella, G. Bisignano, *Int. J. Antimicrob. Agents* **20** (2002) 293
11. D. Markin, L. Duek, I. Berdicevsky, *Mycoses* **46** (2003) 132
12. A. P. Pereira, I. C. Ferreira, F. Marcelino, P. Valentao, P. B. Andrade, R. Seabra, L. Estevinho, A. Bento, J. A. Pereira, *Molecules* **12** (2007) 1153
13. S. Lee-Huang, L. Zhang, P. L. Huang, Y. T. Chang, *Biochem. Biophys. Res. Commun.* **307** (2003) 1029
14. V. Micol, N. Caturla, L. Perez-Fons, V. Mas, L. Perez, A. Estepa, *Antiviral Res*. **66** (2005) 129
15. H. K. Hamdi, R. Castellon, *Biochem. Biophys. Res. Commun.* **334** (2005) 769
16. L. Abaza, T. P. N. Talorete, P. Yamada, Y. Kurita, M. Zarrouk, H. Isoda, *Biosci. Biotechnol. Biochem.* **71** (2007) 1306
17. A. Pieroni, D. Heimler, L. Pieters, B. van Poel, A. J. Vlietinck, *Pharmazie* **51** (1996) 765
18. J. Meirinhos, B. M. Silva, P. Valentao, R. M. Seabra, J. A. Pereira, A. Dias, P. B. Andrade, F. Ferreres, *Nat. Prod. Res.* **68** (2005) 189
19. S. Kwiecien, T. Brzozowski, S. J. Konturek, *J. Physiol. Pharmacol.* **53** (2002) 39
20. V. L. Singleton, R. Orthofer, R. M. Lamuela-Raventós, in *Methods in Enzymology, Oxidants and Antioxidants* (Part A), L. Packer, Ed., Academic Press, San Diego, CA, 1999, p. 152
21. *European Pharmacopoeia 6.0*, Council of Europe, Strasbourg, 2008, p. 255
22. Weißdornblätter mit Blüten, in *Deutsches Arzneibuch, Band 2, Monographien R-Z*, Amlitche Ausgabe Deutscher Apotheker Verlag, Govi-Verlag GmbH, Stuttgart, 1991
23. R. Rucker, D. Storms, *J. Nutr.* **132** (2002) 2999
24. R. B. Rucker, *J. Anim. Physiol. Anim. Nutr*. **91** (2007) 148
25. ImageJ, Image Processing and Analysis in Java, http://rsb.info.nih.gov/ij/ (May, 2008)
26. O. S. Zayachkivska, S. J. Konturek, D. Drozdowicz, P. C. Konturek, T. Brzozowski, M. R. Ghegotsky. *J. Physiol. Pharmacol.* **56** (2005) 219

27. R. J. Nijveldt, E. van Nood, D. E. C. van Hoorn, P. G. Boelens, K. van Norren, P. A. M. van Leeuwen, *Am. J. Clin. Nutr.* **74** (2001) 418
28. I. U. Asuzu, O. U. Onu. *Int. J. Crude Drug. Res.* **28** (1990) 27
29. F. Borelli, A. A. Izzo, *Phytother. Res.* **14** (2000) 581
30. R. O. Ramirez, C. C. Roa, Jr., *Clin. Hemorheol. Microcirc.* **29** (2003) 253
31. E. Speroni, M. C. Guerra, A. Minghetti, N. Crespi-Perellino, P. Pasini, F. Piazza, *Phytother. Res.* **12** (1998) S98
32. I. Andreadou, E. K. Iliodromitis, E. Mikros, M. Constantinou, A. Agalias, P. Magiatis, A. L. Skaltsounis, E. Kamber, A. Tsantili-Kakoulidou, D. Th. Kremastinos**,** *J. Nutr.* **136** (2006) 2213
33. O. Benavente-Garcia, J. Castillo, J. Lorente, A. Ortuno, J. A. Del Rio, *Food Chem.* **68** (2000) 457
34. R. Briante, M. Paturni, S. Terenziani, E. Bismuto, F. Febbraio, R. Nucci, *J. Agric. Food Chem.* **50** (2002) 4934
35. N. De Laurentis, L. Stefanizzi, M. A. Milillo, G. Tantillo, *Ann. Pharm. Fr*. **56** (1998) 268
36. C. Alarcon de la Lastra, M. J. Martin, V. Motilva, *Pharmacology* **48** (1994) 56
37. G. Di Carlo, N. Mascolo, A. A. Izzo, F. Capasso, *Life Sci.* **65** (1999) 337
38. M. J. Martin, C. La Casa, C. Alarcon de la Lastra, J. Cabezza, I. Villegas, V. Motilva, *Z. Naturforsch.* **53** (1998) 82
39. V. M. Tadić, S. Dobrić, G. M. Marković, S. M. Đorđević, I. A. Arsić, N. R. Menković, T. Stević, *J. Agric. Food Chem.* **56** (2008) 7700
40. S. B. Olaleye, E. O. Farombi. *Phytother. Res.* **20** (2006) 14
41. S. Đorđević, S. Petrović, S. Dobrić, M. Milenković, D. Vučićević, S. Žižić, J. Kukić, *J. Ethnopharmacol.* **109** (2007) 458
42. M. P. Germano, V. D'Angelo, T. Biasini, T. C. Miano, A. Braca, M. De Leo, R. De Pasquale, R. Sanogo, *J. Ethnopharmacol.* **115** (2008) 271
43. F. Visioli, C. Galli, F. Bornet, A. Mattei, R. Patelli, G. Galli, D. Caruso, *FEBS Lett*. **468** (2000) 159
44. M. N. Vissers, P. L. Zock, A. J. C. Roodenburg, R. Leenen, M. B. Katan, *J. Nutr.* **132** (2002) 409.

Journal of the Serbian Chemical Society
JSCS@tmf.bg.ac.rs • www.shd.org.rs/JSCS
J. Serb. Chem. Soc. 74 (4) 379–388 (2009)
JSCS–3839
UDC 577.112.383+66.097.8+547.995
Original scientific paper

Inhibition of trypsin by heparin and dalteparin, a low molecular weight heparin

OLIVERA M. BOSNIĆ[1], KRISTINA R. GOPČEVIĆ[2*#], MIROSLAV M. VRVIĆ[3#] and IVANKA M. KARADŽIĆ[2#]

[1]School of Medicine, Department of Physiology, University of Belgrade, Višegradska 26, 11000 Belgrade, [2]School of Medicine, Department of Chemistry, University of Belgrade, Višegradska 26, 11000 Belgrade, and [3]Faculty of Chemistry, University of Belgrade, Studentski trg 12–16, 11000 Belgrade, Serbia

(Received 28 August, revised 19 September 2008)

Abstract: The interaction between trypsin, a prototype S1 serine protease, with heparin and its low molecular weight derivative dalteparin were investigated. Direct inhibition of the proteolytic activity of trypsin by heparin and dalteparin, used in concentrations typical for their clinical application, was detected. The half-maximum inhibition of the trypsin activity was achieved at 15.25±1.22 μg/mL for heparin and was estimated to be at 58.47±15.20 μg/mL for dalteparin. Kinetic analyses showed that heparin and its low molecular weight derivative dalteparin inhibited trypsin by occupation of an exosite, producing noncompetitive and mixed inhibition, respectively. Heparin as a noncompetitive inhibitor with constant of inhibition $K_{i1,2}$ = 0.151±0.019 μM and dalteparin with K_{i1} = 0.202±0.030 μM and K_{i2} = 0.463±0.069 μM in mixed inhibition both represent moderate inhibitors of serine protease trypsin. The obtained constants of inhibition indicate that under the clinically applied concentrations of heparin and dalteparin, trypsins and their homolog S1 serine proteases could be directly inhibited, influencing the delicate control of proteolytic reactions in homeostasis.

Keywords: serine proteases; heparin; dalteparin; inhibition.

INTRODUCTION

Trypsin (EC 3.4.21.4) is a member of the serine protease S1 family. The catalytic activity of the S1 trypsin family is provided by a charge relay system involving serine, histidine and aspartic acid. The sequences in the vicinity of the serine and histidine residues in the active site are well conserved in this family.[1] Proteases known to belong to the serine protease S1, often called trypsin family, are: blood coagulation factors VIIa, IXa, Xa, XIa and XIIa, thrombin (IIa), plas-

* Corresponding author. E-mail: kgopcevic@yahoo.com
# Serbian Chemical Society member.
doi: 10.2298/JSC0904379B

min, activated protein C, trypsins I, II, III, and IV, chymotrypsins, *etc*.[2] Several distinct mechanisms exist for the control of peptidase activity, but inhibition is of particular importance. Peptidases from the family S1 are inhibited by diverse group of inhibitors, including low molecular weight natural and synthetic inhibitors for research or therapeutic purposes, and also natural proteinaceous inhibitors. Natural inhibitors of proteases represent a structurally heterogeneous group of substances from low-molecular weight to macromolecular, originating from animals, plants and microorganisms.[2] Their great importance and particular reason for intensive and constant investigation are related to their potential application in therapy of different diseases, including such serious ones as Alzheimer or AIDS.[3,4]

Heparin is naturally occurring polyanionic glycosaminoglycan with a molecular mass of about 15–20 kDa, and extreme acidic properties.[5] Heparin causes significant structural and functional alterations of trypsin, as the prototype S1 serine protease, in a paradoxical manner which strongly depends on heparin dose, trypsin–heparin ratio and the experimental conditions (pH, presence of salts, time),[5] including inhibition at concentrations of up to 60 mg/L and almost complete losts of activity at concentrations from 120–400 mg/L.[6] Specific, but less intense alterations of the structure and function of trypsin caused by heparin in concentrations from 6–60 mg/L have been recognized as an oxidative mechanism of radical generating binding property of heparin.[6] Actually, it was demonstrated that heparin is capable of generating radicals after its binding to trypsin, which is of particular physiological importance. Additionally, even at the lowest concentrations which trigger radical production, heparin specifically binds to trypsin.[6] Acting as a very efficient anticoagulant, heparin binds to serpin (serin protease inhibitor) peptidase inhibitor antithrombin III (AT-III), which inactivates thrombin and other proteases involved in blood clotting.[7] It should be mentioned that from an administrated dose of heparin of about 32000 U per 24 h for 70 kg patients, by continuous infusion of 40 U/mL, only one third binds to antithrombin.[8] It was found that the inhibitory effect of heparin is mostly indirect, even though it may affect proteolytic enzymes through direct inhibition.[9]

Low-molecular-weight-heparin (LMWH), dalteparin, has a molecular mass of 4–6 kDa and a chain length of 13–22 sugars. Results obtained in clinical trials of heparin and dalteparin as anticoagulants confirmed the significance of both used glycosaminoglycans in anticoagulation by an indirect inhibition of blood clotting serine proteases.[10]

The specific interactions between heparin and LMWH with S1 serine proteases from blood clotting have been investigated and described.[11,12] However, to date, no kinetic data of the direct inhibition of S1 serine proteases by heparin and low molecular weight heparin have been reported. The present investigation was designed as a model system to evaluate the interaction between the prototype S1 serine protease trypsin with heparin and its derivative dalteparin, as inhibitory

substances. Kinetic data and an inhibition model of heparin and dalteparin on the proteolytic activity of serine protease trypsin were determined.

EXPERIMENTAL

Chemicals

Bovine trypsin (T-4665, Sigma Chemicals Co., St. Louis, MO) was used without further purification. Heparin (Galenika, Belgrade, Serbia) and LMWH – dalteparin (Hemopharm, Vršac, Serbia, in cooperation with Sanofipharm, France) were used in appropriate dilutions in the corresponding buffers. BAPNA (N^{α}-benzoyl-DL-arginine-*p*-nitroanilide) and casein Hammerstein were purchased from Sigma Chemicals Co., St. Louis, USA. All chemicals were of analytical grade.

Standard enzyme assays

The proteolytic activity of trypsin on N^{α}-benzoyl-DL-arginine-*p*-nitroanilide as the substrate was determined according to a modified method of Erlanger.[13] BAPNA, in a final concentration of 10 mM (stock solution), was prepared by dissolving in 0.050 M Tris buffer pH 8.2 containing 0.020 M $CaCl_2$ and 2 % (v/v) dimethylformamide. Into 0.50 mL of the BAPNA solution (4.5 mM), 0.10 mL of enzyme solution, containing 0.10 mg of trypsin (9.0 μg/mL) (specific activity on N^{α}-benzoyl-L-arginine-ethyl ester hydrochloride (BAEE): 8750 U/mg) was added, the volume adjusted to the final 1.1 mL with Tris buffer pH 8.2 and the reaction mixture was incubated 15 min at 37 °C. The absorbance of the clear supernatant was measured at 410 nm using a spectrophotometer, Ultrospec K, Sweden. The concentration of *p*-nitroaniline was calculated using a standard curve. One unit of enzyme activity was defined as the amount of enzyme that liberated 1.0 μmol of *p*-nitroaniline per minute under the test conditions.

The proteolytic activity on casein as the substrate was determined according to a modified method of Kunitz[14] and Van der Walt.[15] Casein was dissolved in Tris buffer pH 8.5 to a final concentration of 1.0 % (m/v). Into 0.50 mL of casein solution, 0.10 mL of enzyme solution containing 0.10 mg of lyophilized trypsin powder (9.0 μg/mL, specific activity on BAEE 8750 U/mg) was added and reaction mixture was incubated 15 min at 37 °C. The reaction was stopped with 1.0 mL of trichloroacetic acid (TCA) solution (30 %) and centrifuged at 3000 rpm for 10 min. The absorbance of the clear supernatant was measured at 280 nm. One unit of enzyme activity was defined as the amount of enzyme that decreased the absorbance by 0.0010 after 15 min under the test conditions.

The effect of heparin and dalteparin on the trypsin activity

The effect of different concentrations of heparin: 500 IU (0.21 μM), 1000 IU (0.42 μM), 1500 IU (0.63 μM), 2000 IU (0.84 μM), 2500 IU (1.05 μM); and dalteparin: 1025 IU (1.31 μM), 2050 IU (2.62 μM), 3075 IU (3.93 μM), 4100 IU (5.24 μM), 5125 IU (6.55 μM) on the trypsin activity (the same concentration as in the standard assay) against BAPNA and casein was performed. A mixture of total volume of 1.1 mL containing: 0.10 mL of enzyme solution and 1.0 mL of inhibitor solution was pre-incubated for 5 min at 37 °C. After the addition of 0.50 mL of BAPNA or casein solution, activity was monitored as described in the standard assay methods. The control was the enzyme solution without inhibitors, supplemented with buffer solution to a final volume of 1.1 mL. The activity of the control was defined as 100 %. The half-maximum inhibitory concentrations (IC_{50} values) of heparin and dalteparin for trypsin were determined mathematically by derivation of the best-fit line using an online IC_{50} calculator from BioFitData software package (ChangBioscience).[16]

Kinetic parameters

Enzyme assays on trypsin were performed with BAPNA as the substrate, in concentrations of: 10.0 mM, 5.00 mM, 2.50 mM, 1.25 mM, 0.623 mM and 0.313 mM and different concentrations of inhibitors, *i.e.*, heparin: 0.84 μM, 0.42 μM, 0.21 μM; and dalteparin: 3.93 μM, 2.62 μM, 1.31 μM. The final volume of 1.1 mL of the reaction mixture contained: 0.10 mL of enzyme solution and 1.0 mL of inhibitor. After pre-incubation for 5 min at 37 °C, 0.50 mL of BAPNA solution was added and absorbance at 410 nm was monitored after the 1st and 2nd minute of reaction. The control was the enzyme solution without inhibitor.

To determine kinetic parameters and mode of action of the tested substances on the trypsin activity, the curve fitting software package Ez-fit was used.[17] All enzyme assays were performed in duplicate with the control (test without inhibitor) and the data were fitted to the equations:

$$V_0 = \frac{V_{max}[S]}{\alpha K_m[S]} \text{ for competitive,}$$

$$V_0 = \frac{V_{max}[S]}{\alpha K_m[S] + \alpha[S]} \text{ for noncompetitive,}$$

$$V_0 = \frac{V_{max}[S]}{\alpha' K_m[S] + [S]} \text{ for uncompetitive and}$$

$$V_0 = \frac{V_{max}[S]}{\alpha' K_m[S] + \alpha[S]} \text{ for mixed type of inhibition.}$$

The kinetic constants (V_{max}, K_m and K_i values) and statistical parameters, including the Akaike information criterion (*AIC*), were calculated by the Ez-fit software. By comparing the values of Akaike's information criterion (*AIC*) for the tested inhibition models, the preferred fit was chosen as the one at least 2 units smaller than the rival model.[18] Lineweaver–Burk graphs were plotted using the Microcal Origin program (version 6.1).

Statistical analysis

Graphs were plotted using the Microcal Origin program (version 6.1). The kinetic constants and their standard errors are presented as means ± *SEM* (obtained by linear regression analysis). The statistical comparisons were performed by the Student's *t*-test for paired observations. The means of at least five observations is quoted in the text and $p < 0.01$ was considered statistically significant.

ESI-MS of trypsin

Mass measurements of proteins were performed on a MS system consisting of a 6210 Time-of-Flight LC/ESI-MS (G1969A, Agilent Technologies). A sample of trypsin was dissolved in a mobile phase consisting of a 50:50 mixture of solvent A (0.20 % formic acid in water) and solvent B (acetonitrile). The mass spectrometer was run in the positive electron spray ionization (ESI) mode. A personal computer system running Agilent MassHunter Workstation Software was used for data acquisition and Agilent MassHunter Workstation Software and Analyst QS were used for data processing.

RESULTS AND DISCUSSION

Enzyme and substrate selection

Of many animal trypsins, bovine trypsin has been studied and used for many years as the prototype of serine endopeptidases from the S1 family. The forms of

trypsins present in higher animals share not only high structural but also sequence identity.[2] From the list of trypsins available at the MEROPS database, as one of the protease information systems, only bovine and human trypsins were selected for comparison. Sequences of bovine and human trypsins were aligned using the SIB BLAST network service and trypsins with high identities are given in Table I.[19]

TABLE I. Similarity search of bovine and human trypsins using SIB BLAST Network Service of ExPASy Proteomics Server

Entry name in UniProtKB/-/Swiss-Prot	Accession number	Protein name	Synonyms	No. of amino acids[a]	Identity	Score
TRY1_BOVIN	P00760	Cationic trypsin (precursor)	EC 3.4.21.4 Beta-trypsin	243	243/243 (100 %)	462 bits (1188)
TRY2_BOVIN	Q29463	Anionic trypsin (precursor)	EC 3.4.21.4	247	165/223 (73 %)	362 bits (928)
TRY1_HUMAN	P07477	Cationic trypsin-1 (precursor)	EC 3.4.21.4 Trypsin I Cationic trypsinogen Serine protease 1 Beta-trypsin	247	168/223 (75 %)	364 bits (935)
TRY2_HUMAN	P07478	Anionic trypsin-2 (precursor)	EC 3.4.21.4 Trypsin II Anionic trypsinogen Serine protease 2	247	166/223 (74 %)	355 bits (911)
TRY3_HUMAN	P35030	Trypsin-3 (precursor)	EC 3.4.21.4 Trypsin III Brain trypsinogen Mesotrypsinogen Trypsin IV Serine protease 3 Serine protease 4	303	162/223 (72 %)	351 bits (901)

[a]The length of the sequence of the unprocessed precursor

The high similarity between bovine and human cationic trypsin is obvious. The native form of bovine trypsin, referred to as cationic trypsin or β-trypsin, consists of a single chain polypeptide of 223 amino acid residues. A molecular mass of 23305 Da was computed using Expasy ProtParam Tool. The bovine trypsin preparation (*ex* Sigma) used in this research was analyzed by ESI-MS to confirm the presence of the dominant trypsin form. Intensive signals at 23294 and 23312 Da corresponding to β- and α-trypsin, were detected, similar to a reported

ESI-MS spectrum of bovine trypsin.[20] The cationic form of bovine trypsin, widely used in a variety of medical and scientific applications, is well characterized in terms of kinetic parameters, particularly for low molecular weight synthetic substrates with ester and amide bonds.[21,22] To compare the potential inhibition of trypsin activity by heparin, a proteinaceous substrate casein and a synthetic substrate BAPNA (Fig. 1) were preliminarily investigated. As Fig. 1 shows, the inhibition patterns obtained by both substrates were similar, although the chromogenic substrate BAPNA seemed slightly more suitable for investigations of inhibittion. For the further kinetic study, bovine trypsin and the BAPNA chromogenic substrate were selected.

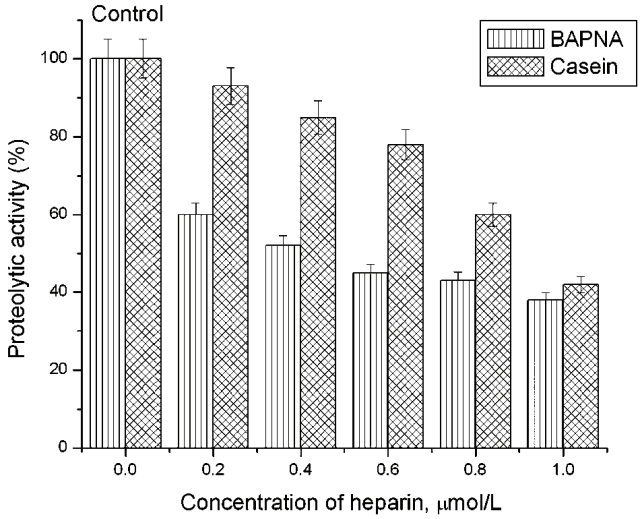

Fig.1. Activity of trypsin in the presence of different concentrations of heparin on BAPNA and casein. The activity of trypsin without inhibitors was 100 %. The results are expressed as the mean percentage of enzyme activity, from at least three independent experiments, performed in triplicate.

The effect of heparin and dalteparin on the activity of trypsin

The results of a preliminary experiment designed to evaluate the effects of different concentrations of heparin and dalteparin on the activity of trypsin are shown in Fig. 2.

Heparin at a concentration of 1.05 μM reduced the trypsin activity to 37 % ($p < 0.05$), while LMWH – dalteparin at a concentration of 7.55 μM inhibited the trypsin activity by 40 % ($p < 0.05$). It is clear from Fig. 2 that the inhibitory effects are dose-dependent, *i.e.*, increasing the concentration of the test substances decreased the proteolytic activity of trypsin on BAPNA as the substrate. In micro-molar concentrations, heparin and dalteparin act as inhibitors of the S1 serine protease trypsin.

The half-maximum inhibition concentration (IC_{50}) of heparin on trypsin was found to be 15.25±1.22 μg/mL. By derivation of the best-fit line, the IC_{50} value of dalteparin was mathematically estimated to be 58.47±15.20 μg/mL. The obtained IC_{50} values for heparin and LMWH were slightly higher than those referenced.[23]

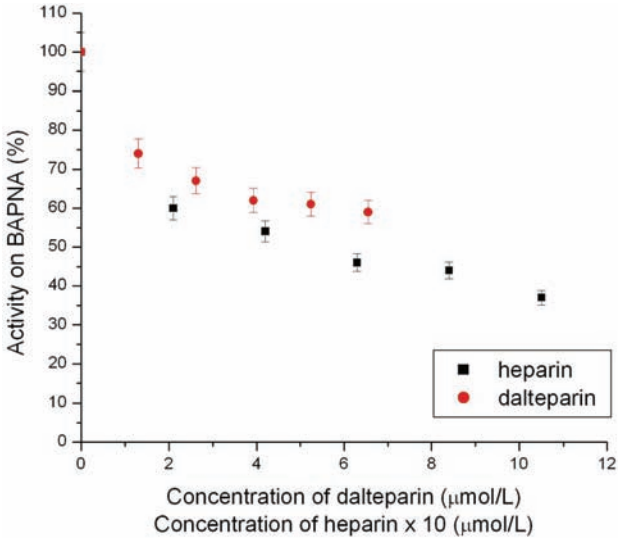

Fig. 2. The effect of different concentrations of heparin and dalteparin on the activity of trypsin on BAPNA. The activity of trypsin without inhibitors was 100 %. The results are expressed as a mean percentage of enzyme activity, from at least three independent experiments, performed in triplicate.

Kinetic study

To investigate the type of inhibition of the trypsin activity by heparin and dalteparin, kinetic analysis of the inhibition pattern using the Ez-fit software package was undertaken. Initial velocity data obtained from the inhibition of trypsin activity were fitted to four inhibition models. The Akaike information criterion (*AIC*) for competitive, uncompetitive, noncompetitive and mixed model of trypsin inhibition by heparin and dalteparin is shown in Table II. Based on a comparison of the values of the Akaike information criterion, the inhibition model was selected that was at least 2 units smaller than the rival model.

It is obvious from the *AIC* values that neither of the tested substances showed competitive inhibition. In addition, uncompetitive inhibition, in which the inhibitor binds to the enzyme–substrate complex, is unlikely to occur. Finally, inhibition in which the inhibitor binds to a site different from the active site, with possibility to bind to either the free enzyme or the enzyme–substrate complex with the same (non-competitive) or different (mixed) constants of inhibition, are the most likely scenarios. Both substances, with the lowest *AIC* for heparin of 177.44

TABLE II. The Akaike information criterion (*AIC*) for competitive, uncompetitive, noncompetitive and mixed model of trypsin inhibition by heparin and LMWH – dalteparin. The kinetic constants and *AIC* were calculated by Ez-fit software. By comparing the *AIC* values for the tested inhibition models, the preferred fit was chosen as the one at least 2 units smaller than the rival model

Tested substance	*AIC* (competitive inhibition)	*AIC* (mixed inhibition)	*AIC* (noncompetitive inhibition)	*AIC* (uncompetitive inhibition)
Heparin	196	179.14	177.44	180.38
Dalteparin	237.17	113.14	115.02	134.55

for noncompetitive and for dalteparin of 113.14 for mixed inhibition (Table II), actually inhibit trypsin by binding to an exosite. A recently identified activity modulation of serine protease fIXa as a homolog of trypsin by occupation of the heparin-binding exosite[11,12] supports the data obtained in this kinetic study. The obtained kinetic data clearly show that there is a specific interaction between trypsin and the tested substances based on the binding of heparin and dalteparin to an exosite of the enzyme, demonstrating a mixed or noncompetitive inhibition pattern. Lineweaver–Burk graphs of the most probable inhibition models of trypsin by heparin and dalteparin are shown in Fig. 3.

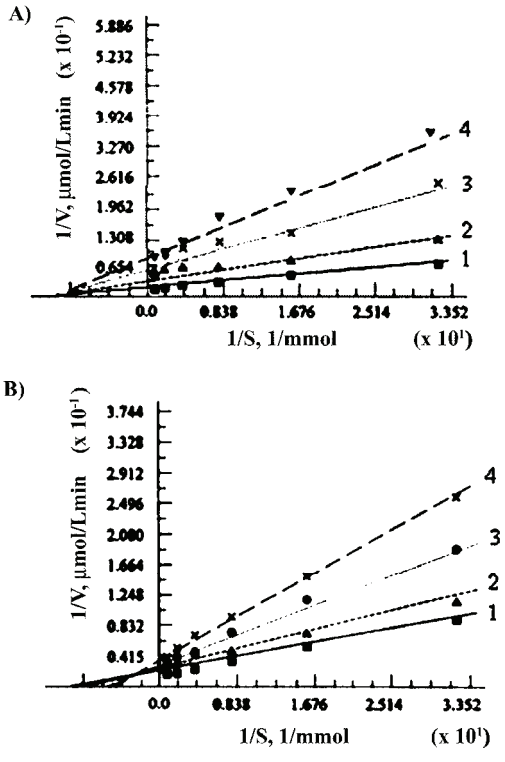

Fig. 3. Lineweaver–Burk plot of a series of kinetic measurements of trypsin activity on BAPNA in the presence of different concentrations of A) heparin and B) dalteparin. Enzyme assays on trypsin were performed with BAPNA as the substrate, in the concentration range 0.313–10.0 mM and different concentrations of inhibitors, *i.e.*, heparin: 0.42–0.84 µM, and dalteparin: 2.9–8.79 µM. The kinetic parameters and mode of action of the tested substances on the trypsin activity were determined using the curve fitting software package Ez-fit. All enzyme assays were performed in duplicate with a control. A) The concentrations of heparin: 1, 0 µM; 2, 0.21 µM; 3, 0.42 µM and 4, 0.84 µM. B) The concentrations of dalteparin: 1, 0 µM; 2, 1.31 µM; 3, 2.62 µM and 4, 3.93 µM.

Heparin, with constant of inhibition $K_{i1,2}$ = 0.151±0.019 μM for noncompetitive inhibition, and dalteparin, with K_{i1} = 0.202±0.030 μM and K_{i2} = 0.463± ±0.069 μM for mixed inhibition, represent moderate inhibitors of the serine protease trypsin. In addition to the constants of inhibition, it was found that the K_m value for BAPNA of 0.99 mM (the K_m for BAPNA is referenced to be 0.94 mM)[22] was not changed in noncompetitive inhibition by heparin, while it was found to be 1.35 mM in mixed inhibition. Data for comparison of S1 serine protease inhibition by heparin and LMWH were not found. However, some inhibitions of fIXa, one of the serine proteases in the human blood-coagulation cascade, were found to be: K_i = 3.2 μM for the 8-hydroxyquinoline family of inhibitors[24] and K_i = 1.73 nM for KFA-1411, a synthetic low molecular weight inhibitor, the inhibition constant of which on trypsin was K_i = 6.1 μM.[17]

CONCLUSIONS

Being involved in complex biological processes, the activity of serine proteases is regulated by sophisticated mechanisms, including the delicate balance between proteolytic and inhibitory reactions in homeostasis. The present model study clearly shows the potential of well known substances, such as heparin and LMWH, to act as inhibitors of trypsin, the reference serine protease.

Research of peptidase inhibitors is an active and rapidly growing field focused mainly on two objectives: construction and screening of new chemical entities with inhibitory activity, and the search for natural proteinaceous inhibitors. A high throughput screening of non-proteinaceous chemical entities for identification of serine protease inhibitors, potentially applicable as drugs has been employed and robust data collections have been generated to date. However, the activity of some well-known (“old”) molecules, such as heparin and LMWH, as potential inhibitors has not been evaluated yet. The present study shows that heparin and dalteparin can specifically inhibit trypsin, producing noncompetitive and mixed kinetic inhibition pattern.

Acknowledgments. This study was supported by the Ministry of Science and Technological Development of the Republic of Serbia (Project No 142018B). Our special thanks go to Dr Lidija Izrael-Živković and Dr Danijela Krstić for their editorial comments during the final preparation of the manuscript.

ИЗВОД

ИНХИБИЦИЈА ТРИПСИНА ХЕПАРИНОМ И ДАЛТЕПАРИНОМ

ОЛИВЕРА БОСНИЋ[1], КРИСТИНА ГОПЧЕВИЋ[2], МИРОСЛАВ ВРВИЋ[3] и ИВАНКА КАРАЏИЋ[2]

[1]Институт за физиологију, Медицински факултет, Универзитет у Београду, Вишеградска 26, 11000 Београд, [2]Институт за хемију, Медицински факултет, Универзитет у Београду, Вишеградска 26, 11000 Београд и [3]Хемијски факултет, Универзитет у Београду, Студентски трг 12–16, 11000 Београд

У раду је испитивана интеракција трипсина, као прототипа S1 серин-протеазе, са хепарином и његовим нискомолекулским дериватом далтепарином фрагмином. Утврђена је ди-

ректна инхибиција трипсина како хепарином тако и далтепарином, у концентрацијама типичним за њихову клиничку употребу. Одређена је IC_{50} трипсина хепарином: 15,25±1,22 μg/mL и далтепарином: 58,47±15,20 μg/mL. Кинетичка анализа је показала да хепарин и његов нискомолекулски дериват далтепарин инхибирају трипсин по моделу некомпетитивне и мешовите инхибиције, редом. Хепарин са константом инхибиције $K_{i1,2}$ =0,151±0,019 μM (некомпетитивна) и далтепарин са K_{i1} = 0,202±0,030 μM и K_{i2} = 0,463±0,069 μM (мешовита), представљају умерене инхибиторе трипсина, као референтне серин-протеазе. Добијене константе инхибиције указују да при клинички апликованим концентрацијама хепарина и далтепарина, трипсини и хомологе S1 серин-протеазе могу бити директно инхибиране и тиме утицати на деликатну контролу активности серин-протеаза у хомеостази.

(Примљено 28. августа, ревидирано 19. септембтра 2008)

REFERENCES

1. A. J. Barret, N. D. Rawlings, *Handbook of proteolytic enzymes*, 1st Ed. on CD, Academic Press, London, 1998
2. A. J. Barrett, N. D. Rawlings, E. A. O' Brien, *J. Struct. Biol.* **134** (2001) 95
3. G. Hook, V. Y. Hook, M. Kindy, *Biol. Chem.* **388** (2007) 979
4. B. Luna, M. U. Townsend, *Clin. Ther.* **29** (2007) 2309
5. P. Finotti, S. Manente, *Biochim. Biophys. Acta* **1207** (1994) 80
6. P. Finotti, C. Corvaja, A. Pagetta, *Free Radic. Biol. Med.* **27** (1999) 1378
7. T. S. Olson, B. E. Pock, J. Kvassman, U. J. D. Shore, D. A. Lawrence, D. Ginsburg, I. Bjork, *J. Biol. Chem.* **270** (1995) 30007
8. J. Hirsh, T. Warkentin, S. Shaughnessy, S. Anand, J. Halperin, R. Raschke, C. Granger, E. Ohman, J. Dalen, *Chest* **119** (2001) 64S
9. P. A. Patson, M. Schapira, *Biochem. Biophys. Res. Comm.* **230** (1997) 597
10. I. Ahrens, K. Peter, C. Bode, *Haemostaseologie* 27 (2007) 328
11. P. F. Neuenschwander, *Biochemistry* **43** (2004) 2978
12. P. F. Neuenschwander, S. R. Williamson, A. Nalian, K. J. Baker-Deadmond, *J. Biol. Chem.* **281** (2006) 23066
13. B. F. Erlanger, N. Kokowsky, W. Cohen, *Arch. Biochem. Biophys.* **95** (1961) 271
14. M. Kunitz, *J. Gen. Physiol.* **30** (1947) 291
15. S. J. Van der Walt, F. J. Joubert, *Toxicon* **9** (1971) 153
16. BioDataFit 1.02, *Data Fit for Biologists* (http//www.changbioscience.com/stat/ec50.html), Chang Bioscience Inc., 2008
17. W. F. Perella, *Anal. Biochem.* **174** (1988) 437
18. R. H. Jones, E. B. Reeve, G. D. Swanson, *Comp. Biomed. Res.* **17** (1984) 277
19. S. F. Altschul, T. L. Madden., A. A. Schäffer, J. Zhang, Z. Zhang, W. Miller, D. J. Lipman, *Nucleic Acids Res.* **25** (1997) 3389
20. D. S. Ashton, A. E. Ashcroft, C. R. Beddlerl, D. J. Cooper, B. N. Green, R. W. A. Oliver, *Biochem. Biophys. Res. Commun.* **199** (1994) 694
21. K. A. Walsh, *Methods Enzymol.* **19** (1970) 41
22. K. D. Johnson, A. Clark, S. Marshal, *Comp. Biochem. Physiol. B* **131** (2002) 423
23. E. Glusa, C. Adam, *Br. J. Pharmacol.* **133** (2001) 422
24. N. H. Mueller, N. Pattabiraman, C. Ansarah-Sobrinho, P. Viswanathan, T. C. Pierson, R. Padmanabhan, *Antimicrob. Agents Chemother.* **52** (2008) 3385.

Journal of the Serbian Chemical Society
JSCS@tmf.bg.ac.rs • www.shd.org.rs/JSCS

J. Serb. Chem. Soc. 74 (4) 389–400 (2009)
JSCS–3840

UDC 546.982–386:548.7:535.441
Original scientific paper

Palladium(II) complexes with R_2edda derived ligands. Part I. Reaction of diisopropyl (*S*,*S*)-2,2'-(1,2-ethanediyldiimino)-dipropanoate with $K_2[PdCl_4]$

BOJANA B. KRAJČINOVIĆ[1#], GORAN N. KALUĐEROVIĆ[1,2*#], DIRK STEINBORN[2], HARRY SCHMIDT[2], CHRISTOPH WAGNER[2], KURT MERZWEILER[2], SREĆKO R. TRIFUNOVIĆ[3] and TIBOR J. SABO[4#]

[1]*Department of Chemistry, Institute of Chemistry, Technology and Metallurgy, University of Belgrade, Studentski trg 14, 11000 Belgrade, Serbia,* [2]*Institut für Chemie, Martin-Luther--Universität Halle-Wittenberg, Kurt-Mothes-Straße 2, D-06120 Halle, Germany,* [3]*Department of Chemistry Faculty of Science, University of Kragujevac, 34000 Kragujevac and* [4]*Faculty of Chemistry, University of Belgrade, P.O. Box 158, 11001 Belgrade, Serbia*

(Received 24 June, revised 6 October 2008)

Abstract: The reaction of $K_2[PdCl_4]$ with (*S*,*S*)-(*i*-Pr)$_2$eddip diester (diisopropyl (*S*,*S*)-2,2'-(1,2-ethanediyldiimino)dipropanoate) resulted in {$PdCl_2$[(*S*,*S*)-(*i*--Pr)$_2$eddip-κ^2*N*,*N*']} (**1**) and {PdCl[(*S*,*S*)-(*i*-Pr)eddip-κ^2*N*,*N*',κ*O*]} (**2**) with one hydrolyzed ester group. The compounds were characterized by spectroscopic methods and it was proved that the reaction is diastereoselective (^{1}H- and ^{13}C-NMR) in the case of **2** (one diastereoisomer of four possible). The structure of **2** was determined by X-ray diffraction analysis, indicating that the product is the (*R*,*R*)-*N*,*N*' configured isomer. In contrast, the reaction yielding **1** produced two of three possible diastereoisomers. DFT calculations support the formation of two diastereoisomers of **1** and of one diastereoisomer of **2**.

Keywords: palladium complexes; crystal structure; EDDP ligands; DFT calculations.

INTRODUCTION

In a previous study, platinum(IV) complexes with R_2edda (esters of ethylenediamine-*N*,*N*'-diacetic acid) ligands were prepared (R = Me, Et or *n*-Pr; Fig. 1, **I**).[1] In contrast, reactions between homologous propionate ligands (R_2eddp = = $ROOCCH_2CH_2NHCH_2CH_2NHCH_2CH_2COOR$; R = Me, Et, *n*-Pr, *n*-Bu or *n*-Pe), and potassium hexachloroplatinates(IV) gave different products depending on the R moiety (Fig. 1, **II** and **III**)[2,3]. For R = Me, Et or *n*-Pr, these reactions

* Corresponding author. E-mail: goran@chem.bg.ac.yu
# Serbian Chemical Society member.
doi: 10.2298/JSC0904389K

proceeded with the hydrolysis of the ester groups yielding [$PtCl_2$(eddp-κ^2*N*,*N*',κ^2*O*,*O*')] (Fig. 1, **II**). Structural analysis gave proof of the *trans*-dichloro arrangement. When R was *n*-butyl or *n*-pentyl, the isolated platinum(IV) complexes [$PtCl_4$(R_2eddp-κ^2*N*,*N*')] maintained the ester functions of the ligand intact, see **III** in Fig. 1.[2]

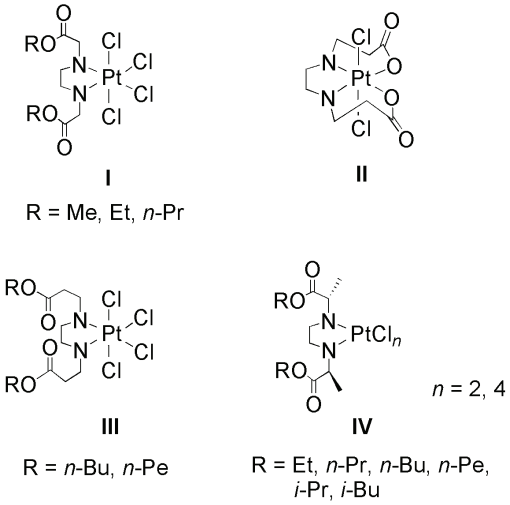

Fig. 1. Platinum complexes containing R_2edda derived ligands.

Furthermore, the work was extended by synthesizing chiral branched-chain esters, (*S*,*S*)-R_2eddip = ROOC$C^{(S)}$H(CH_3)NHCH_2CH_2NH$C^{(S)}$H(CH_3)COOR (R = = Et, *n*-Pr, *n*-Bu, *n*-Pe, *i*-Pr or *i*-Bu), and the corresponding platinum(II/IV) complexes, {$PtCl_n$[(*S*,*S*)-R_2eddip]} (*n* = 2 or 4; Fig. 1, **IV**).[4] Also here, as in the reaction of R_2edda and hexachloroplatinate(IV), the ligands maintained their ester functional groups without hydrolyzing in the obtained complexes. Studies on the antitumoral activity of some Pt(IV) complexes with R_2edda derived ligands showed higher cytotoxicity than cisplatin and the kinetics of the tumor cell death process induced by these complexes was considerably faster in comparison to that induced by cisplatin.[5,6]

The coordination mode of palladium(II) and platinum(II) is analogous, but the palladium(II) complexes are kinetically less stable than the platinum(II) complexes.[7,8] Due to the similar coordination modes and chemical properties of palladium(II) and platinum(II) compounds, it was also decided to synthesize and characterize complexes of palladium(II) with edta tetraalkyl esters and ethylene-diammonium-*N*,*N*'-di-3-propanoic acid.[9,10] In the light of the increasing interest in the biological activity of palladium(II) complexes, their antiproliferative activity is also of interest.[11–13]

The complexes {$PdCl_2$[(*S*,*S*)-(*i*-Pr)$_2$eddip]} (**1**) and {PdCl[(*S*,*S*)-(*i*-Pr)eddip]} (**2**) were prepared and spectroscopically and structurally characterized. In addition, DFT calculations were conducted on the diastereoisomers of **1** and **2**.

EXPERIMENTAL

General

[(*S*,*S*)-H_3eddip]Cl and [(*S*,*S*)-H_2(*i*-Pr)$_2$eddip]$Cl_2 \cdot H_2O$ were prepared as previously reported.[4,14-16] $K_2[PdCl_4]$ was obtained from Merck and used as received. The infrared spectra were recorded on a Perkin-Elmer FTIR 31725-X spectrophotometer using the KBr pellet technique (4000–400 cm^{-1}). The ^1H- and ^{13}C-NMR spectra were recorded on Varian Gemini 200 (200 MHz) (**1**) and Varian Unity 500 (500 MHz) spectrometers (**2**) in $CDCl_3$ and DMF-d_7, respectively. Elemental analyses for C, H and N were performed on a Vario III CHNOS Elemental Analyzer, Elementar Analysensysteme GmbH.

Synthesis of complexes

$K_2[PdCl_4]$ (0.158 g, 0.512 mmol) was dissolved in water (20 ml) at 40 °C and [(*S*,*S*)-H_2(*i*-Pr)$_2$eddip]$Cl_2 \cdot H_2O$ (0.194 g, 0.512 mmol) was added. During 2 h of stirring, 10 ml of 0.10 M LiOH was added in small portions to the reaction solution. On cooling to room temperature, a yellow precipitate of **1** was obtained. The precipitate was filtered off and the filtrate was left for several days at room temperature. The mother liquor produced crystals of **2** suitable for X-ray measurement.

*X-ray crystallography of **2***

Intensity data were collected on a STOE IPDS diffractometer at 220(2) K using graphite monochromatized Mo–K_α radiation (λ = 0.71073 Å). A summary of the crystallographic data, the data collection parameters and the refinement parameters are given in Table I. The structure was solved by direct methods with SHELXS-96 and refined using full-matrix least-squa-

TABLE I. Crystallographic data for **2**

Empirical formula	$C_{11}H_{21}ClN_2O_4Pd$
M_r	387.17 g mol^{-1}
Crystal system	monoclinic
Space group	$P\,2_1$
a / Å	5.877(1)
b / Å	9.672(2)
c / Å	14.424(3)
β / °	100.78(2)
V / Å^3	805.5(3)
Z	2
D_{calc} / g cm^{-3}	1.584
μ(Mo–K_α) / mm^{-1}	1.328
F(000)	392
θ Range / °	2.55–25.80
Refln. collected	1637
Refln. observed ($I > 2\sigma(I)$)	1543
Refln. independent	1637
Data/restraints/parameters	1637/1/177
Goodness-of-fit on F^2	1.079
$R1$, $wR2$ [$I > 2\sigma(I)$]	0.0316, 0.0789
$R1$, $wR2$ (all data)	0.0338, 0.0797
Largest diff. peak and hole / e Å^{-3}	1.02/–1.64

res routines against F^2 with SHELXS-97.[17,18] Non-hydrogen atoms were refined with anisotropic displacement parameters. The hydrogen atoms were refined isotropically. They were placed in the calculated positions with fixed displacement parameters (riding model), except for H12 atom, which was found in the electron density map. The large displacement parameters of atoms C5, C6 and O1 are explained by oscillation in the crystal structure and because these atoms are far away from the palladium atom. The Diamond program was used for the representation of the structure.[19]

The Cambridge Crystallographic Data Centre, CCDC No. 681419, contains supplementary crystallographic data for this paper.*

Computational details

Geometry optimizations were performed with the Gaussian 03 package.[20] All structures were optimized using the MPW1PW91 functional.[21] The SDD basis set for all atoms was employed in the calculations.[22,23] All systems were optimized without symmetry restrictions. The resulting geometries were characterized as equilibrium structures by the analysis of the force constants of normal vibrations. Supplementary data associated with the quantum chemical calculations can be obtained from the authors upon request.

RESULTS AND DISCUSSION

The addition of an aqueous solution containing the ligand precursor [(*S*,*S*)-H_2(*i*-Pr)$_2$eddip]Cl_2 to a solution of $K_2[PdCl_4]$ followed by the addition of the stoichiometric amount of base (molar ratio 1:1:2) results in the formation of a yellow precipitate of **1** (56 % yield). The mother liquor was left for several days at room temperature and crystals of **2** (20 % yield) suitable for X-ray analysis were obtained (Scheme 1). The $\kappa^2N,N',\kappa O$ coordination mode of the [(*S*,*S*)-(*i*-Pr)-eddip]$^-$ ligand in complex **2** arises from the hydrolysis of one of the two ester groups of the original (*S*,*S*)-(*i*-Pr)$_2$eddip ligand.

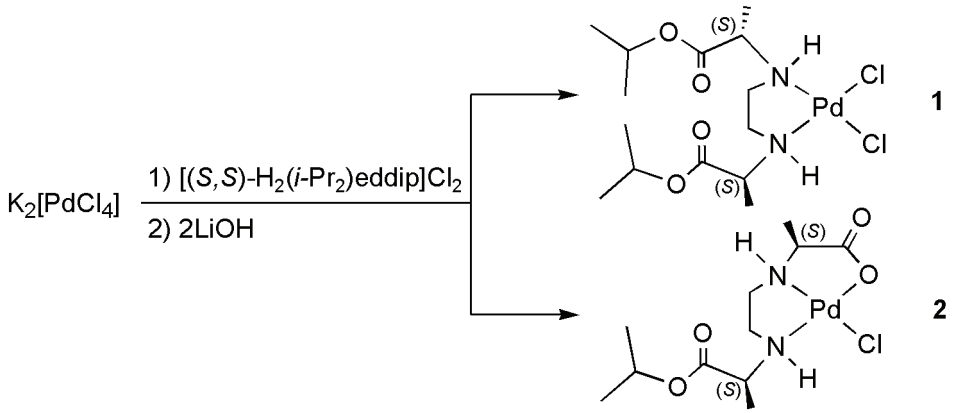

Scheme 1. Reaction of $K_2[PdCl_4]$ with [(*S*,*S*)-H_2(*i*-Pr)$_2$eddip]Cl_2.

*These data can be obtained free of charge *via* www.ccdc.cam.uk/conts/retrieving.html (or from the CCDC, 12 Union Road, Cambridge CB2 1EZ, UK; fax: +44 1223 336033; E-mail: deposit@ccfdc/cam.ac.uk).

Characterization of the complexes

*{PdCl$_2$[(*S,S*)-(i-*Pr*)$_2$eddip]} (**1**)*. Yield: 0.13 g (56 %). Anal. Calcd. for $C_{14}H_{28}Cl_2N_2O_4Pd$: C, 36.11; H, 6.06; N, 6.02. Found: C, 35.79; H, 6.33; N, 5.77 %. IR (KBr, cm^{-1}): 3448, 3153, 2983, 1734, 1380, 1224, 1187, 1143, 1105, 918, 830, 754, 430. ^{1}H-NMR* (200 MHz, $CDCl_3$, δ / ppm): 1.25/1.32 (*d*/*d*, 12H, $^3J_{H,H}$ = 6.60/7.80 Hz, $C_{5,6}H_3$), 1.61/2.00 (*d*/*d*, 6H, $^3J_{H,H}$ = 7.00/7.60 Hz, $C_{3,9}H_3$), 2.44/3.21 and 2.81/3.68 (*m*/*m*, 4H, AA'BB', $C_{10,11}H_2$), 4.09/4.52 (*m*/*m*, 2H, $C_{2,8}H$), 5.03/5.15 (*m*/*m*, 2H, C_4H), 6.12–6.26/6.31–6.42 (*m*/*m*, 2H, NH). ^{13}C-NMR (50 MHz, $CDCl_3$, δ / ppm): 14.6/16.0 (*s*/*s*, $\mathbf{C}_{3,9}$), 21.7/21.7 (*s*/*s*, $\mathbf{C}_{5,6}$), 48.7/51.9 (*s*/*s*, $\mathbf{C}_{10,11}$), 57.4/59.0 (*s*/*s*, $\mathbf{C}_{2,8}$), 69.3/69.9 (*s*/*s*, $\mathbf{C}_4$), 169.4/170.9 (*s*/*s*, $\mathbf{C}_{1,7}$).

*{PdCl$_2$[(*S,S*)-(i-*Pr*)eddip]} (**2**)*. Yield: 0.04 g (20 %). IR (KBr, cm^{-1}): 3441, 3357, 3127, 2985, 1737, 1644, 1389, 1219, 1104, 944, 833, 590, 430. ^{1}H-NMR (500 MHz, DMF-d_7, δ / ppm): 1.23 (*d*, 6H, $^3J_{H,H}$ = 6.95 Hz, $C_{5,6}H_3$), 1.75 (*d*, 3H, $^3J_{H,H}$ = 7.21 Hz, C_3H_3), 1.76 (*d*, 3H, $^3J_{H,H}$ = 7.21 Hz, C_9H_3), 2.73 and 2.90 (*m*, 4H, $C_{10,11}H_2$), 3.69 (*m*, 1H, C_8H), 4.05 (*m*, 1H, C_2H), 4.96 (*m*, 1H, C_4H), 6.55–6.65 (*m*, 1H, N_1H), 6.68–6.77 (*m*, 1H, N_2H). ^{13}C-NMR (125 MHz, DMF-d_7, δ, ppm): 14.8 (*s*, $\mathbf{C}_3$), 15.6 (*s*, $\mathbf{C}_9$), 21.0 (*s*, $\mathbf{C}_{5,6}$), 49.4 (*s*, $\mathbf{C}_{11}$), 52.5 (*s*, $\mathbf{C}_{10}$), 56.4 (*s*, $\mathbf{C}_2$), 62.2 (*s*, $\mathbf{C}_8$), 68.9 (*s*, $\mathbf{C}_4$), 169.6 (*s*, $\mathbf{C}_1$), 181.1 (*s*, $\mathbf{C}_7$).

Spectroscopic properties

The IR spectrum of **1** shows specific absorption bands: ν(C=O) at 1734 cm^{-1} (strong), (typical absorption for aliphatic esters), ν(C–O) at 1236 cm^{-1} (strong) and ν(CH_3) at 2983 cm^{-1} (medium). For comparison [(*S*,*S*)-H_2(i-Pr)$_2$eddip]Cl_2 exhibited the corresponding bands at 1734, 1239 and 2982 cm^{-1}, respectively.[4] The band for the C=O group is at the same position as in the spectrum of the free ligand, meaning that the oxygen atoms of the COOR moieties are not coordinated. In the IR spectrum of **2**, there are two absorption bands for ν(C=O) at 1737 and 1644 cm^{-1}, indicating two different C=O groups, which is in correspondence with the hydrolysis of one of the isopropyl groups and the coordination of the residual oxygen atom. The ν(N–H) absorption bands at 3153 (for **1**) and 3127 cm^{-1} (for **2**) (both typical absorptions for secondary amino groups) may indicate that the coordination occurred *via* the nitrogen atoms.[2–4]

For both complexes **1** and **2**, the NMR spectroscopic measurements gave proof for their constitution. Selected data are given in Table II. The coordination of the N atoms gives rise to the formation of chiral centers, thus in principle, three diastereoisomers can be formed for [PdCl$_2${(*S*,*S*)-(*i*-Pr)$_2$eddip}] (**1**) ((*R*,*R*), (*R*,*S* ≡ *S*,*R*) and (*S*,*S*), Fig. 2). Two sets of signals of about the same intensity (for each diastereoisomer one set of signals) were found (Table II). Two of these

* The values for the two diastereoisomers are separated by a slash. The assignment was verified by COSY experiments.

three possible diastereoisomers (*S*,*S*)- and (*R*,*R*)-*anti*-**1**, will give rise (due to C_2 symmetry) to one set of resonances each for their ester branches. The third diastereoisomer, (*R*,*S*)-*syn*-**1**, is expected to give rise to two sets of signals, since the ester branches are non-equivalent in symmetry, although these two sets may coincide by chance.

TABLE II. Selected ^{1}H- and ^{13}C-NMR data (δ / ppm)[a] of {$PdCl_2$[(*S*,*S*)-(*i*-Pr)$_2$eddip]} (**1**) and {PdCl[(*S*,*S*)-(*i*-Pr)eddip]} (**2**)

Complexes	$C^{3,9}\mathbf{H}_3$	$C^4\mathbf{H}$	$C^{5,6}\mathbf{H}_3$	$\mathbf{C}^{3,9}$	$\mathbf{C}^4$	$\mathbf{C}^{1,7}$OO	$\mathbf{C}^{5,6}H_3$
1[b]	1.61	5.03	1.25	14.6	69.3	169.4	21.7
	2.00	5.15	1.32	16.0	69.9	170.9	21.7
2	1.75	4.96	1.23	14.8	68.9	169.6	21.0
	1.76			15.6		181.1	

[a]Numbering as in Fig. 3 and analogous for {$PdCl_2$[(*S*,*S*)-(*i*-Pr)$_2$eddip]}; [b]diastereoisomers of **1**

In the ^{1}H-NMR spectrum, the signals of the methylene hydrogen atoms from the ethylenediamine moiety show coordination induced shifts of up to 0.9 ppm, which indicates that the coordination occurred *via* the nitrogen atoms. Chemical shifts arising from ester carbon atoms are found at the expected position for this class of compounds.[1,3,4]

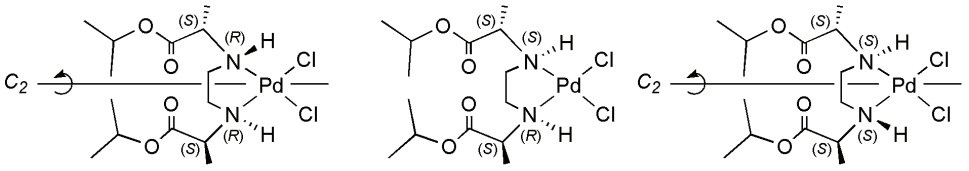

Fig. 2. Diastereoisomers of {$PdCl_2$[(*S*,*S*)-(*i*-Pr)$_2$eddip]} (**1**).

In contrast, four diastereoisomers are possible in **2**: (*S*,*S*)- and (*R*,*R*)-*anti*-**2** and (*S*,*R*)- and (*R*,*S*)-*syn*-**2**, but only one set of signals was found in both the ^{1}H- and ^{13}C-NMR spectra (Table II). In the ^{13}C-NMR spectrum, it can be seen that two signals assigned to carbon atoms from the COO moieties are at very different shift values. Comparison with [(*S*,*S*)-H_2(*i*-Pr)$_2$eddip]Cl_2 gave proof that the signal at 169.6 ppm belongs to the ester carbon atom and the signal at 181.1 ppm belongs to the carbon atom of the carboxyl group that participates in the coordination *via* its oxygen atom.

*Solid state structure of **2***

{PdCl[(*S*,*S*)-(*i*-Pr)eddip]} was found to crystallize in the monoclinic crystal system in the chiral space group $P2_1$. The molecular structure is shown in Fig. 3, and selected bond lengths and angles are listed in Table III.

The Pd atom was found in square–planar coordination geometry with one [(*S*,*S*)-(*i*-Pr)eddip]$^-$ ligand coordinated through one carboxylic oxygen and two

nitrogen atoms (κ^2*N*,*N*',κ*O* coordination mode). The remaining coordination site is occupied by the chloro ligand. The crystal structure represents the (*R*,*R*)–*N*,*N*' configured isomer.

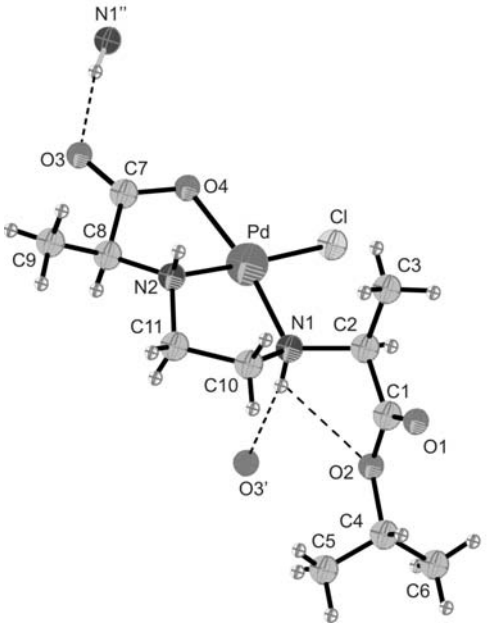

Fig. 3. Molecular structure of {PdCl[(*S*,*S*)-(*i*-Pr)eddip]} (**2**). The dashed lines represent H-bonds.

TABLE III. Selected experimentally found bond lengths (Å) and angles (°) in the molecular structure of **2** and the calculated values (2**c**) for the diastereoisomers of **2**

Bond	Compound				
	2	(*R*,*R*)-*anti*-**2c**	(*R*,*S*)-*anti*-**2c**	(*S*,*R*)-*anti*-**2c**	(*S*,*S*)-*anti*-**2c**
Pd–N2	1.995(5)	2.039	2.045	2.032	2.034
Pd–O4	2.019(5)	2.003	2.012	2.002	2.006
Pd–N1	2.047(6)	2.078	2.077	2.079	2.055
Pd–Cl	2.325(1)	2.344	2.340	2.350	2.353
C1–O1	1.190(1)	1.234	1.234	1.241	1.243
C1–O2	1.314(1)	1.374	1.376	1.353	1.351
C4–O2	1.441(1)	1.495	1.500	1.495	1.497
C7–O3	1.216(8)	1.242	1.242	1.242	1.243
C7–O4	1.316(8)	1.334	1.337	1.336	1.337
C10–N2	1.476(8)	1.494	1.502	1.494	1.504
C11–N1	1.508(8)	1.502	1.500	1.515	1.508
N2–Pd–N1	86.3(2)	86.5	85.5	87.2	86.5
N2–Pd–Cl	177.1(1)	177.2	178.3	176.8	175.2
O4–Pd–N1	167.7(2)	168.9	166.2	169.8	169.1
O4–Pd–Cl	95.2(1)	98.2	97.8	98.6	101.6
N1–Pd–Cl	96.6(1)	92.2	95.4	91.5	88.8
N2–C10–C11	108.2(6)	108.4	110.6	109.6	111.5

TABLE III. Continued

Bond	Compound				
	2	(*R*,*R*)-*anti*-**2c**	(*R*,*S*)-*anti*-**2c**	(*S*,*R*)-*anti*-**2c**	(*S*,*S*)-*anti*-**2c**
N1–C11–C10	108.9(5)	109.9	109.8	112.3	113.1
C3–C2–N1	112.0(6)	114.1	114.1	113.3	113.8
N2–C8–C9	113.0(5)	113.2	113.3	113.2	112.8
C11–N1–Pd	106.9(4)	106.1	102.6	106.2	103.3
C7–O4–Pd	113.7(4)	114.6	113.2	114.3	113.5

The Pd–N bond lengths (1.995(5)–2.047(6) Å) are shorter than those found in palladium complexes with edta tetra-alkyl ester ligands (2.098(4)–2.106(7) Å).[9,24–26] The Pd–N1 bond length is in the range for Pd(II) complexes with ethylenediamine ligands (2.03–2.09 Å).[14,27] The Pd–O bond length of 2.019(5) Å in **2** is consistent with the range of values (1.999(6)–2.105(3) Å) reported for five- and six-membered chelates containing Pd–O bonds.[28,29] The Pd–Cl bond length (2.325(1) Å) is in the same range as those in $[PdCl_2(R_4edta)]$ and $[PdCl_2(H_4edta)]\cdot xH_2O$ (R = Me or Et; x = 5 or 6; 2.287(2)–2.298(2) and 2.30(1) Å, respectively).[9,25,26]

In the structure of **2**, intramolecular hydrogen bonds N1–H···O2 (N1···O2 = = 2.838(9) Å, N1–H···O2 = 102°) and intermolecular N1–H···O3 hydrogen bonds (N1···O3 = 2.997(8) Å, N1–H···O3 = 170°, Fig. 3), which fulfill the geometric parameters given in the literature,[30–33] were found. As the H atoms could not be located in the electron density map, the discussion of these hydrogen bonds is restricted to the heavy atoms. It may be possible that the hydrogen on the N1 atom participates in a bifurcated hydrogen bond, giving rise to the formation of one-dimensional chains in the crystals of **2**.

Quantum chemical calculations

To investigate the selectivity of the formation of only one of the four possible isomers of **2** and to presume which two isomers were formed in the case of **1**, quantum chemical calculations were employed. DFT calculations were conducted for the isomers arising from the coordination of [(*S*,*S*)-(*i*-Pr)$_2$eddip] and its partly hydrolyzed derivative [(*S*,*S*)-(*i*-Pr)eddip]$^-$ to palladium(II). The optimized structures of the {$PdCl_2$[(*S*,*S*)-(*i*-Pr)$_2$eddip]} (**1c**) and {PdCl[(*S*,*S*)-(*i*-Pr)eddip]} (**2c**) complexes are represented in Figs. 4 and 5, respectively. The structures were fully optimized without any symmetry constraints and were found to represent equilibria structures.

In the case of complex **1c**, the results showed that (*R*,*R*)-*anti*-**1c** and (*R*,*S*)-*syn*-**1c** diastereoisomers appear to be structurally and synthetically feasible (Fig. 4). Namely, the energy difference between the (*R*,*R*)-*anti*-**1c** and (*R*,*S*)-*syn*-**1c** isomers amounts to 0.7 kcal/mol (2.9 kJ/mol), which is within the error of DFT calculations, so that these isomers are of the same energy. The third diastereoisomer (*S*,*S*)-

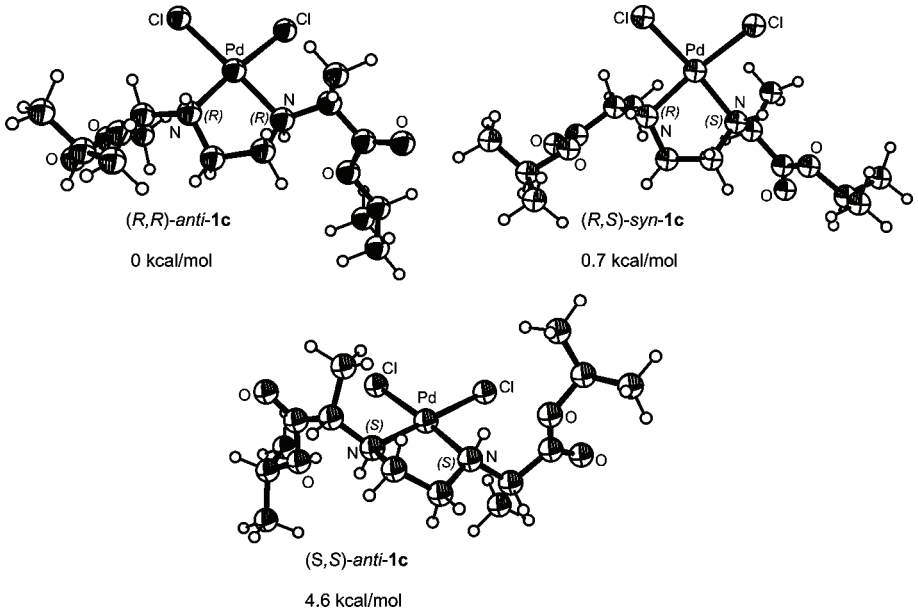

Fig. 4. Calculated structures of {$PdCl_2${(*S*,*S*)-(*i*-Pr)$_2$eddip]} (**1c**) (the energies are relative to the most stable isomer (*R*,*R*)-*anti*-**1c**).

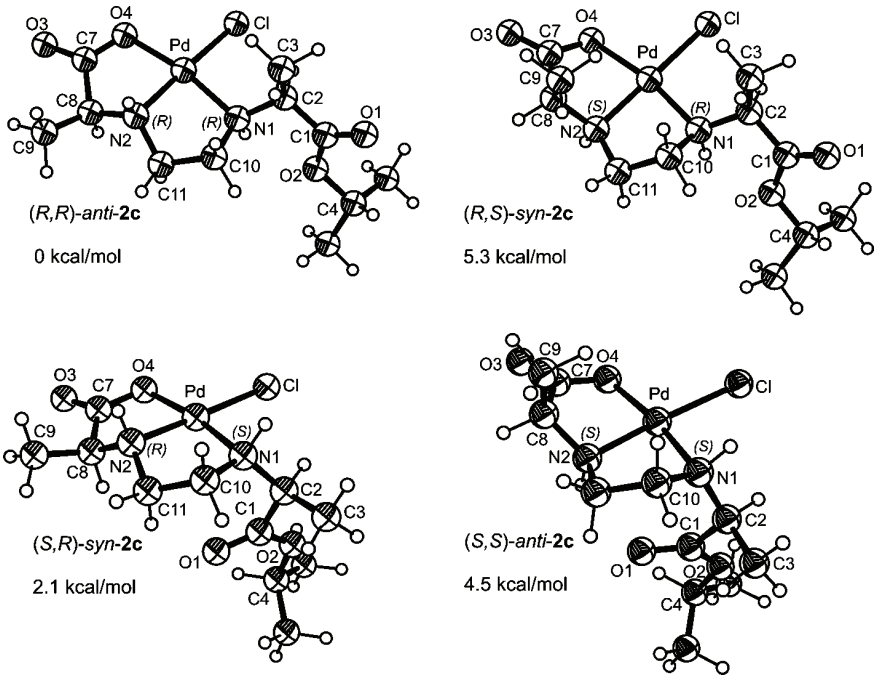

Fig. 5. Calculated structures of {PdCl[(*S*,*S*)-(*i*-Pr)eddip]} (**2c**) (the energies are relative to the most stable isomer (*R*,*R*)-*anti*-**2c**).

-*anti*-**1c** is 4.6 kcal/mol (19.2 kJ/mol) higher in energy than (*R*,*R*)-*anti*-**1c** and the formation of this isomer is not to be expected. This indicates that the obtained two isomers of **1**, proved by NMR spectroscopy (within the sensitivity limits of NMR spectroscopy), could be assigned as (*R*,*R*)-*anti*-**1c** and (*R*,*S*)-*syn*-**1c**. This is consistent with a recently reported study on DFT calculations of platinum(II) complexes with the Et_2edda ligand.[1]

Furthermore, from the quantum chemical calculations, it is apparent that three of the four isomers of **2c** have more strain and that they are higher in energy than (*R*,*R*)-*anti*-**2c** by 2.1–5.3 kcal/mol (8.8–22.2 kJ/mol) (Fig. 5). Thus, this indicates that the (*R*,*R*)-*anti*-**2c** isomer is thermodynamically more stable than the other isomers and that the energy differences correlate well with the results from X-ray crystallography and NMR spectroscopic investigations. As can be seen from a comparison of the calculated and experimental bond lengths and angles shown in Table III, the calculated values for (*R*,*R*)-*anti*-**2c** are in good agreement with the results obtained from X-ray structural analysis.

CONCLUSIONS

The present investigation shows that the [(*S*,*S*)-H_2(*i*-Pr)$_2$eddip]Cl_2 ligand precursor reacts with $K_2[PdCl_4]$ yielding the corresponding {$PdCl_2$[(*S*,*S*)-(*i*-Pr)$_2$eddip]} complex (**1**) and the palladium(II) complex with a partly hydrolyzed ester {PdCl[(*S*,*S*)-(*i*-Pr)eddip]} (**2**). In case of **1**, two from the three possible isomers were detected (^{1}H- and ^{13}C-NMR spectroscopy). In contrast, the reaction yielding **2** is diastereoselective, only one from the four possible diastereoisomers was formed, (*R*,*R*)-*anti*-**2** (^{1}H- and ^{13}C-NMR spectroscopy, X-ray structural analysis). Quantum chemical calculations for **1** proposed the formation of the (*R*,*R*)-*anti*-**1** and (*S*,*R*)-*anti*-**1** diastereoisomers and confirmed the formation of the (*R*,*R*)-*anti*-**2** diastereoisomer for **2**.

Acknowledgement. G. N. Kaluđerović gratefully acknowledges the financial support from the Alexander von Humboldt Foundation. The authors are grateful to the Ministry of Science and Technological Deveplopment of the Republic of Serbia for financial support (Grants No. 142010 and 142008). We thank Sebastian Schwieger (Universität Halle) for helpful discussions.

ИЗВОД

КОМПЛЕКСИ ПАЛАДИЈУМА(II) СА ЛИГАНДИМА R_2EDDA ТИПА. ДЕО I. РЕАКЦИЈА ДИИЗОПРОПИЛ-(*S*,*S*)-2,2'-(1,2-ЕТАНДИИЛДИИМИНО)ДИПРОПАНОАТА СА $K_2[PdCl_4]$

БОЈАНА Б. КРАЈЧИНОВИЋ[1], ГОРАН Н. КАЛУЂЕРОВИЋ[1,2], DIRK STEINBORN[2], HARRY SCHMIDT[2], CHRISTOPH WAGNER[2], KURT MERZWEILER[2], СРЕЋКО Р. ТРИФУНОВИЋ[3] и ТИБОР Ј. САБО[4]

[1]*Институт за хемију, технологију и металургију – Центар за хемију,Универзитет у Београду, Студентски трг 14, 11000 Београд,* [2]*Institut für Chemie, Martin-Luther-Universität Halle-Wittenberg, Kurt-Mothes-Straße 2, D-06120 Halle, Germany,* [3]*Департман за хемију, ПМФ, Универзитет у Крагујевцу, 34000 Крагујевац и* [4]*Хемијски факултет, Универзитет у Београду, п.пр. 158, 11001 Београд*

У реакцији $K_2[PdCl_4]$ са (*S*,*S*)-(*i*-Pr)$_2$eddip диестром [диизопропил-(*S*,*S*)-2,2'-(1,2-етандиилдиимино)дипропаноат] добијају се {$PdCl_2$[(*S*,*S*)-(*i*-Pr)$_2$eddip-κ^2*N*,*N*']} (**1**) и {PdCl[(*S*,*S*)-(*i*-

-Pr)eddip-κ^2*N*,*N*',κ*O*]} (**2**) са једном хидролизованом естарском групом. Једињења су окарактерисана спектроскопским методама и доказано је да је ова реакција дијастереоселективна (^{1}H- и ^{13}C-NMR) у случају **2** (један дијастереоизомер од могућа четири). Структура једињења **2** је одређена рендгенском структурном анализом и нађено је да је добијени производ (*R*,*R*)–*N*,*N*' изомер. Супротно томе, у случају једињења **1** добијени производ је смеша два од три могућа дијастереоизомера. DFT прорачуни потврђују формирање два дијастереоизомера једињења **1** и једног дијастереоизомера једињења **2**.

(Примљено 24. јуна, ревидирано 6. октобра 2008)

REFERENCES

1. G. N. Kaluđerović, H. Schmidt, S. Schwieger, Ch. Wagner, R. Paschke, A. Dietrich, T. Müller, D. Steinborn, *Inorg. Chim. Acta* **361** (2008) 1395
2. T. J. Sabo, G. N. Kaluđerović, S. R. Grgurić-Šipka F. W. Heinemann, S. R. Trifunović, *Inorg. Chem. Commun.* **7** (2004) 241
3. G. N. Kaluđerović, V. M. Đinović, Z. D. Juranić, T. P. Stanojković, T. J. Sabo, *J. Inorg. Biochem.* **99** (2005) 488
4. B. B. Krajčinović, G. N. Kaluđerović, D. Steinborn, H. Schmidt, Ch. Wagner, Ž. Žižak, Z. D. Juranić, S. R. Trifunović, T. J. Sabo, *J. Inorg. Biochem.* **102** (2008) 892
5. G. N. Kaluđerović, D. Miljković, M. Momčilović, V. M. Đinović, M. Mostarica-Stojković, T. J. Sabo, V. Trajković, *Int. J. Cancer* **116** (2005) 479
6. S. Mijatović, D. Maksimović-Ivanić, J. Radovica, D. Miljković, G. N. Kaluđerović, T. J. Sabo, V. Trajković, *Cell. Mol. Life Sci.* **62** (2005) 1275
7. J. Ruiz, J. Lorenzo, L. Sanglas, N. Cutillas, C. Vicente, M. D. Villa, F. X. Avilés, G. López, V. Moreno, J. Pérez, D. Bautista, *Inorg. Chem.* **45** (2006) 6347
8. E. R. Jamieson, S. J. Lippard, *Chem. Rev.* **99** (1999) 2467
9. G. N. Kaluđerović, H. Schmidt, Ch. Wagner, K. Merzweiler, D. Steinborn, *Collect. Czech. Chem. Commun.* **72** (2007) 560
10. G. N. Kaluđerović, F. W. Heinemann, N. Ž. Knežević, S. R. Trifunović, T. J. Sabo, *J. Chem. Crystallogr.* **34** (2004) 185
11. I. Brudzińska, Y. Mikata, M. Obata, Ch. Ohtsuki, Sh. Yano, *Bioorg. Med. Chem. Lett.* **14** (2004) 2533
12. B. T. Khan, J. Bhatt, K. Najmuddin, S. Shamsuddin, K. Annapoorna, *J. Inorg. Biochem.* **44** (1991) 55
13. C. Navarro-Ranninger, J. M. Pérez, F. Zamora, V. M. González, J. R. Masaguer, C. Alonso, *J. Inorg. Biochem.* **52** (1993) 37
14. S. Baggio, L. M. Amzel, L. N. Becka, *Acta Crystallogr. B* **26** (1970) 1698
15. G. N. Kaluđerović, T. J. Sabo, *Polyhedron* **21** (2002) 2277
16. D. B. Haydock, T. P. C. Mulholland, *J. Chem. Soc. C* (1971) 2389
17. G. M. Sheldrick, *SHELXS-96, Programs for Crystal Structure Solution*, University of Göttingen, Göttingen, Germany, 1997
18. G. M. Sheldrick, *SHELXS-97, Programs for the Refinement of Crystal Structures*, University of Göttingen, Göttingen, Germany, 1997
19. K. Branderburg, *Diamond, Release 2*, Crystal Impact GbR, Bonn, 1997
20. M. J. Frisch, G. W. Trucks, H. B. Schlegel, G. E. Scuseria, M. A. Robb, J. R. Cheeseman, J. A. Montgomery, Jr. T. Vreven, K. N. Kudin, J. C. Burant, J. M. Millam, S. S. Iyengar, J. Tomasi, V. Barone, B. Mennucci, M. Cossi, G. Scalmani, N. Rega, G. A. Petersson, H.

Nakatsuji, M. Hada, M. Ehara, K. Toyota, R. Fukuda, J. Hasegawa, M. Ishida, T. Nakajima, Y. Honda, O. Kitao, H. Nakai, M. Klene, X. Li, J. E. Knox, H. P. Hratchian, J. B. Cross, V. Bakken, C. Adamo, J. Jaramillo, R. Gomperts, R. E. Stratmann, O. Yazyev, A. J. Austin, R. Cammi, C. Pomelli, J. W. Ochterski, P. Y. Ayala, K. Morokuma, G. A. Voth, P. Salvador, J. J. Dannenberg, V. G. Zakrzewski, S. Dapprich, A. D. Daniels, M. C. Strain, O. Farkas, D. K. Malick, A. D. Rabuck, K. Raghavachari, J. B. Foresman, J. V. Ortiz, Q. Cui, A. G. Baboul, S. Clifford, J. Cioslowski, B. B. Stefanov, G. Liu, A. Liashenko, P. Piskorz, I. Komaromi, R. L. Martin, D. J. Fox, T. Keith, M. A. Al-Laham, C. Y. Peng, A. Nanayakkara, M. Challacombe, P. M. W. Gill, B. Johnson, W. Chen, M. W. Wong, C. Gonzalez, *GAUSSIAN 03, Revision C.02*, Gaussian, J.A. Pople, Inc., Wallingford, CT, 2004

21. C. Adamo, V. Barone, *Chem. Phys. Lett.* **274** (1997) 242
22. T. H. Dunning Jr., P. J. Hay, *Modern Theoretical Chemistry*, 3rd Ed., Vol. 3, Plenum, New York, 1976, pp. 1–28
23. D. Andrae, U. Häußermann, M. Dolg, H. Stoll, H. Preuß, *Theor. Chem. Acc.* **77** (1990) 123
24. M. Kaplun, M. Sandström, D. Boström, A. Shchukarev, P. Peresson, *Inorg. Chim. Acta* **358** (2005) 527
25. D. J. Robinson, C. H. L. Kennard, *J. Chem. Soc. A* (1970) 1008
26. X.-M. Luo, X.-H. Chen, S. Shanmuga Sundara Raj, H.-K. Fun, L.-G. Zhu, *Acta Crystallogr. C* **55** (1999) 1220
27. J. R. Wiesner, E. C. Lingafelter, *Inorg. Chem.* **5** (1966) 1770
28. A. K. Singh, J. Sooriyakumar, S. Husebye, K. W. Tornroos, *J. Organomet. Chem.* **612** (2000) 46
29. D. R. Billodeaux, F. R. Fronczek, A. Yoneda, G. R. Newkome, *Acta Crystallogr. C* **C54** (1998) 1439
30. C. S. A. Fraser, H. A. Jenkins, M. C. Jennings, R. J. Puddephatt, *Organometallics* **19** (2000) 1635
31. C. J. Adams, A. Angeloni, A. G. Orpen, T. J. Podesta, B. Shore, *Cryst. Growth Des.* **6** (2006) 411
32. M. Yamada, H. Hagiwara, H. Torigoe, N. Matsumoto, M. Kojima, F. Dahan, J.-P. Tuchagues, N. Re, S. Iijima, *Chem. Eur. J.* **12** (2006) 4536
33. J. C. Mareque Rivas, E. Salvagni, R. T. M. de Rosales, S. Parsons, *Dalton Trans.* (2003) 3339.

Journal of the Serbian Chemical Society
JSCS@tmf.bg.ac.rs • www.shd.org.rs/JSCS

J. Serb. Chem. Soc. 74 (4) 401–406 (2009)
JSCS–3841

UDC 546.763'723–386:66.095.62.094.25
Original scientific paper

Synthesis and characterization of novel oxo-bridged, trinuclear mixed-metal complexes of Cr(III) and Fe(III)

MOHAMMAD YAZDANBAKHSH, IMAN KHOSRAVI* and HAMAN TAVAKKOLI

Department of Chemistry, Faculty of Science, Ferdowsi University of Mashhad, Mashhad, Iran

(Received 3 October 2008)

Abstract: Two new heterotrinuclear *p*-chlorobenzoates, $[Fe_2CrO(C_7H_4O_2Cl)_6(py)_3]NO_3$ (**1**) and $[Cr_2FeO(C_7H_4O_2Cl)_6(py)_3]NO_3$ (**2**) were prepared as nitrate salts and characterized by elemental analyses (CHN), spectroscopic (infrared, electronic) studies and atomic absorption spectroscopy. These complexes are a new type of oxo-bridged mixed-metal complex in which the carboxylate ligand is *p*-chlorobenzoic acid. Bridging coordination modes for the carboxylates were indicated by the presence of ν_{asym} ($M_2M'O$) vibrations in the infrared spectra.

Keywords: carboxylates; oxo-bridged complexes; *p*-chlorobenzoic acid; IR spectra.

INTRODUCTION

Transition-metal carboxylate chemistry has played a key role in the conceptual development of modern inorganic chemistry. Extensive structural and physicochemical studies of these compounds were crucial for increasing the understanding of the bonding and electronic interactions between proximate metal centers, topics with implications ranging from industrial catalysis and industrial magnetism to the structure and function of mixed-metal compounds.[1–3] The current interest in trinuclear, oxo-centered metal carboxylate assemblies of the general composition $[M_3O(RCOO)_6(L)_3]^z$ (where M is a trivalent 3d metal, L is a monodentate ligand, such as methanol, pyridine (py), *etc*., and *z* is +1 for $M(III)_2M'(III)$ and 0 for $M(III)_2M'(II)$) is due to these complexes having served as important models to test theories of electronic coupling between metal ions[4,5] (Fig. 1).

Heterotrinuclear complexes have been known for more than half a century, $[Fe(III)_2M(II)O(MeCOO)_6(H_2O)_3]$ complexes (M = Co, Ni) were originally prepared in 1928 by Weinland and Holtmeier[6] and the structures proved in 1980 by Yokubov.[7]

These heterotrinuclear complexes exhibited antiferromagnetic exchange interactions and the central O atom provided the main super exchange pathway,[8] in which the p-orbitals of the oxygen atom in the M_3O plane were especially effect-

* Corresponding author. E-mail: khosraviiman@yahoo.com
doi: 10.2298/JSC0904401Y

tive. It is apparent that the number of d-electrons in $M(III)_2M'(III)O$ compounds is one less than that in $M(III)_2M'(II)O$ compounds, hence the chemical properties of these complexes may be quite different.[9]

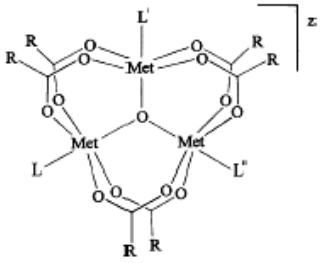

Fig. 1. Structure of the cluster unit $[M_3O(RCOO)_6(L)_3]^z$.

This paper describes the synthesis of new trinuclear oxo-centered complexes containing a *p*-chlorobenzoate ligand, with the general formula:

$$[M_2M'O(C_7H_4O_2Cl)_6(py)_3]NO_3,$$

where M, M' = Fe, Cr.

EXPERIMENTAL

Materials and analytical methods

Organic solvents (Qualigens) were dried and distilled before use by standard methods. All reagents used in this study were of analytical grade and purchased from the Merck Company.

C, H and N analyses were performed on a Thermo Finnigan Flash model EA1112 elemental analyzer. Atomic absorption analyses were performed on a Shimadzu model AA-670 atomic absorption spectrometer. IR spectra of KBr discs (600–4000 cm^{-1}) were recorded on a Buck 500 spectrometer.

*Preparation of $[Fe_2CrO(C_7H_4O_2Cl)_6(py)_3]NO_3$ (**1**)*

$C_7H_5O_2Cl$ (1.6 g, 10 mmol) was dissolved in pyridine (3.0 ml)–acetone (20 ml) mixture and stirred, then a mixture of $Fe(NO_3)_3{\cdot}9H_2O$ (0.80 g, 2.0 mmol) and $Cr(NO_3)_3{\cdot}9H_2O$ (0.40 g, 1.0 mmol) was added and refluxed for 2 h. The resulting brown solution was allowed to cool and stored for 3 days at 20 °C. The brown crystals were filtered off, washed copiously with Et_2O and dried *in vacuo* (yield: 70 %); m.p.: 267 °C. Anal. Calcd. for $C_{57}H_{39}Cl_6CrFe_2N_4O_{16}$ (1411.5 g/mol): C, 48.45; H, 2.76; N, 3.96; Fe, 6.2; Cr, 2.9. Found: C, 47.65; H, 2.66; N, 3.72; Fe, 6.2; Cr 2.8 %. IR (selected data, KBr, cm^{-1}): 310 (*w*), 435 (*m*), 572 (*m*), 740 (*s*), 1415 (*s*), 1607 (*s*), 3000 (*m*).

*Preparation of $[Cr_2FeO(C_7H_4O_2Cl)_6(py)_3]NO_3$ (**2**)*

$Cr(NO_3)_3{\cdot}9H_2O$ (1.5 g, 4.0 mmol) and $Fe(NO_3)_3{\cdot}9H_2O$ (0.40 g, 1.0 mmol) and $C_7H_5O_2Cl$ (1.6 g, 10 mmol) were dissolved in a solvent mixture comprising acetone (20 ml) and pyridine (3.0 ml) and refluxed for 3 h to give a red-purple solution. After cooling, purple crystals were grown by slow evaporation at room temperature (20 °C) for 3 days. The crystals were filtered off, washed copiously with Et_2O and dried *in vacuo* (yield: 75 %); m.p.: 275 °C. Anal. Calcd. for $C_{57}H_{39}Cl_6Cr_2FeN_4O_{16}$ (1407.6 g/mol): C, 48.59; H, 2.77 N, 3.97; Cr, 7.1, Fe, 3.8. Found: C 48.52; H 2.66; N 3.89; Cr 7.0; Fe 3.4 %; IR (selected data, KBr, cm^{-1}): 305 (*w*), 441 (*m*), 565 (*m*), 710 (*s*), 1413 (*s*), 1611 (*s*), 2870 (*m*).

RESULTS AND DISCUSSION

Mixed-metal oxo-centered complexes were synthesized by the reaction of Fe(III) and Cr(III) nitrates with *p*-chlorobenzoic acid and pyridine in acetone under reflux (Eqs. (1) and (2)):

$$2Fe(NO_3)_3{\cdot}9H_2O + Cr(NO_3)_3{\cdot}9H_2O + 6C_7H_5O_2Cl \xrightarrow{C_3H_6O,\ py} \xrightarrow{C_3H_6O,\ py} [Fe_2Cr(O)(C_7H_4O_2Cl)_6(py)_3]NO_3 + 26H_2O + 8HNO_3 \quad (1)$$

$$2Cr(NO_3)_3{\cdot}9H_2O + Fe(NO_3)_3{\cdot}9H_2O + 6C_7H_5O_2Cl \xrightarrow{C_3H_6O,\ py} \xrightarrow{C_3H_6O,\ py} [Cr_2Fe(O)(C_7H_4O_2Cl)_6(py)_3]NO_3 + 26H_2O + 8HNO_3 \quad (2)$$

After cooling the products to room temperature, the crystals were grown by slow evaporation for 3 days. The use of acetone as the solvent was a very suitable choice for these reactions because this solvent cannot covalently link to the metal ions as a terminal ligand.

The complexes had sharp melting points and both decomposed at around 350–400 °C.

Infrared spectra

In the infrared spectra of both complexes, one band was observed in the region 2800–3000 cm^{-1}, which indicates the presence of C–H aromatic stretching vibration of the carboxylic acid. The IR data for compounds **1** and **2** are given in Table I. A band at ≈ 710 cm^{-1} (C–Cl stretching) was also found in the spectra of the complexes. Two strong bands were observed at ≈ 1610 cm^{-1} and ≈ 1415 cm^{-1}, corresponding to ν_{asym}(OCO) and ν_{sym}(OCO) stretching vibrations, respectively. The coordination mode of the carboxylate ligand can be assigned on the basis of the difference ($\Delta\nu \approx 195$ cm^{-1}) of these two frequencies, which indicates the presence of a bridging mode of coordination of the ligand in the complexes[10] (Fig. 2).

TABLE I. Selected IR bands (cm^{-1}) for the complexes

Complex	ν_{asym}(COO)	ν_{sym}(COO)	$\nu(M_3O)$	ν(C–H)	ν(C–Cl)
1	1415	1607	435–572	3000	740
2	1413	1611	441–565	2870	710

For a new series of trinuclear mixed-metal complexes, Cannon and co-workers[11] assigned the IR spectra and identified the vibrational modes of the central M_3O core. They found that a reduction in the site geometry from D_3h to C_2v lifted the degeneracy of the asymmetric M_3O stretching vibtrations and two bands were seen. IR spectra in the range 400–800 cm^{-1} were used for the identification of the metal–oxygen bands of the M_3O groups.[12] The band observed for the asymmetric vibration associated with the $M_2M'O$ unit was split into two

components, A_1 and B_2.[13] These spectra showed characteristic bands for the valence oscillations $\nu_{asym}(M_2M'O)$ around 570 (A_1) and 450 cm^{-1} (B_2).

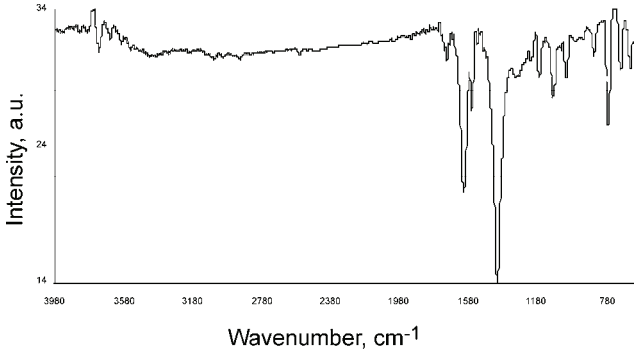

Fig. 2. IR spectrum of $[Cr_2FeO(C_7H_4O_2Cl)_6(py)_3]NO_3$.

Electronic spectroscopy

Oxo-centered complexes involve electronic transitions that are similar to other inorganic compounds. Thus, UV–Vis spectroscopy is one of the useful methods for characterizing oxo-centered complexes.

Electronic spectra of the complexes were recorded in the range 15000––50000 cm^{-1} in dichloromethane solution. The spectra exhibited two spin-allowed bands in the regions 17250 and 22200 cm^{-1}, which could be assigned to the transition from $^4A_2g(F)$ to $^4T_2g(F)$ (ν_1) and $^4T_1g(F)$ (ν_2), respectively. These bands should be attributed to the existence of Cr(III) (d^3) ion in these complexes. The room-temperature electronic spectrum of complex **2** is shown in Fig. 3.

The spectra may be interpreted on the basis of an octahedral environment for chromium(III) in these complexes. The position of the third spin-allowed transition ν_3 ($^4A_2g(F)$ to $^4T_2g(P)$) could be calculated together with the ligand field splitting energy (10 *Dq*), the interelectronic repulsion parameter (*B*) and the covalency factor (β) using the equations of Underhill and Billing:[14]

$$340Dq^2 - 18(\nu_2 + \nu_3)Dq + \nu_2\nu_3 = 0 \quad (1)$$

$$B = (\nu_3 + \nu_2 - 3\nu_1)/15 \quad (2)$$

$$\beta = B_{complex}/B_{free\ ion} \quad (3)$$

The values of the interelectronic repulsion parameter (*B*) were found to be below the free ion value for the chromium(III) ion (933 cm^{-1}),[15] which indicates a considerable covalent nature of the metal–ligand bond in both the complexes, with the covalency factor (β) varying in the range 0–7.0. The UV spectra of these complexes exhibit a strong band in the region 41,000 cm^{-1} which is related to ($\pi \rightarrow \pi^*$) transitions of pyridine (py) ligand. The bands are shifted to higher energy when L = py. The electronic spectroscopy data are given in Table II, which were assigned and characterized on the basis of literature data.[16]

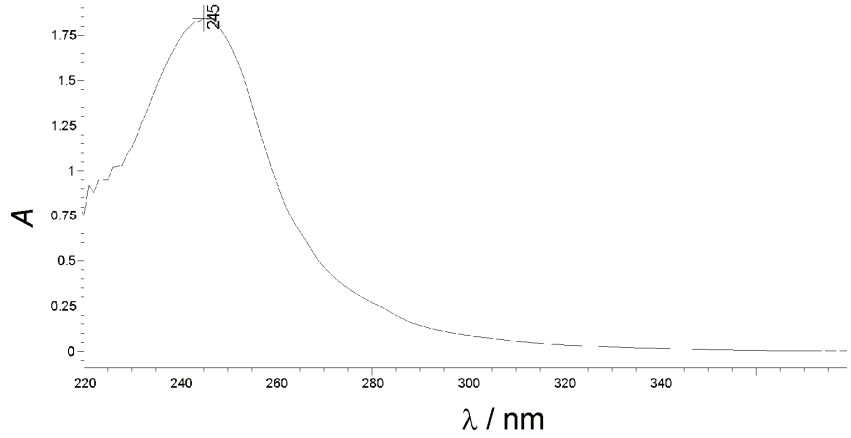

(a)

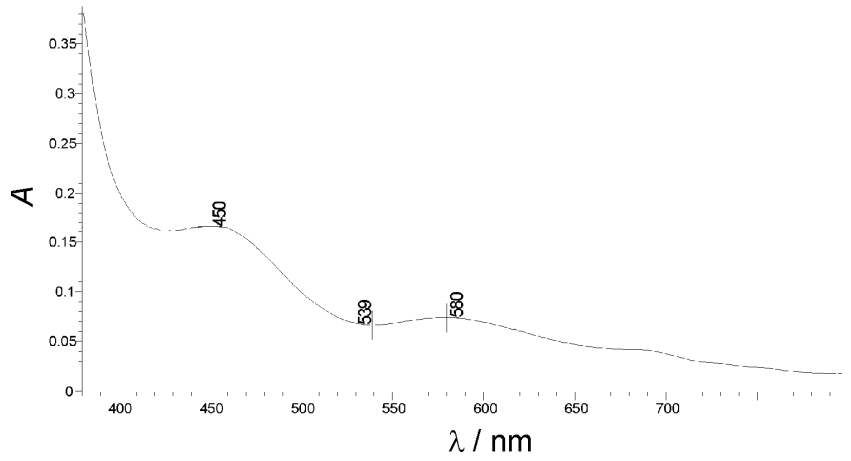

(b)

Fig. 3. UV (a) and Vis (b) spectra of $[Cr_2FeO(C_7H_4O_2Cl)_6(py)_3]NO_3$.

Table II. Electronic absorption spectral data of complexes **1** and **2** in dichloromethane solution

Compound	Transitions ($\pi \rightarrow \pi^*$), nm	Transitions ($d \rightarrow d$), nm
1	247	459–598
2	245	450–580

CONCLUSIONS

In this study, two new complexes of the formula:

$[Fe_2CrO(C_7H_4O_2Cl)_6(py)_3]NO_3$ (**1**) and

$[Cr_2FeO\ (C_7H_4O_2Cl)_6(py)_3]NO_3$ (**2**)

were prepared by the direct reaction of the metal ions with the carboxylic acid. These compounds were characterized by elemental analyses (CHN), infrared and electronic spectroscopy and atomic absorption spectroscopy.

The IR spectra of these compounds showed two strong bands at ≈1610 and ≈ 1415 cm^{-1}, corresponding to $\nu_{asym}(OCO)$ and $\nu_{sym}(OCO)$ stretching vibrations. The difference in these values indicates a bridging mode of coordination of the carboxylic ligand in these complexes.

Acknowledgment. The authors are very grateful for the financial support from the Ferdowsi University of Mashhad, Iran.

ИЗВОД

СИНТЕЗА И КАРАКТЕРИЗАЦИЈА НОВИХ ТРИНУКЛЕАРНИХ МЕШОВИТО МЕТАЛНИХ КОМПЛЕКСА Cr(III) И Fe(III) СА ОКСО КООРДИНАЦИЈОМ

MOHAMMAD YAZDANBAKHSH, IMAN KHOSRAVI и HAMAN TAVAKKOLI

Department of Chemistry, Faculty of Science, Ferdowsi University of Mashhad, Mashhad, Iran

Добијена су два нова хетеротринулкеарна *p*-хлоробензоата: $[Fe_2CrO(C_7H_4O_2Cl)_6(py)_3]NO_3$ (**1**) и $[Cr_2FeO(C_7H_4O_2Cl)_6(py)_3]NO_3$ (**2**) и окарактерисана елементалном (CHN) и спектралном анализом (инфрацрвеном и електронском) и атомском апсорпционом спектроскопијом. Ово је нови тип мешовито металних комплекса са оксо координацијом у којима је карбоксилатни лиганд *p*-хлоробензоева киселина. Ови типови координације карбоксилата су доказани присуством $\nu_{asym}(M_2M'O)$ вибрацијама у инфрацрвеним спектрима.

(Примљено 3. октобра 2008)

REFERENCES

1. R. F. Weinland, *Chem. Ztg.* **32** (1908) 812
2. I. Bertini, H. B. Gray, S. J. Lippard, J. S. Valentine, *Bioinorganic Chemistry*, Viva Books Pvt. Ltd., New Delhi, 1998
3. F. A. Cotton, G. Wilkinson, C. A. Murillo, M. Bochmann, *Advanced Inorganic Chemistry*, 6th Ed., Wiley, New York, 1999
4. R. D. Cannon, R. P. White, *Prog. Inorg. Chem.* **36** (1988) 195
5. S. P Pali, D. E. Richardson, M. L. Hansen, B. B. Iversen, F. K. Larsen, L. Singerean, G. A. Timco, N. V. Gerbeleu, K. R. Jennings, J. R. Eyler, *Inorg. Chim. Acta* **319** (2001) 23
6. R. Weinland, H. Holtmeier *Z. Anorg. Allg. Chem.* **173** (1928) 49
7. K. M. Yakubov, V. V. Zelentsov, V. R. Fisher, *Dokl. Akad. Nauk SSSR* **250** (1980) 402 (in Russian)
8. T. Sale, M. V. Sargen, *J. Chem. Soc. Chem. Commun*. (1978) 253
9. L. Helmholz, W. R. Foster, *J. Am. Chem. Soc*. **72** (1950) 4971
10. M. Yazdanbakhsh, M. H. Alizadeh, H. Z. Khorramdel, W. Frank, *Z. Anorg. Allg. Chem*. **633** (2007) 1193
11. L. Meesuk, U. A. Jayasooriya, R. D. Cannon, *Spectrochim. Acta A* **43** (1987) 687
12. A. K. Boudalis, N. Lalioti, G. A. Spyroulias, C. P. Raptopoulou, A. Terzis, *Inorg. Chem.* **41** (2002) 6474
13. C. Turta, S. Shova, D. Prodius, V. Mereacre, M. Gdaniec, Y. Simonov, J. Lipkowski, *Inorg. Chim. Acta* **657** (2004) 4396.75
14. B. P. Baranwal, T. Fatma, *J. Mol. Struct.* **750** (2005) 72
15. B. N. Figgis, M. A. Hitchman, *Ligand Field Theory and its Applications*, Wiley, New York, 2000, p. 207
16. T. J. Mizoguchi, R. M. Davydov, S. J. Lippard, *Inorg. Chem.* **38** (1999) 4098.

Journal of the Serbian Chemical Society
JSCS@tmf.bg.ac.rs • www.shd.org.rs/JSCS
J. Serb. Chem. Soc. 74 (4) 407–415 (2009) UDC 547.466.64+544.72.023.221+66.097.8:620.193
JSCS–3842 *Original scientific paper*

Electrochemical and molecular simulation studies on the corrosion inhibition of L-glutamine monolayers on an iron surface

ZHE ZHANG[1], SHENHAO CHEN[1,2]*, YUANYUAN FENG[3], YUNQIAO DING[1], JUANJUAN ZHOU[1] and HENGLEI JIA[1]

[1]*Department of Chemistry, Shandong University, Jinan 250100,* [2]*State Key Laboratory for Corrosion and Protection, Shenyang 110016 and* [3]*Department of Chemistry Qufu Normal University, Qufu 273165, P.R. China*

(Received 19 September, revised 10 November 2008)

Abstract: L-Glutamine was used to form monolayers for the inhibition of the corrosion of iron in 0.50 mol dm^{-3} H_2SO_4. The protection ability of the films was examined by electrochemical impedance spectroscopy. The mechanism of adsorption is discussed using quantum chemical calculations and molecular simulations. Scanning electron microscopy was applied to confirm the formation of L-glutamine monolayers and the inhibitive effect. The results indicate that the molecules of L-glutamine are able to form films on the surface of iron and longer immersion time of the iron electrode in the solution results in a stronger inhibition ability of the films. The films are formed spontaneously by the adsorption of L-glutamine with a specific affinity of its head-group to the iron surface, hence, the densely and ordered monolayers can be considered as self-assembled.

Keywords: L-glutamine; iron; corrosion; self-assembled monolayer; EIS.

INTRODUCTION

Self-assembled monolayers (SAMs) have been intensively studied in the past two decades because of their applications in corrosion prevention, metal ion sensors and biosensors.[1–4] SAMs are able to adsorb spontaneously on the metal surface and form compact and stable films which protect the metal from corrosion.[5] Many attempts have been made to enhance the resistance of iron and Cu against corrosion in a corrosive environment.[6–10] Iron is a widely used metal with extensive industrial application because of its interesting properties, such as electrical conductivity, malleability, ductility, *etc*. Hence, work aimed at investigating its corrosion mechanism is very important in order to prevent it from corrosion.

* Corresponding author. E-mail: shchen@sdu.edu.cn
doi: 10.2298/JSC0904407Z

Felhosi *et al.*[11] studied the kinetics of self-assembled monolayers formation on iron. Much work has been performed on the use alkanethiols and alkanamine SAMs on iron and stainless steel surfaces for corrosion protection.[12–13] However, a large number of the effective inhibitors are toxic, hence there has recently been a growing trend to study environment friendly inhibitors. L-Glutamine is an amino acid, just like a protein. It is the most abundant free amino acid in muscle tissue and it plays a principal role in protein metabolism and anti-catabolism. It is a kind of innocuous compound; however, few related literature on the adsorption of the amino-group in amides monolayers on iron surface have been reported.

In this work, L-glutamine monolayers were prepared on an iron surface. The structural formula of L-glutamine is shown in Fig. 1. Electrochemical impedance spectroscopy was performed to study the inhibition ability of the films in 0.50 mol dm^{-3} H_2SO_4. Scanning electron microscopy was used to examine the inhibitive effect of the films on the iron surface. Quantum chemical calculations and molecular simulations were used to discuss the adsorption mechanism and structure of the molecules on the iron surface.

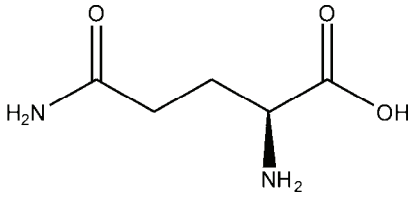

Fig. 1. Molecular structure of the L-glutamine.

EXPERIMENTAL

Electrochemical measurements

The reagents in this experiment were all analytical grade chemicals. L-Glutamine was dissolved in anhydrous ethanol to form a solution with the concentration of 1.0×10^{-4} mol dm^{-3}. The electrolyte solution was 0.50 mol dm^{-3} H_2SO_4, which was prepared with ultra pure water.

The electrochemical measurements were performed using a conventional three-electrode cell. The working electrode was made of an iron rod (Aldrich, 99.9 %, 2.0 mm diameter), which was embedded in epoxy resin, leaving only its cross-section exposed. The reference electrode was a saturated calomel electrode (SCE) and the counter electrodes were two platinum foils (1 cm×1.8 cm). Before each experiment, the exposed surface was polished with 1600# and 2000# emery paper until its surface became smooth and mirror-like bright, then it was cleaned with ultra pure water and anhydrous ethanol as quickly as possible and dried in a stream of pure nitrogen gas. Subsequently, the iron electrode was immersed in L-glutamine solution to form monolayers. The assembly time ranged from 0.50 to 38 h. The iron electrode was immersed in 0.50 mol dm^{-3} H_2SO_4 for 20 min for stabilization before each electrochemical impedance spectroscopy (EIS) test.

The EIS measurements were performed using a Zahner IM6 electrochemical workstation. The sinusoidal potential perturbation was 5 mV in amplitude and frequencies ranged from 60 kHz to 20 mHz. The whole measurement process was accomplished in a still electrolyte system at room temperature (25±1°C).

Scanning electron microscopy (SEM)

Samples for SEM experiments were iron sheets (8 mm×8 mm×1 mm). The polishing procedure was the same as that mentioned above. The immersion time was 4 h. A Jeol JSM--6700F field emission scanning electron microscope was used to observe the morphology of the iron sheets, including the bare iron sheet and the L-glutamine modified iron sheet after corrosion in 0.50 mol dm^{-3} H_2SO_4 for 2 h.

Quantum chemical calculations and molecular simulations

In order to investigate the adsorbate–surface interaction, theoretical calculations of the L-glutamine films on an iron surface were performed using *ab initio* quantum chemical calculations and molecular simulations of the molecular mechanics. The geometrical structures were optimized at the HF/6-311+G (*d*,*p*) basic levels and then the Natural Bond Orbital (NBO) method was used to analyze the natural atomic charge of the L-glutamine molecule.[14,15] These calculations were performed using the GAUSSIAN03 program passage. The interaction of the L-glutamine molecule with an iron surface was simulated using molecular dynamics simulation through the COMPASS force field. The molecular simulations were performed using the C2 package.[16]

RESULTS AND DISCUSSIONS

Electrochemical impedance spectroscopy

A lot of useful information about a metal corrosion process can be obtained through EIS measurements, such as the charge-transfer resistance, the polarization resistance, the double-layer capacitance and the pseudo-capacitance.[17] The Nyquist impedance spectra for the bare and L-glutamine-modified iron electrodes and the equivalent circuit used to analyze and fit the whole impedance spectra are represented in Fig. 2. In the circuit, R_S is the resistance of solution between the

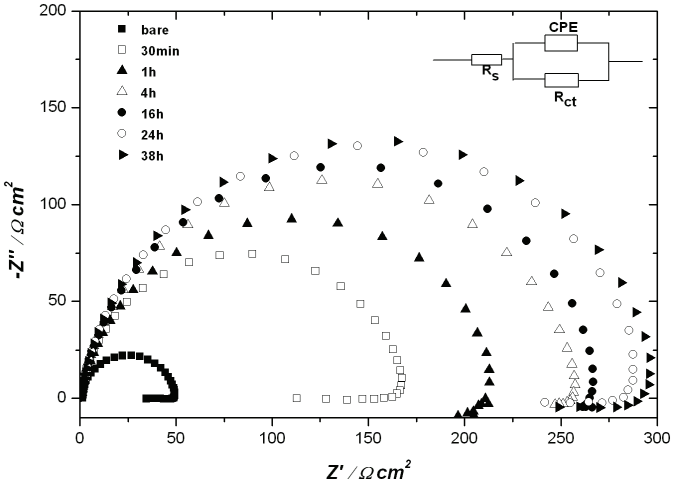

Fig. 2. Nyquist impedance spectra for the bare iron electrode and L-glutamine-modified iron electrodes in 0.50 mol dm^{-3} H_2SO_4 with increasing immersion time in 1.0×10^{-4} mol dm^{-3} L-glutamine and the equivalent circuit for fitting.

iron electrode and the reference electrode and R_{ct} is the charge-transfer resistance, corresponding to the corrosion reaction at the metal substrate/solution interface.[18] The double-layer usually behaves as a constant phase element (CPE) rather than a pure capacitor. The CPE is substituted for a pure capacitor so that it fits the impedance spectra better. The admittance and impedance of a CPE are, respectively, defined as:

$$Y_{CPE} = Y_0 (j\omega)^n \text{ and } Z_{CPE} = \frac{1}{Y_0}(j\omega)^{-n} \quad (1)$$

where Y_0 is the modulus, ω is the angular frequency and n is the phase. The depression degree of the impedance loops depend on the phase of the CPE.[19]

The protection efficiency was calculated using the following equation:

$$PE = \frac{R'_{ct} - R_{ct}}{R'_{ct}} \times 100 \quad (2)$$

where R_{ct} and R'_{ct} represent the charge-transfer resistance of bare electrode and L-glutamine-modified electrodes, respectively.

All impedance spectra exhibited a capacitive loop and all loops were not regular semicircles but depressed to some extent, which is defined by a dispersing effect and is concerned with the state of electrode surface.[20] The diameter of the semicircle represents the charge-transfer resistance. The bare iron electrode had a small charge transfer resistance, because iron reacts with hydrogen ions quickly in acidic solution. After modified with L-glutamine, the electrodes showed a larger charge-transfer resistance than that of the bare electrode, which means that the monolayers block the transfer of the electrons from the iron surface to the solution. By comparing the loops of iron electrode at different immersion time, it was shown that longer immersion times lead to larger loops and higher protection efficiency. It can be seen from Table I that the R_{ct} of the L-glutamine-modified iron electrode was larger than that of the bare iron, which indicates that L-glutamine monolayers were formed and the presence of the monolayers could effectively protect iron from corrosion. With longer immersion times, the L-glutamine-

TABLE I. Equivalent circuit parameters determined by fitting the impedance spectra in Fig. 2 and the calculated values of the protection efficiency (*PE*)

Self-assembly time, h	CPE		R_{ct} / Ω cm^2	*PE* / %
	Y_0 / 10^{-6} Ω^{-1} cm^{-2} s^n	*n*		
0	0.860	0.93	48.10	–
0.50	0.730	0.92	169.0	71.5
1.0	1.13	0.90	215.8	77.7
4.0	0.810	0.91	258.6	81.4
16	0.810	0.90	272.1	82.3
24	0.910	0.91	295.3	83.7
38	0.790	0.91	301.9	84.1

-modified iron electrodes had larger loops and, accordingly, the monolayer had higher protection abilities. It was also found that when the immersion time was prolonged after 4 h, the protection efficiency of L-glutamine did not increase as fast as during the first 4 h because the films became very packed after long immersion times. The maximal protection efficiency obtained in these experiments was approximately 84 %.

There are two controversial processes at the electrode surface, the adsorption and desorption of L-glutamine molecules. At the beginning of the immersion, more and more L-glutamine molecules adsorb on the iron surface. With increasing immersion time, the films become denser and more stable, the adsorption/-/desorption process attains equilibrium. This might be the reason that the increase of the PE was not so obvious after 4 h of immersion. After the films were formed, the electrode was rinsed with ethanol and ultra pure water and dried in a stream of nitrogen. Thus, only the chemisorbed L-glutamine molecules remained on the iron surface. The L-glutamine molecule can be adsorbed on the iron surface through lone pair electrons entering into the empty orbital of iron, hence, the monolayers formed on the iron surface could be considered as self-assembled.

SEM Analysis

SEM was applied to confirm that the self-assembled films on the iron surface can protect the metal from corrosion. The SEM surface morphologies of the bare and L-glutamine-modified iron sheets after corrosion for 2 h in 0.50 mol dm^{-3} H_2SO_4 solutions are shown in Fig. 3. It can be observed that there are distinct differences between the two microphotographs. The former one had suffered more severe corrosion than the latter one. The surface of the bare iron sheet was completely damaged, while the L-glutamine-modified iron sheet was not so severely damaged. This means the presence of L-glutamine films can effectively protect iron from corrosion.

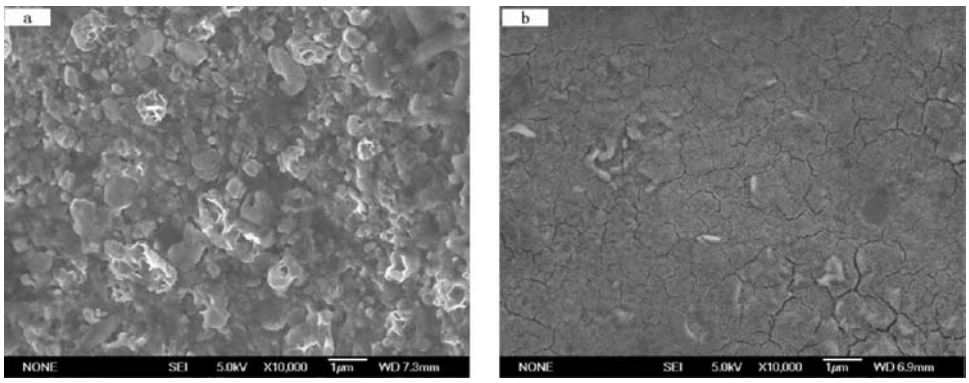

Fig. 3. SEM Images of iron electrodes after corrosion in 0.50 M H_2SO_4 for 2 h. Bare iron electrode (a); L-glutamine modified iron electrode (b).

Quantum chemical calculations and molecular simulations

The optimized structure of L-glutamine is shown in Fig. 4a. The Arabic numbers on the atoms are the natural charges obtained using the Natural Bond Orbital (NBO) analysis of the B3LYP method at 6-311+G (*d*,*p*) basic levels.[21,22] For comparison, the same calculation was performed for the *n*-hexylthiol molecule because alkanethiols can be intensely adsorbed on a metal surface.[23] The optimized structure of *n*-hexylthiol is shown in Fig. 4b. Comparing the two molecules, it can be seen that the N or O atoms in L-glutamine bear much more negative charges than the S atom in *n*-hexylthiol, which indicates the structure of the former is more preferable to interact with the iron surface than that of the latter. Two N atoms and two O atoms in the L-glutamine molecule cannot only interact with an iron surface through lone pair electrons entering into the empty 3*d* orbital of iron but also through the π-electrons in the molecule inserting into the empty 3*d* orbital.

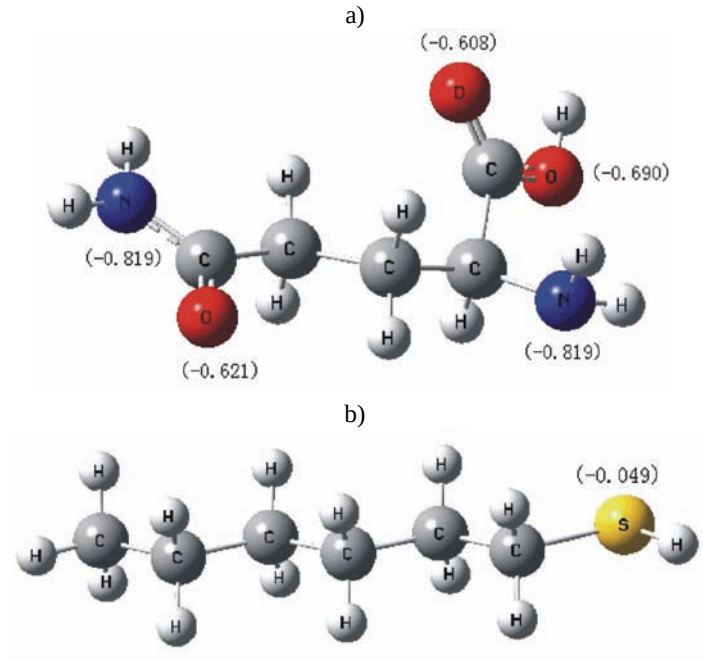

Fig. 4. Optimized structures of L-glutamine (a) and *n*-hexylthiol (b).

To verify the above prediction, a series of molecular dynamics simulations were performed in the next stage. Docking L-glutamine onto an optimized three-layer Fe (110) surface was the calculation model. An L-glutamine molecule was placed onto the surface according to five possible models and the five interaction configurations of L-glutamine with the Fe (110) surface were obtained by mini-

mization using COMPASS force field. The minimization algorithm used by default is the Smart algorithm; it is a cascade of methods using successively steepest descent and conjugate gradient algorithms. As shown in Fig. 5, the models I, II, III and VI are the adsorption models of L-glutamine on an iron surface adsorbing through different N and O atoms; model V is adsorption by the simultaneous action of N and O atoms and the π-electrons with the metal surface.

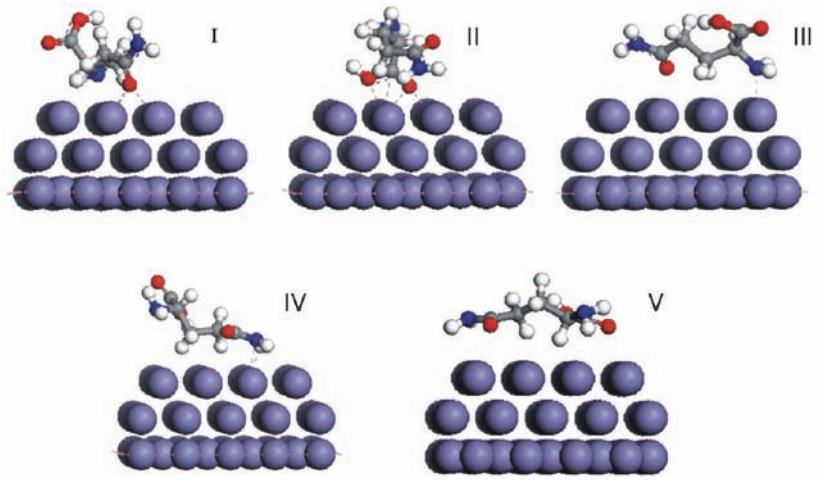

Fig. 5. Adsorption configurations of L-glutamine with a Fe (110) surface.

Based on the optimized configuration, the interaction energy of adsorption between L-glutamine and the iron surface was calculated using the following equation:

$$E_{\text{interaction}} = E_{\text{total}} - (E_{\text{surface}} + E_{\text{L-G}}) \quad (3)$$

where E_{total} is the energy of surface adsorption by an L-glutamine molecule, E_{surface} is the energy of the bare iron surface, and $E_{\text{L–G}}$ is the energy of an L-glutamine molecule. The values of $E_{\text{interaction}}$ and E_{total} are listed in Table II, which shows that configuration V is the most stable adsorption structure of the five models, the next are configurations III and IV. Configurations I and II are unstable adsorption structures because the values of $E_{\text{interaction}}$ are too positive. This verifies the above prediction and shows that L-glutamine can vary easily form monolayers on an iron surface and the possible adsorption structures are configuration III, VI and V.

TABLE II. Calculated interaction energy between L-glutamine and Fe for different adsorption configurations

Configuration	I	II	III	IV	V
$E_{\text{interaction}}$ / kJ mol^{-1}	1.89	105.06	-216.12	-229.38	-246.95

CONCLUSIONS

With increasing immersion time of an iron electrode in an ethanolic L-glutamine solution, more molecules assembled on the iron surface. The highest inhibition efficiency of L-glutamine in 0.50 mol dm^{-3} H_2SO_4 was 84 %. Furthermore, SEM analysis showed that L-glutamine is able to adsorb on an iron surface and the formed monolayers can effectively protect iron against corrosion. Quantum chemical calculations and molecular simulations were able to explain the experimental results to some extent.

Acknowledgements. The authors thank sincerely the Chinese National Science Fund (20573069) and Special Funds for the Major State Basic Research Projects (2006CB605004) for their support of this research.

И З В О Д

ЕЛЕКТРОХЕМИЈСКА ИСПИТИВАЊА И МОЛЕКУЛСКЕ СИМУЛАЦИЈЕ МОНОСЛОЈЕВА ИНХИБИТОРА КОРОЗИЈЕ L-ГЛУТАМИНА НА ГВОЖЂУ

ZHE ZHANG[1], SHENHAO CHEN[1,2], YUANYUAN FENG[3], YUNQIAO DING[1], JUANJUAN ZHOU[1] и HENGLEI JIA[1]

[1]Department of Chemistry, Shandong University, Jinan 250100, [2]State Key Laboratory for Corrosion and Protection, Shenyang 110016 и [3]Department of Chemistry, Qufu Normal University, Qufu 273165, P.R. China

L-Глутамин у монослоју је коришћен као инхибитор корозије гвожђа у 0,50 mol dm^{-3} H_2SO_4. Заштитна моћ слоја је испитивана спектроскопијом електрохемијске импеданције (СЕИ). Механизам адсорпције је дискутован на основу квантно-механичких израчунавања и молекулских симулација. Помоћу скенирајуће електронске микроскопије потврђено је формирање монослојева L-глутамина и њихов инхибициони ефекат. Резултати указују на то да молекули L-глутамина могу да формирају филмове на површини гвожђа и да је инхибициони ефекат филма већи уколико је гвожђе дуже урођено у раствор L-глутамина. Филмови се формирају спонтано адсорпцијом L-глутамина чије терминалне групе поседују специфичан афинитет према површини гвожђа, те се густо паковани монослојеви могу сматрати самоуређеним типом слојева.

(Примљено 19. септембра, ревидирано 10. новембра 2008)

REFERENCES

1. G. Che, Z. Li, H. Zhang, C. R. Cabrera, *J. Electranal. Chem.* **453** (1998) 9
2. W. Yang, J. J. Gooding, D. B. Hibbert, *J. Electranal. Chem.* **516** (2001) 10
3. W. Guo, S. Chen, H. Ma, *J. Serb. Chem. Soc.* **71** (2006) 167
4. G. Liu, S. Chen, H. Ma, X. Liu, *J. Serb. Chem. Soc.* **72** (2007) 475
5. C. Wang, S. Chen, H. Ma, C. S. Qi, *J. Appl. Electrochem.* **33** (2003) 179
6. I. Felhősi, E. Kálmán, *Cor. Sci.* **47** (2005) 695
7. K. Aramaki, T. Shimura, *Cor. Sci.* **48** (2006) 209
8. T. Shimura, K. Aramaki, *Cor. Sci.* **49** (2007) 1378
9. G. K. Jennings, J. C. Munro, T. H. Yong, P. E. Laibinis, *Langmuir* **14** (1998) 6130
10. D. Taneichi, R. Haneda, K. Aramaki, *Cor. Sci.* **43** (2001) 1589
11. I. Felhosi, J. Telegdi, G. Pálinkás, E. Kálmán, *Electrochim. Acta* **47** (2002) 2335
12. K. Nozawa, H. Nishihara, K. Aramaki, *Cor. Sci.* **39** (1997) 1625

13. C. Ruan, T. Bayer, S. Meth, C. N. Sukenik, *Thin Solid Films* **419** (2002) 95
14. A. E. Reed, L. A. Curtiss, F. Weinhold, *Chem. Rev.* **88** (1988) 899
15. R. McWeeny, G. Dierksen, *J. Chem. Phys.* **49** (1968) 4852
16. Y. Feng, S. Chen, J. You, W. Guo, *Eletrochim. Acta* **53** (2007) 1743
17. Y. Feng, W. K. Teo, K. S. Siow, Z. Gao, K. L. Tan, A. K. Hsieh, *J. Electrochem. Soc.* **144** (1997) 55
18. M. Gojić, *Cor. Sci.* **43** (2001) 919
19. H. Ma, X. Cheng, G. Li, S. Chen, Z. Quan, S. Zhao, L. Niu, *Cor. Sci.* **42** (2000) 1669
20. S. Muralidharan, K. L. N. Phani, S. Ravichandran, S. V. K. Iyer, *J. Electrochem. Soc.* **142** (1995) 1478
21. A. D. Becke, *Phys. Rev. A.* **38** (1988) 3098
22. C. Lee, W. Yang, R. G. Parr, *Phys. Rev. B* **37** (1988) 785
23. G. Grundmeier, C. Reinartz, M. Rohwerder, M. Stratmann, *Eletrochim. Acta* **43** (1998) 165.

Journal of the Serbian Chemical Society
JSCS@tmf.bg.ac.rs • www.shd.org.rs/JSCS

J. Serb. Chem. Soc. 74 (4) 417–425 (2009)
JSCS–3843

UDC 633.822+66.061:665.52/.54
Original scientific paper

Supercritical CO_2 extraction of mentha (*Mentha piperita* L.) at different solvent densities

ZORAN ZEKOVIĆ[1*#], ŽIKA LEPOJEVIĆ[1#], SLAVICA MILIĆ[1], DUŠAN ADAMOVIĆ[2] and IBRAHIM MUJIĆ[3]

[1]*University of Novi Sad, Faculty of Technology, Department of Biotechnology and Pharmaceutical Engineering, Bulevar Cara Lazara 1, 21000 Novi Sad,* [2]*Institute of Field and Vegetable Crops, Maksima Gorkog 30, 21000 Novi Sad, Serbia and* [3]*University of Bihać, Biotechnical Faculty, Kulina Bana 2, 77000 Bihać, Bosnia and Herzegovina*

(Received 20 May, revised 28 October 2008)

Abstract: The chemical composition of mentha essential oil and mentha extracts obtained at different pressures/temperatures by supercritical fluid extraction (SFE) were studied by GC–MS. The menthol content was also determined spectrophotometrically. The predominant compounds in the essential oil and in the CO_2 extract obtained at 100 bar were L-menthon and menthole but at higher pressures (from 150 to 400 bar), squalene was dominant. The equation of Naik *et al*. was used for modelling the mentha–supercritical CO_2 system.

Keywords: *Mentha piperita* L.; essential oil; supercritical fluid extraction; extraction pressure and temperature; GC–MS.

INTRODUCTION

The *Labiatae* family has several members with significant essential oil contents. Mentha essential oil is an important material for perfumery, as a flavour, for liquors, *i.e*., in cosmetics, in toothpastes, as well as spices in the food industry. Parts of the mint-family plant, mainly dry leaves, are used for tea worldwide. Commercial oils could be classified by their menthol or carvone content.[1–3]

The classical procedures for the separation of the active substances from plant material, *i.e*., steam distillation and extraction with organic solvents (*e.g*., dichloromethane) have serious drawbacks. The distillation procedure allows only the separation of volatile compounds (essential oils), which, to a greater or lesser extent, are transformed under the influence of the elevated temperature. On the other hand, extraction with organic solvents can hardly render an extract free of traces of the organic solvent, which are undesirable for organoleptic and/or health reasons. In addition, organic solvents are insufficiently selective, hence, in addi-

* Corresponding author. E-mail: zzekovic@tehnol.ns.ac.rs
# Serbian Chemical Society member.
doi: 10.2298/JSC0904417Z

tion to the active substances, some concomitant compounds are also dissolved. For these reasons, supercritical fluid extraction (SFE) with carbon dioxide (CO_2) has recently gained in importance as an alternative to the classical procedures. Extraction procedures involving supercritical CO_2 belong to "clean technologies", with no secondary products polluting the environment. CO_2 is the most widely used medium in SFE because it is simple to use, inexpensive, non-flammable, non-toxic, chemically stable, shows great affinity to volatile (lipophilic) compounds and can be easily and completely removed from any extract. By changing the pressure and/or temperature above the critical point of CO_2 (t_c = = 31.3 °C; p_c = 72.8 bar; d_c = 0.467 g/ml), a pronounced change in the density and dielectric constant, *i.e.*, solvent power, of supercritical CO_2, can be achieved.[4–7] SFE of the essential oil from different mentha varieties, as well as GC analysis of the mentha essential oil and other extracted compounds have been investigated by many authors.[1–3,8–10]

In this study, the chemical composition of mentha essential oil (EO) and the mentha extracts obtained at different pressures and temperatures by supercritical fluid extraction (SFE) using CO_2 were studied. The chemical composition of the mentha EO and CO_2 extracts were compared. The SFE–CO_2 kinetics was described by the well-known model equation of Naik *et al.*[11]

EXPERIMENTAL

Plant material and chemicals

Mentha (*Mentha piperita* L.) was grown by the Institute of Field and Vegetable Crops, Novi Sad, Serbia (year 2004). The dry and milled (mean particle size 0.60 mm) leaves of mentha were used in this work.

Standard sample of (–)-menthol (Fluka AG, Switzerland) was used. Commercial carbon dioxide (Tehno-gas, Novi Sad, Serbia) was employed as the extracting agent. All other chemicals were of analytical reagent grade.

Procedures

The mentha essential oil (EO) content (3.19 %; v/w) was extracted by steam distillation, using the prescribed procedure in Ph. Jug. IV.[12]

The supercritical fluid extraction (SFE) with carbon dioxide was performed using a previously described laboratory-scale high pressure extraction plant – HPEP (Nova-Swiss, Effretikon, Switzerland).[13] The main parts and characteristics (manufacturer's specification) of the plant are: a diaphragm-type compressor (up to 1000 bar), extractor with an internal volume of 200 ml (p_{max} = 700 bar), separator with an internal volume 200 ml (p_{max} = 250 bar) and maximum CO_2 flow rate of about 5.7 kg/h. The mass of mentha (mean particle size 0.6 mm) in the extractor was 50 g and a CO_2 flow rate of 3.225 g/min was employed. The pressure and temperature were varied (see Tables I and II). The separator conditions were: pressure: 15 bar and temperature: 25 °C.

Analyses

A basic standard solution of menthol (10 mg/100 ml in 95 % ethanol) was used for obtaining the solutions with different menthol concentrations (from 0.05 to 0.70 mg/10 ml). To each standard solution (2 ml), a 0.10 % solution (3 ml) of *p*-dimethylaminobenzaldehyde

in cc. H_2SO_4 was added. After 10 min, absorbance of solution was measured at 510 nm. Obtained values were used for the construction of a calibration curve for the menthol content.

TABLE I. Operating conditions and extraction yields obtained at 40 °C

Extract No.	Pressure, bar	CO_2 density, g/ml	Extraction time, h	Extraction yield, %
1	100	0.630	2.5	3.57
2	150	0.790	0.5	0.44
3	200	0.840	0.5	0.40
4	300	0.910	0.5	0.23
5	400	0.957	0.5	0.21

TABLE II. Operating conditions, extraction yield and menthol content in the extracts obtained at different extraction temperatures (pressure: 100 bar, extraction time: 2.5 h)

Extract No.	Temperature, °C	CO_2 density g/ml	Extraction yield, %	Menthol content in extract %
1	35	0.735	2.94	32.04
2	40	0.630	3.57	28.54
3	45	0.520	2.71	26.53
4	50	0.375	2.91	33.62

The dependence of the menthol mass (m_M in mg) on the absorbance (A) could be expressed as:

$$m_M = \frac{A + 3.71 \times 10^{-3}}{6.8625} \quad (1)$$

with a linear regression coefficient was 0.987. The content of menthol in the oil and extracts was calculated using Eq. (1).

The GC–MS measurements were realise using a GCD HP G 1800 A (Hewlett-Packard, Palo Alto, CA, USA) instrument with HP-5 MS column (30.0 m×0.25 mm i.d., film thickness 0.25 μm). The carrier gas was helium at a flow rate of 0.80 ml/min. The temperatures of the injector and detector (45-425 D) were 250 and 280 °C, respectively. The column was heated from the initial 50 °C (3 min) with a linear increase of 20 °C/min to 130 °C (1 min) and 9 °C/min until the final 280 °C (10.33 min). The total analysis time was 35 min. The injected volume of sample solution in dichloromethane was 1 μL. The compounds were identified using the Wiley data base.

All investigations were performed in triplicate and the given results are mean values.

RESULTS AND DISCUSSION

The menthol content in the mentha essential oil as determined by the spectrophotometric method was 30.67 %.

The GC–MS method was used to determine the qualitative and quantitative composition of obtained mentha essential oil (EO) (Table III). The contents of the compounds the EO are expressed as % on the basis of the menthol content obtained by the spectrophotometric method, as well as by the external standard method using standard sample of (–)-menthol. The content of menthol determined by these two methods for quantification was similar and for calculation of other compounds, the mean value of the menthol content was used.

TABLE III. Composition of the essenial oil (EO) obtained by steam distillation and extracts obtained at 40 °C under different extraction pressures

Compound	Content of compound, %					
	EO	Pressure, bar				
		100	150	200	300	400
D,L-Limonene	0.46	0.23	–	–	–	–
Limonene	0.98	0.54	–	–	–	–
Cineole	4.04	2.32	–	–	–	–
β-Terpineol	2.90	2.73	0.40	0.35	–	–
L-Menthone	37.15	27.08	2.18	1.98	1.74	–
Iso-menthone	10.33	8.79	0.79	0.76	–	–
Menthol	30.67	28.54	5.47	6.54	6.09	3.39
4-Terpineol	1.48	1.22	–	–	–	–
α-Terpineol	0.48	0.70	–	–	–	–
Pulegone	2.40	2.22	0.22	–	–	–
Piperitone	0.95	0.76	–	–	–	–
Menthyl acetate	5.46	4.67	0.69	0.84	0.72	–
β-Caryophyllene	0.76	4.34	0.80	1.05	0.90	–
Nerolidol	–	0.58	–	–	–	–
Germacrene-D	–	5.03	0.86	0.97	0.92	–
Bicyclogermacrene	–	1.65	1.31	0.35	–	–
β-Bisabolene	–	0.35	–	–	–	–
β-Elemene	–	0.23	–	0.15	–	–
Viridiflorol	–	0.39	–	0.15	–	–
trans-Pinene	–	0.17	0.19	0.50	0.43	1.62
Palmitic acid	–	–	1.16	0.98	0.83	0.80
9,12,15-octadecatriene-1-ol	–	–	3.77	3.81	5.57	8.96
Linoleic acid	–	–	0.47	0.31	0.41	–
Diethylmethylborane	–	–	3.08	1.90	–	–
Vitamin K_1	–	–	–	2.68	–	–
14-β-Pregnane	–	–	0.98	0.34	5.49	6.99
Hexacosane	–	0.59	7.29	7.27	16.20	18.60
Octacosane	–	0.28	1.71	1.09	1.39	1.50
Vitamine E	–	–	16.20	2.38	11.72	16.91
8-Hydroxysclerodine	–	–	5.95	2.54	0.73	1.30
Neophytadiene	–	0.49	0.60	2.08	2.27	3.60
Tricosane	–	–	29.26	28.32	3.00	–
Tetratriacontane	–	–	–	0.45	1.00	1.73
Heptacosane	–	–	0.92	0.68	1.88	1.85
Stigmast-5-en-3-ol	–	–	–	5.18	–	–
Ergost-5-en-3-ol	–	–	–	5.16	–	–
Squalene	–	1.76	4.92	11.40	25.67	23.55
Nonadecane	–	–	3.17	3.78	4.29	4.33
Triacontane	–	0.52	4.32	2.27	3.27	0.54
Total	98.06	96.18	96.71	96.26	94.53	95.67

L-Menthone was present in the highest amount (37.15 %) in the mentha EO. The most important mentha compound, menthol had a content of 30.67 %. In addition, the other predominant compounds of the mentha EO were iso-menthone (10.33 %) and menthyl acetate (5.46 %). These four compounds made up 83.61 % of the mentha EO.

The SFE of mentha by CO_2 was performed at a pressure of 100 bar and a temperature of 40 °C for 2.5 h (*i.e.*, the same time as prescribed for steam distillation by Ph. Jug. IV[12]), whereby the first extract was obtained (extract No. 1). The same mentha sample was extracted at a higher pressure (150 bar) for 0.5 h whereby the second extract was separated (extract No. 2). The extraction yields obtained under different extraction conditions are shown in Table I.

The results of the GC–MS analysis of the extracts No. 1 to No. 5 are shown in Table III.

The extraction yield of extract No. 1 (obtained at a pressure of 100 bar and 40 °C; solvent density 0.630 g/ml) was higher (3.57 %) by about 12 % than the amount of EO obtained by steam distillation (3.19 %). Extract No. 1 had a similar composition to mentha EO. However, because of the co-extraction of compounds not present in the EO obtained by steam distillation, the contents of L-menthone and menthol were lower (27.08 and 28.54 %, respectively). In this extract, the total % of the four main compounds (menthone, iso-menthone, menthol and menthyl acetate) was also lower (69.08 %) than in the EO (83.61 %).

By increasing the pressure to 150 bar (and subsequently to 200, 300 and 400 bar), an attempt was made to perform selective extractions, *i.e.*, to determine the remaining components in the mentha sample without the EO. The yield of the remaining components obtained at 150 bar was only 0.44 % (Table III shows the content the compounds in extract No. 2). The predominant compounds of extract No. 2 were tricosane (29.26 %) and Vitamin E (16.20 %), with traces of the mentha EO compounds. Primarily, the yields of menthol and menthone show the incomplete extraction of EO (*i.e.*, only about 24 mg of menthol and 10 mg of menthone were extracted in the steam distillation in comparison to 1019 mg of menthol and 967 mg of menthone obtained from 100 g of menthe present in extract No. 1).

By increasing the pressure to 200 bar, the extraction yield was a lower (0.40 %) than that obtained at 150 bar (0.44 %). The predominant compounds in extract No. 3 were tricosane (28.32 %) and squalene (11.40 %). Menthol (6.54 %) and menthone (1.98 %) were still present in this extract. Then, the extraction was continued at a pressure of 300 bar and extract No. 4 was obtained in very low yield (0.23 %). Menthol (6.09 %) and menthone (1.74 %) were detected, but the predominant compounds of extract No. 4 were squalene (25.67 %) and hexacosane (16.20 %), as well as Vitamin E (11.72 %). Finally, the extraction at 400 bar yielded in 0.21 % of dry extract (extract No. 5). Menthone was not detected in

the final extract, but menthol was (3.39 %). This percent of menthol corresponded to about 7 mg/100 g of mentha leaves. The predominant compounds of extract No. 5 were squalene (23.55 %), hexacosane (18.60 %) and Vitamin E (16.91 %). The total % of the four important mentha compounds (menthone, iso-menthone, menthol and menthyl acetate) in extracts No. 2 to No. 5 were 9.13, 10.12, 8.55 and 3.33 %, respectively.

For the investigation of the influence of temperature on the SFE of mentha, a pressure of 100 bar was chosen. The temperatures of extraction were 35, 40, 45 and 50 °C. The extraction procedure, as well as extraction yield and menthol content in the obtained extracts are shown in Table II.

The highest extraction yield was 3.57 % at a temperature of 40 °C (*i.e.*, 1019 mg/100 g of mentha leaves of menthol were extracted). The highest content of menthol in the extract obtained at 50 °C (33.62 %) corresponds to a menthol extraction yield of 980 mg/100 g of mentha leaves. The effect of operating temperature on the extraction yield, as well as on menthol yield, could be explained through the solvent density obtained at the investigated temperatures. The solubility of the mentha compounds was the highest at a CO_2 density of 0.630 g/ml, *i.e.*, at a temperature of 40 °C and a pressure of 100 bar than at the other investtigated densities, *i.e.*, temperatures (Table II).

For modelling of the investigated extraction system, mentha–supercritical carbon dioxide, the simple equation of Naik *et al.*[11] was employed:

$$y = \frac{y_\infty t}{b + t} \tag{2}$$

where: y is the extraction yield after time t; y_∞ is the maximum extraction yield and b is a constant.

The linear form of Eq. (2):

$$\frac{1}{y} = \frac{b}{y_\infty}\frac{1}{t} + \frac{1}{y_\infty} \tag{3}$$

was used for calculating the parameters of Eq. (2). The obtained values for modelling the system through total extract yield and menthol yield for SFE of mentha are shown in Tables IV and V, respectively.

TABLE IV. Values of y_∞ and b for mentha total extract

t / °C	y_∞ / %	b	Correlation coefficient, r	Mean relative deviation (MRD[a]), %
35	6.29	101.96	0.977	14.75
40	5.47	62.32	0.990	7.72
45	3.62	42.31	0.999	1.95
50	5.59	91.86	0.978	10.85

[a] $MRD = \frac{\sum\left|\frac{y_c - y_e}{y_e}\right| 100}{n}$, where y_c is the calculated value, y_e the experimental value and n the number of points

TABLE V. Values of y_∞ and b (Eq. (3)) for menthol extraction

t / °C	y_∞ / %	b	Correlation coefficient, r	Mean relative deviation (*MRD*), %
35	1.85	101.93	0.976	14.60
40	1.56	62.32	0.990	7.73
45	1.09	42.16	0.999	1.88
50	1.84	110.40	0.979	12.56

The obtained model equations, as well as experimental points, are shown in Figs. 1 and 2 for the total yield of extract and for the menthol yield, respectively.

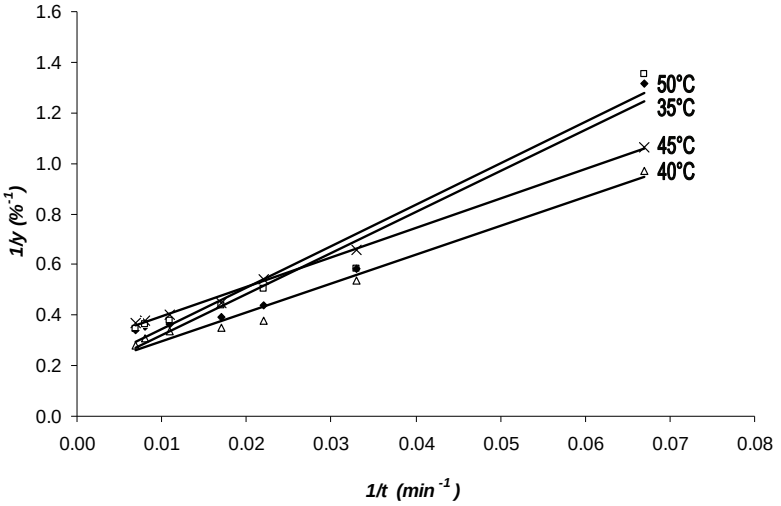

Fig. 1. Dependence of 1/y on 1/t for mentha total extract.

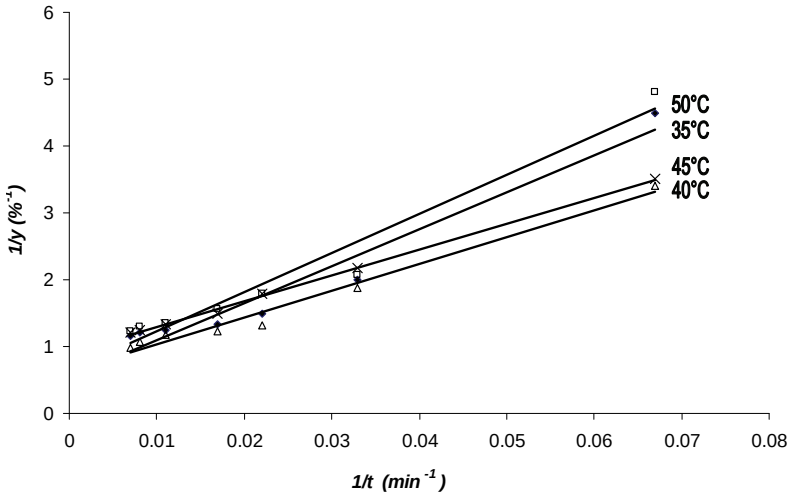

Fig. 2. Dependence of 1/y on 1/t for menthol extraction. Legend: ♦ – 35 °C; Δ – 40 °C; × – 45 °C and □ – 50 °C.

The obtained values of the mean relative deviation (Tables IV and V) show the possibility of using the equation of Naik *et al.*[11] for the extraction process of the investigated system mentha–supercritical carbon dioxide through the total extract yield and menthol yield. The applied equation shows a good fit for the extraction process at the temperatures of 40 and 45 °C, but for the temperatures of 35 and 50 °C, some another model equation, with a better fit of the experimental results should be applied.

CONCLUSIONS

The content of mentha essential oil (EO) in mentha leaves was 3.19 %, containing menthol (30.67 %) and L-menthone (37.15 %). These values are in the good agreement with the results of other authors. The SFE conditions, such as the operating temperature and pressure, *i.e.*, solvent density, are very important for an optimum extraction process. Due to this, different combinations of pressure and temperature were investigated in this work. For the production of a mentha most similar to the mentha EO obtained by steam distillation, the extraction conditions are 100 bar, 40 °C and an extraction time of 2.5 h.

For the investigations of the influence of temperature on the SFE mentha with CO_2, the temperatures of 35, 40, 45 and 50 °C (no thermal decomposition of the mentha compounds present), at a pressure of 100 bar, were chosen. The extraction kinetics through the total extract yield, as well as menthol yield, was described by the model equation of Naik *et al*. The applied equation showed a good fit only for the extraction process at the temperatures of 40 and 45 °C.

ИЗВОД

ЕКСТРАКЦИЈА МЕНТЕ (*Mentha piperita* L.) СУПЕРКРИТИЧНИМ CO_2 ПРИ РАЗЛИЧИТИМ ГУСТИНАМА РАСТВАРАЧА

ЗОРАН ЗЕКОВИЋ[1], ЖИКА ЛЕПОЈЕВИЋ[1], СЛАВИЦА МИЛИЋ[1], ДУШАН АДАМОВИЋ[2] и ИБРАХИМ МУЈИЋ[3]

[1]Универзитет у Новом Саду, Технолошки факултет, Катедра за биотехнологију и фармацеутско инжењерство, Булевар Цара Лазара 1, 21000 Нови Сад, [2]Институт за ратарство и повртарство, Максима Горког 30, 21000 Нови Сад и [3]University of Bihać, Biotechnical Faculty, Kulina Bana 2, 77000 Bihać, Bosnia and Herzegovina

Квалитативни и квантитативни састав етарског уља и екстраката менте добијених на различитим притисцима/температурама екстракцијом суперкритичним флуидом су одређени методом GC–MS. Садржај ментола одређен је спектрофотометријски. Доминантне компоненте у етарском уљу су L-ментол и ментон, као и у CO_2 екстракту добијеном при притиску од 100 bar, док је у екстрактима добијеним при већим притисцима (од 150 до 400 bar) доминантна компонента сквален. За моделовање испитиваног екстракционог система мента–суперкритични угљендиоксид примењена је једначина Naik-а и сарадника.

(Примљено 20. маја, ревидирано 28. октобра 2008)

REFERENCES

1. E. Reverchon, A. Ambruosi, F. Senatore, *Flavour Fragr. J.* **9** (1994) 19
2. N. Aghel, Y. Yamini, A. Hadjiakhoondi, S. M. Pourmortazavi, *Talanta* **62** (2004) 407
3. A. Ammann, D. C. Hinz, R. S. Adleman, C. M. Wai, B. W. Wenclawiak, *Fresenius J. Anal. Chem.* **364** (1999) 650
4. Z. Zeković, Ž. Lepojević, A. Tolić, *Sep. Sci. Technol.* **38** (2003) 541
5. Z. Zeković, Ž. Lepojević, Dj. Vujić, *Chromatographia* **51** (2000) 175
6. G. Stojanović, R. Palić, S. Alagić, Z. Zeković, *Flavour Fragr. J.* **15** (2000) 335
7. Z. Zeković, Ž. Lepojević, A. Tolić, *Sep. Sci. Technol.* **36** (2001) 3459
8. N. Aghel, Y. Yamini, A. Hadjiakhoondi, *DARU* **10** (2002) 67
9. M. Gotto, M. Sato, T. Horose, *J. Chem. Eng. Jpn.* **26** (1993) 401
10. Z. Zeković, Ž. Lepojević, D. Adamović, I. Mujić, S. Milić, in *Proceedings of the Eighth Conference on Supercritical Fluids and Their Applications, Tome 1*, Ischia, Italy, (2006), E. Reverchon Ed., (2006), pp. 95–98
11. S. N. Naik, H. Lentz, R. C. Maheshwari, *Fluid Phase Equilib*. **49** (1989) 105
12. *Pharmacopoea Jugoslavica, Editio quarta* (Ph. Jug. IV), Savezni zavod za zdravstvenu zaštitu, Beograd, 1984
13. B. Pekić, Z. Zeković, L. Petrović, A. Tolić, *Sep. Sci. Technol*. **30** (1995) 3575.

Journal of the Serbian Chemical Society
JSCS@tmf.bg.ac.rs • www.shd.org.rs/JSCS

J. Serb. Chem. Soc. 74 (4) 427–440 (2009) UDC 536.2:536.7+547.321'212:541.18.045
JSCS–3844 *Original scientific paper*

Local heat transfer coefficients during the evaporation of 1,1,1,2-tetrafluoroethane (R-134a) in a plate heat exchanger

EMILA ŽIVKOVIĆ[1*#], STEPHAN KABELAC[2] and SLOBODAN ŠERBANOVIĆ[1#]

[1]*Faculty of Technology and Metallurgy, University of Belgrade, Karnegijeva 4, 11120 Belgrade, Serbia and* [2]*Helmut Schmidt University of the Federal Armed Forces, Holstenhofweg 85, D-22043 Hamburg, Germany*

(Received 10 June, revised 30 October 2008)

Abstract: The evaporation heat transfer coefficient of the refrigerant R-134a in a vertical plate heat exchanger was investigated experimentally. The area of the plate was divided into several segments along the vertical axis. For each of the segments, the local value of the heat transfer coefficient was calculated and presented as a function of the mean vapor quality in the segment. Owing to the thermocouples installed along the plate surface, it was possible to determine the temperature distribution and vapor quality profile inside the plate. The influences of the mass flux, heat flux, pressure of system and the flow configuration on the heat transfer coefficient were also taken into account and a comparison with literature data was performed.

Keywords: plate heat exchanger; evaporation; R-134a; heat transfer coefficient.

INTRODUCTION

Plate heat exchangers (PHE) have been widely used for almost a century due to their good thermal performance, modest space requirements, easy accessibility to all areas and lower capital and operating costs in comparison to the most commonly used shell-and-tube heat exchangers. In the past, PHE were extensively used in the food and pharmaceutical industries but their application field has expanded to the chemical, petrochemical and process industries. In refineries and petrochemical plants, PHE are applied to many hydrocarbon processes, including catalytic reforming, desulphurization, isomerization, and aromatic recoveries. Typical applications of PHE in the chemical industry are as coolers of acetic acid, sulfuric acid and organic solutions.

Their high thermal performance and compactness made PHE suitable as evaporators or condensers in many refrigeration, air conditioning, and heat pump systems where the fluid acting as the heat source or heat sink is a liquid. For

* Corresponding author. E-mail: emila@tmf.bg.ac.rs
# Serbian Chemical Society member.
doi: 10.2298/JSC0904427Z

these purposes, various refrigerants have been used as working fluids. Serious depletion of the ozone layer in the atmosphere and global warming problems created a need for the development of new refrigerants, such as R-134a, R143a, R-407c, R-410a, R-417a or R-507, with low values of ozone depletion potential (ODP) and global warming potential (GWP). Application of these refrigerants on the other hand required the knowledge of their thermodynamic, thermophysical, and heat transfer properties.

Literature data on two-phase heat transfer, especially for the new refrigerants in PHE, are relatively scarce. In the past years, experimental data for evaporation heat transfer in PHE were published by a few research groups. Experimental investigations on evaporation heat transfer of different refrigerants in PHE are summarized in a previous paper.[1] Yan and Lin[2] explored the evaporation of the refrigerant R-134a in a plate heat exchanger. Their data, used in this study for comparison, produce the local heat transfer coefficient for a 60° chevron type plate as a function of the vapor quality, mass flux and heat flux. A few years later, using the same setup, Hsieh *et al.*[3] investigated the subcooled flow boiling of R-134a, as well as the heat transfer characteristics of the refrigerant R-410a during evaporation[4] and saturated flow boiling processes.[5] The evaporation and condensation of R-134a were also the subject of our previous investigation.[1,6–8] Previously, heat transfer during the boiling process was explored on different plate geometries and with several refrigerants (R-12, R-22, R-113 and R-717) used as the working fluid.[9]

The aim of this work, which is a continuation of our previous investigations,[1,6–8] was to obtain values of the local heat transfer coefficients as a function of vapor quality for different mass and heat fluxes, system pressures and flow configurations. Local temperature measurements along the plate produced temperature profiles and allowed the calculation of vapor distribution along the plate during evaporation.

EXPERIMENTAL

The experimental system used in the present investigation included two vertical PHE – an evaporator and a condenser. It consisted of two main loops, a refrigerant loop and a water––glycol loop, as well as of a data acquisition unit. A detailed description of the experimental setup can be found in a previous paper[1] and a schematic representation of the system is given in Fig. 1. During the experiments, the temperatures, pressures, and flow rates were measured in both loops of the system. The refrigerant loop contained an evaporator (1), separator (2), expansion valve (3), inner heat exchanger (4), compressor (5), two oil separators (6), condenser (7), refrigerant collector with a level indicator (8), two sight glasses and also two volume flowmeters. A vertical plate and a frame heat exchanger was used as the condenser (7). It consisted of 10 plates forming 4 channels for the refrigerant and 5 for the secondary fluid flow, as shown in Fig. 2. Except the two single plates at each end of the stack, the remaining 6 formed 4 double-plate cassettes, inside of which the refrigerant flow passed. The plate characteristics are given in a previous paper[1] and a schematic representation is shown in Fig. 3.

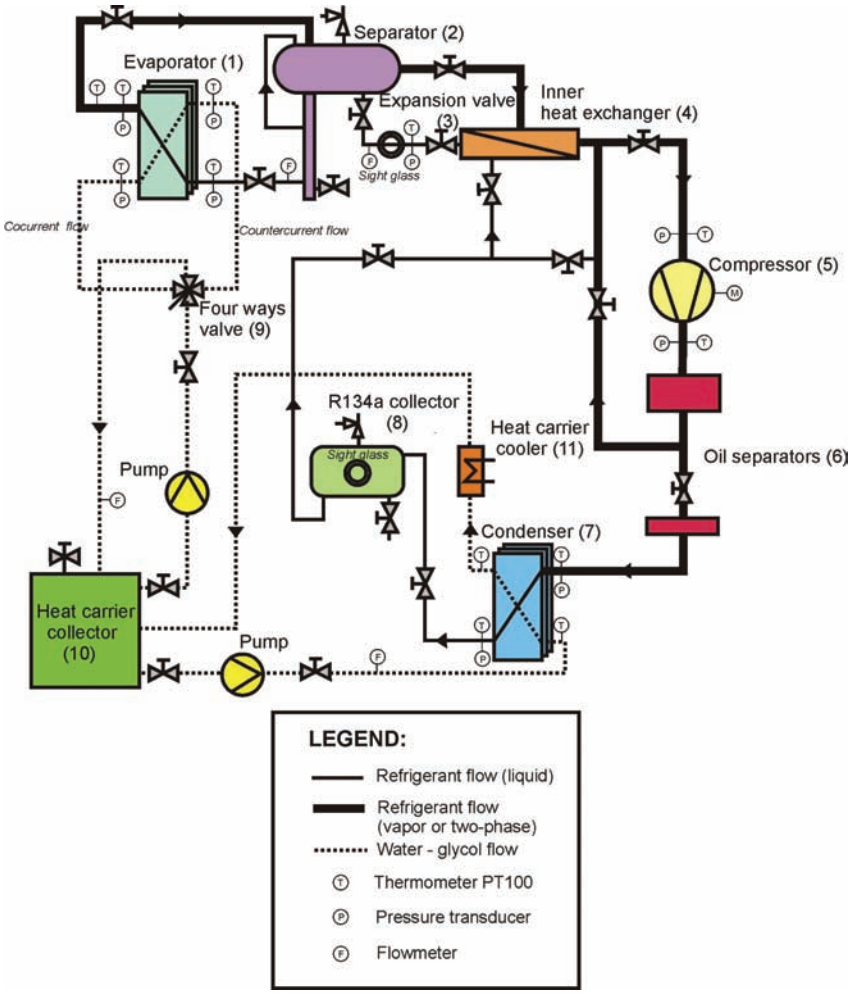

Fig. 1. Experimental setup.

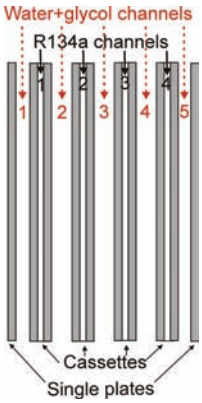

Fig. 2. PHE configuration.

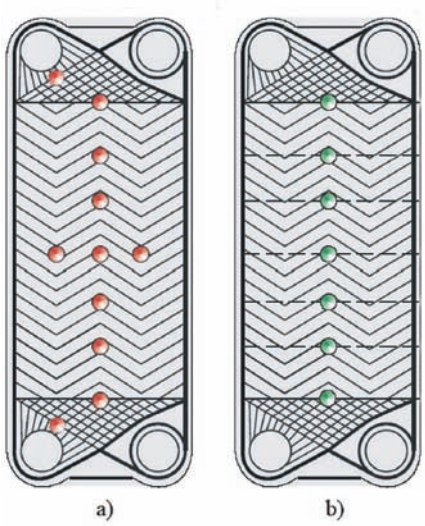

Fig. 3. Plate geometry and thermocouples position; a) wall temperature thermocouples and b) fluid temperature thermocouples.

A special feature of this setup is the measurement of the temperature profile along the plate inside the PHE. Thermocouples (type K, 0.5 mm diameter) were welded along the plate surface in a vertical line on the two middle cassettes for local temperature measurement. The thermocouples were used for measuring the wall temperature on one of the plates and the fluid temperature on the other one, which enabled a direct calculation of local heat transfer coefficients on the water–glycol side. The wall temperature thermocouples were fixed onto the plates *via* small dimples of silver solder, while the fluid temperature thermocouples were fixed a few millimeters below the temperature sensitive head and bent into the middle of the fluid flow channel. The thermocouples were calibrated repeatedly with single phase flow on both sides of the PHE to ensure reliable temperature readings.

In the central horizontal line of the plates, three fluid thermocouples were placed laterally next to each other to check on possible maldistribution within one plate channel. Since their temperature readings agreed within ±1 °C, lateral flow maldistribution seemed to be negligible. Additional thermocouples were installed on each of the remaining two cassettes, at the inlet and at the outlet of the secondary fluid channels, to check on possible maldistribution of the secondary fluid between the plates of the PHE.

Typical temperature profiles along the plate (measured temperatures of the secondary fluid and calculated refrigerant temperatures) are shown in Fig. 4 for concurrent and in Fig. 5 for countercurrent flow. In addition to the measurements by the thermocouples, the temperature of both fluids at the inlet and outlet ports of the condenser were measured by Pt100 resistance thermometers, calibrated against a PTB standard (Physikalish Technische Bundesanstalt Braunschweig, Germany). The differential and absolute pressures were measured using Holox-membrane pressure transducers connected to the inlet and outlet ports of the PHE.

In order to obtain various test conditions, such as the vapor quality at the exit of the evaporator, pressure, flow rate, and imposed heat flux, various water–glycol flow rates were used and the compressor power was changed.

Since the evaporator operated in the thermosyphon mode, the refrigerant mass flux in the evaporator sub-cycle was higher than the mass flux within the loop, thus two flowmeters were required on the refrigerant side. At the evaporator inlet, the volumetric flow rate of the refri-

gerant was measured by a calibrated KROHNE Ultrasonic Flowmeter (type UFM 3030) with an uncertainty of ±1 % and before the expansion valve by a turbine flowmeter, calibrated in--house, with an uncertainty of around 2 %. The water–glycol loop consisted of two sub-cycles, one connected with the evaporator and the other with the condenser. For temperature and pressure measurements of the secondary fluid, Pt100 thermometers and pressure transducers were used at the inlets and outlets of both heat exchangers. The flow rate was measured by a turbine flowmeter with an uncertainty of ±1.5 % in the evaporator sub-cycle and by a TRIMEC Multipulse Positive Displacement MP025 flowmeter with an uncertainty of ±0.5 % in the condenser subcycle. The resistance thermometers, the pressure transducers, and the flowmeters were calibrated repeatedly.

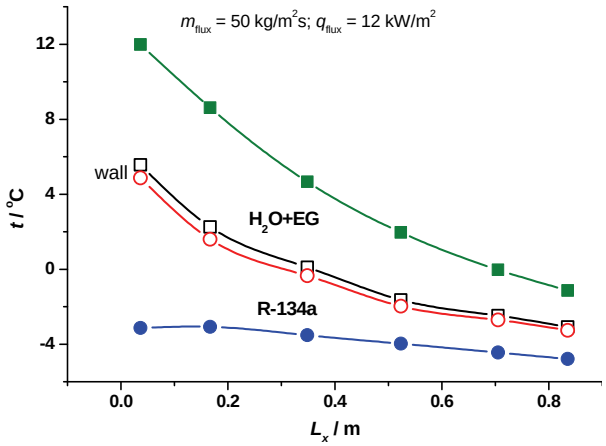

Fig. 4. Temperature profiles of R-134a and the ethylene glycol + water mixture (EG + H_2O) along the plate for concurrent flow.

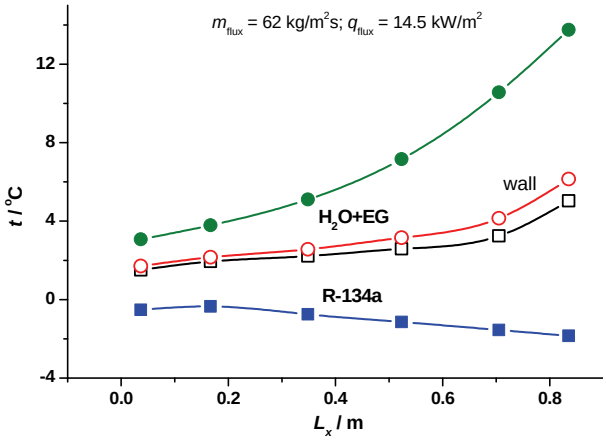

Fig. 5. Temperature profiles of R-134a and the ethylene glycol + + water mixture (EG + H_2O) along the plate for countercurrent flow.

The data acquisition system included a recorder (KETHLEY 2750 Multimeter), a power supply, and a personal computer. The temperature and voltage data were recorded and the collected data signals were then transmitted through a GPIB interface to a computer for further analysis. The experiment was monitored and controlled, and a preliminary balance check was realized by a routine written in the LabVIEW® program.

For calculation purposes, the plate area was divided into several segments along the vertical axis, on the borders of which thermocouples were installed on the cooling liquid side (Fig. 3). The energy balance for each of the segments was checked and the amount of heat transferred calculated. Since the heat transfer coefficients were calculated separately for each segment of the plate, they represent local values.

For every segment of the plate, the heat flux between the two fluids, q_x, was calculated using the water–glycol side data:

$$q_x = m_{\mathrm{h,c}} c_{p,\mathrm{h}} (T_{\mathrm{h},x,\mathrm{i}} - T_{\mathrm{h},x,\mathrm{o}}) / A_x \tag{1}$$

where $m_{\mathrm{h,c}}$ is the mass flow rate of the heating fluid through one channel and $T_{\mathrm{h},x,\mathrm{i}}$ and $T_{\mathrm{h},x,\mathrm{o}}$ are the inlet and outlet temperatures for one segment on the water–glycol side, respectively.

The area of the segment available for heat transfer, A_x, was calculated from the equation:

$$A_x = 2 L_x B_\mathrm{p} \Phi \tag{2}$$

where L_x is the length of the segment, B_p the plate width and Φ the area enhancement factor.

The local heat transfer coefficients for the single phase water–glycol mixture, $\alpha_{\mathrm{h},x}$ were determined as:

$$\alpha_{\mathrm{h},x} = \frac{q_x}{T_{\mathrm{h},x} - T_{\mathrm{w,h},x}} \tag{3}$$

The mean values of the fluid temperature, $T_{\mathrm{h},x}$, and wall temperature, $T_{\mathrm{w,h},x}$, in each segment, from the heating liquid side, were calculated from the measured inlet and outlet temperatures. Wall temperature from the refrigerant side, $T_{\mathrm{w,r},x}$, can be expressed as:

$$T_{\mathrm{w,r},x} = T_{\mathrm{w,h},x} - \frac{q_x \delta_\mathrm{p}}{\lambda_\mathrm{p}} \tag{4}$$

where δ_p and λ_p are the plate thickness and the thermal conductivity of the plate material, respectively.

Finally, local heat transfer coefficients, $\alpha_{\mathrm{r},x}$, were determined from the equation:

$$\alpha_{\mathrm{r},x} = T_{\mathrm{w,h},x} - \frac{q_x}{T_{\mathrm{w,r},x} - T^\mathrm{s}_{\mathrm{r},x}(p^\mathrm{s}_{\mathrm{r},x})} \tag{5}$$

where $T^\mathrm{s}_{\mathrm{r},x}$ is the refrigerant evaporation temperature, determined as a function of the saturation pressure, $p^\mathrm{s}_{\mathrm{r},x}$.

The saturation pressures at the chosen positions along the plate, $p^\mathrm{s}_{\mathrm{r},x}$, were calculated with an uncertainty of less than 10 % from the measured overall pressure drop.

Heat released from the heating fluid was partly used for heating the refrigerant to the saturation point, $q_{\mathrm{r,s,sens}}$, and partly for evaporation, $q_{\mathrm{r,s,lat}}$:

$$q_x = q_{\mathrm{r,s,sens}} + q_{\mathrm{r,s,lat}} \tag{6}$$

$$q_{\mathrm{r},x,\mathrm{sens}} = (T^\mathrm{s}_{\mathrm{r,x}} - T_{\mathrm{r,i}}) m_{\mathrm{r,c}} c_{p,\mathrm{r}} / A_x \tag{7}$$

$$q_{\mathrm{r},x,\mathrm{lat}} = m_{\mathrm{r,c}} \Delta h_\mathrm{v} \Delta x / A_x \tag{8}$$

In Eqs. (6)–(8), $m_{\mathrm{r,c}}$, represents the mass flow rate of the refrigerant through one channel, $T_{\mathrm{r,i}}$ is the refrigerant temperature and Δh_v is the specific enthalpy of vaporization.

Since the sub-cooling of the refrigerant was very small, usually a few degrees, the evaporation process began in the first segment of the plate. In this segment, both terms in Eq. (6)

were taken into account. In all of the following segments, the heat transferred to the refrigerant was used only for evaporation.

The change in the refrigerant vapor quality, Δx, was calculated from Eq. (9):

$$\Delta x = \frac{q_{\mathrm{r},x,\mathrm{slat}} A_x}{m_{\mathrm{r,c,h}} \Delta h_{\mathrm{v}}} \tag{9}$$

An uncertainty analysis was conducted on the basis of a procedure suggested by Moffat.[10] In the cases where a quantity, for example a heat transfer coefficient, could not be directly measured, it could be calculated from a set of measurements using a data fitting program represented by

$$y = f(x_1, x_2, x_3, \ldots x_N) \tag{10}$$

The directly measured variables, $(x_1, x_2, x_3, \ldots x_N)$ were presented in the following form:

$$x_i = x_{i,\mathrm{exp}} + u(x_i) \tag{11}$$

where $x_{i,\mathrm{exp}}$ is the measured value and $u(x_i)$ is the uncertainty based on specific probability.

The uncertainty in the calculated result has to be expressed with the same probability as that used in the estimation of the uncertainties in the measurements. According to Kline and McClintock,[11] the uncertainty in a calculated variable could be estimated with good accuracy using a root-sum-square combination of the effects of each of the individual inputs

$$u(y) = \sqrt{\sum_i \left(\left(\frac{\partial f}{\partial x_i} \right)_{x_{j \neq i}} u(x_i) \right)^2} \tag{12}$$

If the calculation from Eq. (12) involves an expression that is difficult to differentiate, the numerical approach may be used.[10]

For calculation purposes, Eq. (12) was transformed into a more suitable form:

$$u(y) = \sqrt{\sum_i \left(\frac{f(x_i + \delta) - f(x_i - \delta)}{2\delta} u(x_i) \right)^2} \tag{13}$$

where δ is the uncertainty interval.

More details on uncertainty analysis, calculation procedures and possible sources of uncertainties are given in literature.[12] The uncertainties of the thermophysical properties, as well as the uncertainties of the instrumentation, were taken into account and the evaluation results are summarized in Table I.

TABLE I. Estimated uncertainties

Parameter	Uncertainty	
	Relative	Absolute
Geometry of the plates		
Length, width and thickness	±1.5 %	$\pm 5\times10^{-5}$ m
Area	±4.5 %	$\pm 7\times10^{-5}$ m^2
Measuring instruments		
Temperature, PT100	±1.5 %	±0.1 °C
Temperature, TC	±5 %	±0.4 °C
Pressure transducers	±1 %	±200 Pa

TABLE I. Continued

Parameter	Uncertainty	
	Relative	Absolute
Water flowrate – turbine	±1.5 %	±1.0 min^{-1}
Water flowrate – multipulse positive displacement flowmeter	±0.5 %	±0.35 min^{-1}
R134 flowrate – ultrasonic flowmeter	±1 %	±0.15 min^{-1}
R134 flowrate – turbine	±2 %	±0.3 min^{-1}
Evaporation heat transfer		
Heat flux	±7.5 %	±1.7 kW m^{-2}
Vapor quality	±8.5 %	±0.05
Heat transfer coefficient	±15 %	±400 W m^{-2} K^{-1}

RESULTS AND DISCUSSION

A series of experiments on R-134a evaporation in a vertical PHE were conducted under different test conditions. The evaporation temperature was varied from –8.85 to 11.08 °C (saturation pressure from 0.21 to 0.43 MPa), the values of the refrigerant mass flux were between 40 and 90 kg m^{-2} s^{-1} and the corresponding values of the heat flux were from 9 to 15 kW m^{-2}. The experiments involved both concurrent and countercurrent flow of fluids through the evaporator. The working conditions of pressure, mass flux, heat flux and flow configuration during the experiments presented in this paper are summarized in Table II. The

TABLE II. Working conditions during the experiments

Name	Flow configuration	No. of compressor cylinders	Pressure MPa	Heat flux kW/m^2	Mass flux kg/m^2 s
LTEST 1	Concurrent	2	0.33–0.38	9	50
LTEST 2		2			60
LTEST 3		2			75
LTEST 4		2		10	50–55
LTEST 4a	Countercurrent	2			
LTEST 5	Concurrent	2			60
LTEST 5a	Countercurrent	2			
LTEST 6	Concurrent	2			65–70
LTEST 7		2			75–80
LTEST 8	Countercurrent	2			85
LTEST 9	Concurrent	2	0.38–0.44	10	55–60
LTEST 10		2			75–80
LTEST 11		2		11	55–60
LTEST 12		2			60–65
LTEST 13	Concurrent	4	0.25–0.27	12	45–50
LTEST 14	Countercurrent	4		13.5	60–70
LTEST 15	Concurrent	4	0.27–0.30	14.5	50–60
LTEST 15a	Countercurrent	4		14.5	

thermophysical properties of R134-a, necessary for the calculation of the local heat transfer coefficients and pressure drops, were taken from the REFPROP database.[13] The calculated values of the local heat transfer coefficients and pressure drop in each of the segments are graphically presented as functions of the mean vapor quality in the segment. The mean vapor quality, x_m, is the average vapor quality in the segment, estimated from the inlet value x_i and the vapor quality change Δx.

Influences of the refrigerant mass flux, heat flux, system pressure and flow direction on the evaporation heat transfer were analyzed closely. The influence of mass flux on the heat transfer coefficient in the case of concurrent flow is illustrated in Fig. 6. The heat transfer coefficient increases with increasing mass flux, more significantly for higher vapor quality, which would indicate the dominance of the convective boiling regime. A similar dependency is shown in Fig. 7 for the case of countercurrent flow. This tendency could be explained by the fact that with a higher vapor quality, the liquid film on the plate surface is thinner and since this film represents an additional resistance to heat transfer, the resulting effect on the heat transfer coefficient becomes favorable. This behavior is, however, contrary to the usual assumption that for small and medium vapor qualities, nucleate boiling is dominant, hence, the heat transfer coefficient is independent of mass flux and vapor quality. It should be noted here that these local values do

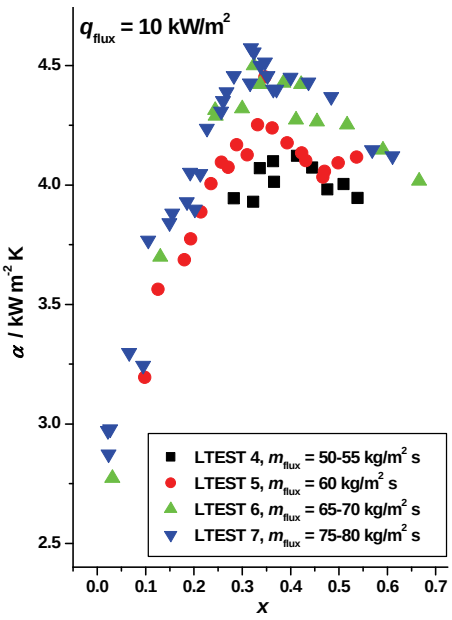

Fig. 6. Influence of mass flux on the heat transfer coefficient; concurrent flow.

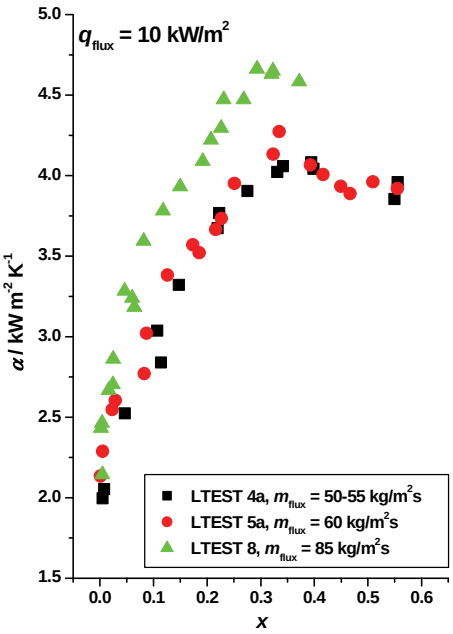

Fig. 7. Influence of mass flux on the heat transfer coefficient, countercurrent flow.

not correspond to the succeeding values along the plate length within one specific run. As the heat flux changes significantly along the plate, the results presented in Figs. 6–8 and 11–12 have been sorted into groups of similar mass and heat fluxes in order to be comparable.

The effect of heat flux on the heat transfer coefficient is shown in Fig. 8 for three heat fluxes, keeping the mass flux and system pressure constant. An increase in the heat flux induces an increase in the heat transfer coefficient, although the effect is not as significant as in the previous case of the influence of mass flux. For smaller heat and mass fluxes, the heat transfer coefficient seems to remain constant, or even slightly drop, after reaching the maximum value, as can be seen in Figs 6–8. A similar behavior was also noticed earlier.[12] For higher values of heat flux (Fig. 8, q_{flux} = 14.5 kW m^{-2}), this tendency does not seem to appear.

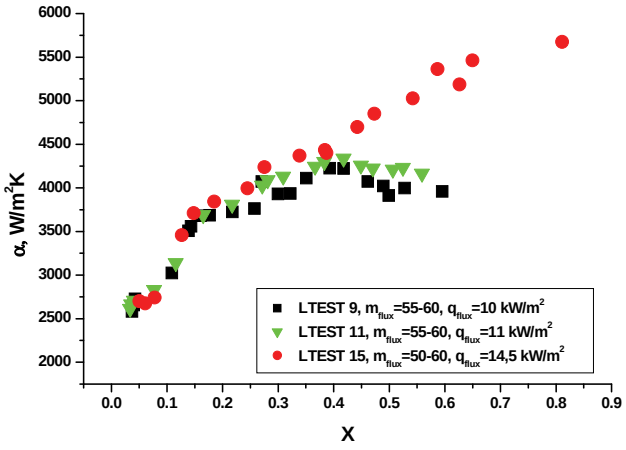

Fig. 8. Influence of heat flux on the heat transfer coefficient.

Concurrent and countercurrent flows are compared and analyzed in Figs. 9 and 10. The concurrent flow seems to give a more than 10 % higher heat transfer coefficient and higher outlet vapor quality than the countercurrent flow, under similar working conditions. In Fig. 10, the vapor quality is shown as a function of the plate position for two countercurrent flow cases and the corresponding concurrent flow cases. The vapor quality increases more quickly in the case of the concurrent flow, as a result of larger temperature difference at the entrance, as can be seen in Fig. 4.

The last analyzed parameter is the system pressure, which exhibits only a smaller influence on the heat transfer coefficient, as can be seen in Fig. 11.

The results of the series of measurements under various experimental conditions are compared with literature data[2] in Fig. 12. Although the measurements of Yan *et al.*[2] were conducted in a PHE of different geometry, satisfactory agreement was achieved.

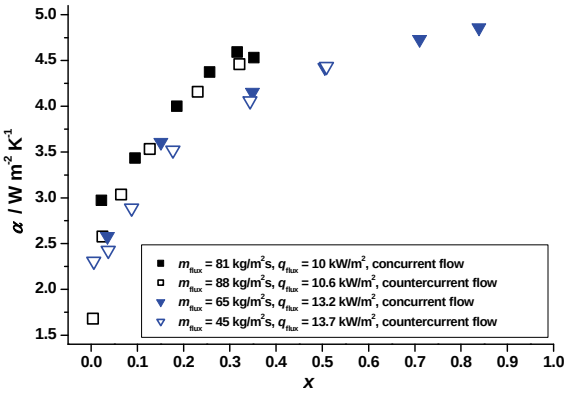

Fig. 9. Influence of flow configuration on the heat transfer coefficient.

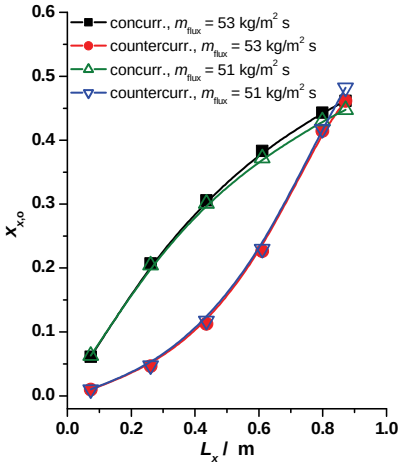

Fig. 10. Evolution of the local vapor quality along the plate for the concurrent and countercurrent flow configurations.

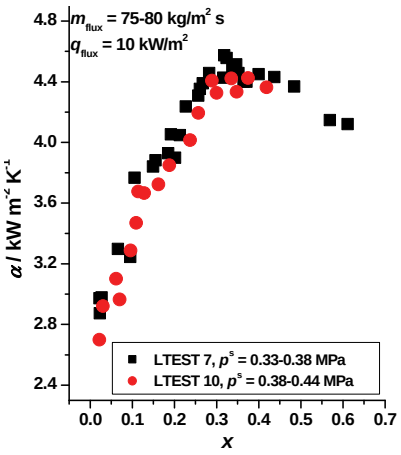

Fig. 11. Influence of system pressure on the heat transfer coefficient.

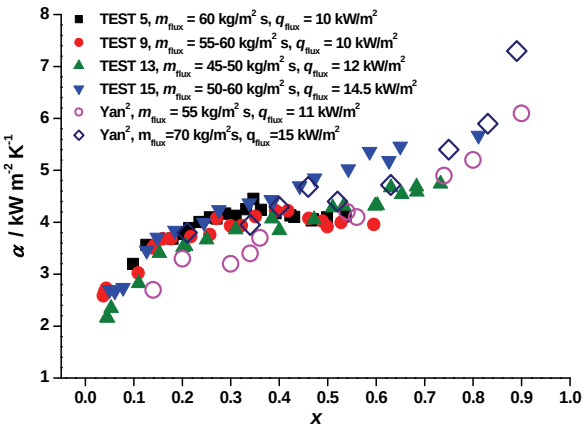

Fig 12. Comparison with previous experimental data.[1]

CONCLUSIONS

The effects of the refrigerant mass flux, heat flux, vapor quality, system pressure and flow configuration on the evaporation heat transfer coefficient were investigated and discussed. A special feature of the employed experimental setup was the measurement of temperature profiles along the plates inside the PHE, which allowed the calculation of local values of the heat transfer coefficient as a function of the vapor quality. As a result of the investigation, the following conclusions can be drawn:

– increasing the vapor quality induces an increase in heat transfer coefficient during R-134a evaporation;

– increasing the refrigerant mass flux and the imposed heat flux results in a better evaporation heat transfer coefficient, although the effect of the heat flux seems to be less significant;

– the question of the dominant boiling mechanism remains unresolved. It seems that convective boiling is dominant, at least for the smaller values of heat flux. More data are required to clarify the limits and the overlap of the relevant boiling mechanisms;

– the concurrent flow configuration gives higher values of the heat transfer coefficient than the countercurrent flow configuration, due to the higher temperature differences between both fluids and faster rise in vapor quality in the entrance region.

NOTATIONS

A	Heat transfer area, m^2
B_p	Width, m
c_p	Specific heat, $J/kg^{-1}\ K^{-1}$
L	Length, m
m	Mass flow rate, kg/s
m_{flux}	Mass flux, $kg/m^{-2}\ s^{-1}$
p^s	Saturation pressure, Pa
q	Heat flux, W/m^2
T	Temperature, K
T^s	Saturation temperature, K
T_w	Wall temperature, K
Δh_v	Specific enthalpy of vaporization, J/kg
$u(y)$	Measurement uncertainty
x	Mean vapor quality

Greek letters

α	Heat transfer coefficient, $W/m^{-2}\ K^{-1}$
δ_p	Thickness of the plate, m
Φ	Area enhancement factor due to corrugation
λ_p	Thermal conductivity of plate material, W/m K
ψ	Angle of plate corrugation, deg.

Subscripts

c Channel
i Inlet
h Hot water-glycol mixture
o Outlet
p Plate
r Refrigerant
x Segment

Acknowledgements. The experimental investigation presented in this paper was conducted in the Laboratory of the Institute of Thermodynamics at the Helmut Schmidt University of the Federal Armed Forces in Hamburg, Germany. The setup was partially supported by GEA Ecoflex GmbH, Sarstedt, Germany. The research visit of the first author in Hamburg was financed by the German Academic Exchange Bureau, DAAD. The results reported in this study are also a part of the scientific project financed by the Ministry of Science and Technological Development of the Republic of Serbia.

ИЗВОД

ЛОКАЛНИ КОЕФИЦИЈЕНТИ ПРЕЛАЗА ТОПЛОТЕ ПРИ ИСПАРАВАЊУ 1,1,1,2-ТЕТРАФЛУОРЕТАНА (R-134a) У ПЛОЧАСТОМ РАЗМЕЊИВАЧУ ТОПЛОТЕ

ЕМИЛА ЖИВКОВИЋ[1], STEPHAN KABELAC[2] и СЛОБОДАН ШЕРБАНОВИЋ[1]

[1]*Технолошко–металуршки факултет, Универзитет у Београду, Карнегијева 4, 11120 Београд и*
[2]*Helmut Schmidt Univerzitet u Hamburgu, Holstenhofweg 85, D-22043 Hamburg, Germany*

У овом раду је експериментално испитиван коефицијент прелаза топлоте при двофазном току расхладног флуида 1,1,1,2-тетрафлуороетана (R-134a) у вертикалном плочастом размењивачу топлоте. Површина плоче је подељена у неколико сегмената дуж вертикалне осе. У сваком од сегмената израчуната је локална вредност коефицијента прелаза топлоте и приказана у функцији средњег степена сувоће у сегменту. Захваљујући термопаровима постављеним дуж површине плоче, било је могуће одредити температурне профиле и расподелу степена сувоће дуж плоче. Испитивани су утицаји масеног флукса, топлотног флукса, радног притиска и конфигурације тока флуида на коефицијент прелаза топлоте и извршено је поређење са одговарајућим литературним подацима.

(Примљено 10. јуна, ревидирано 30. октобра 2008)

REFERENCES

1. E. Đorđević, S. Kabelac, S. Šerbanović, *J. Serb. Chem. Soc.* **72** (2007) 833
2. Y. Y. Yan, T. F. Lin, *ASME J. Heat Transfer* **121** (1999) 118
3. Y. Y. Hsieh, L. J. Chiang, T. F. Lin, *Intern. J. Heat Mass Transfer* **45** (2002) 1791
4. Y. Y. Hsieh, T. F. Lin, *ASME J. Heat Transfer* **125** (2003) 852
5. Y. Y. Hsieh, T. F. Lin, *Int. J. Heat Mass Transfer* **45** (2002) 1033
6. E. Đorđević, S. Kabelac, S. Šerbanović, *J. Serb. Chem. Soc.* **72** (2007) 1015
7. E. Đorđević, S. Kabelac, S. Šerbanović, *Chem. Pap.* **62** (2008) 78
8. E. Đorđević, S. Kabelac, *Int. J. Heat Mass Transfer* **51** (2008) 6235
9. R. Osterberger, B. Slipccevic, *Ki Klima – Kälte – Heizung* **11** (1990) 481
10. R. J. Moffat., *Exp. Therm. Fluid Sci.* **1** (1988) 3
11. S. J. Kline, F. A. McClintock, *Mechan. Eng.* **75** (1953) 3

12. M. Andre, *PhD Thesis*, Hannover University, Germany, 2004
13. M. O. McLinden, S. A. Klein, E. W. Lemmon, A. P. Peskin, *NIST thermodynamic and transport properties of refrigerant mixtures – REFPROP*, Version 6.0, NIST, Boulder, 1998.

Journal of the Serbian Chemical Society
JSCS@tmf.bg.ac.rs • www.shd.org.rs/JSCS

J. Serb. Chem. Soc. 74 (4) 441–453 (2009)
JSCS–3845

UDC 669.018.9:678.632:546.26–037
Original scientific paper

Composite material based on an ablative phenolic resin and carbon fibers

VINETA SREBRENKOSKA[1]*, GORDANA BOGOEVA-GACEVA[2] and DIMKO DIMESKI[1]

[1]*Faculty of Technology, Goce Delčev University, Krste Misirkov b.b., P.O. Box 201, 2000 Štip and* [2]*Faculty of Technology and Metallurgy, Sts.Cyril and Methodius University, MK-1000 Skopje, FYR Macedonia*

(Received 27 July 2007, revised 12 February 2009)

Abstract: In this study, a technological procedure for the production of a molding compound based on short carbon fibers and an ablative phenol–formaldehyde resin for high temperature application was optimized. The starting raw materials were characterized and molding compounds with different fiber/matrix ratios and different fiber lengths were obtained. From the different laboratory samples, molded parts were made by thermocompression. The basic mechanical and thermal properties of the composites were determined. From the obtained results, the optimal fiber/matrix ratio was determined for a production of molding compound for high temperature application. The molding process of the composite material was optimized and all the parameters for good mechanical properties and high thermal stability of the composite were obtained. Optimization of the composite molding process was performed by the application of a numerical method for a planned experiment, *i.e.*, a full three-factorial experimental design with variance of all three parameters (fiber length, temperature and time of the press cycle) on two levels. The obtained mechanical properties (flexural strength: 247 MPa, modulus: 27.6 GPa, impact resistance: 110 (for test moldings 10 mm×10 mm) and 91 kJ/m^2 (for test moldings 15 mm×15 mm)) justified the application of this composite material in the automotive, leisure, military and other industries where high temperature resistance and high mechanical strength is required.

Keywords: molding compound; phenol–formaldehyde resin; carbon fibers; composites; thermocompression.

INTRODUCTION

Phenolic composites reinforced with carbon fibers are mostly used for the production of responsible parts for various industries, among which those for high temperature applications are of particular significance.[1]

* Corresponding author. E-mail: vineta.srebrenkoska@ugd.edu.mk; srebrenkoska@yahoo.com
doi: 10.2298/JSC0904441S

Phenolic resins are known for their excellent thermal properties and chemical stability. In the field of advanced composite materials, phenolic based composites are known for their excellent flame resistance and are excessively used in the rocket industry because of their ablative characteristics.

Carbon fiber-reinforced phenolic resins are particularly effective in resisting high temperatures, since the resin evaporates and burns at the surface creating a thermal protective layer.[2–4]

The gel time (B-time) of phenolic resins at 150 °C ranges from 1 to 3 min. The weight loss at temperatures higher than 500 °C is about 40 %.[5]

Phenolic bulk molding compound (BMC) composites have excellent dimensional stability at high temperatures, excellent strength and heat insulation properties and high durability.[6,7]

The properties of short fiber–polymer composites are strongly dependent on the volume fraction and orientation distribution of the fiber and on the adhesion between the fibers and matrices. The fiber volume fraction is usually fairly tight controlled, although some segregation of fibers and polymer may occur during fabrication. The fiber orientation distribution changes when the molding conditions change, but it is difficult to control.[8,9]

Thermosetting short fiber reinforced composites have unique property combinations. Thus, typical strength values are in the range from 150 to 200 MPa and Young's modulus values are in the range 10–18 GPa.[8] The differences in fiber orientation distribution usually occurs within the moldings, particularly through the wall thickness, and this can lead to a composite with unequal mechanical properties.[8]

In this study, the influence of the basic processing parameters and length of the carbon fibers on the basic mechanical and thermal properties of phenol–formaldehyde composites were investigated. According to the test results, the optimal processing parameters of the compound were determined. One of the possible applications of such a composite is expected to be for the production of load-bearing and high temperature resistant parts of anti-hail rockets, such as the nozzles.

EXPERIMENTAL

For the production of the molding compound, a resol-type phenol formaldehyde resin (under the trade name Borofen DX 30), see Table I, and carbon fiber type T800 (under the trade name Toray), see Table II, were used.

Thermal characterization of the resin was performed by thermogravimetry, TG, (Thermo Gravimetric Analyzer 980 of Du Pont de Numerous), differential scanning calorimetry, DSC, (Perkin Elmer DSC-7 analyzer) and through determination of the gel time at different temperatures.

The molding compound was produced by mixing resin and carbon fibers (cut at different lengths, 25 and 50 mm) in a universal mix and knead machine (Werner Pfleiderer, Germany). The produced molding compound was dried at 80 °C for 30 min. The content of volatile materials was kept at 2–3.5 %.

TABLE I. Characteristics of phenol–phormaldehide resin, Borofen DX30 resol type, dissolved in 2-propanol

Property		Value
Appearance		Clear dark red solution
pH		7.3–7.8
Dry material content, %		68–72
Viscosity (Ford, 4mm), s		140–160
Content of free phenol, %		Max. 6
Content of free formaldehyde, %		Max. 2
Gel-time, min	120 °C	8.0–11
	150 °C	1.0–1.5

TABLE II. Characteristics of carbon fiber

Property	Value
Trade name	"Toray" T800H
Producer	Toray Industries Inc., Tokyo, Japan
Filaments count	12000
Density, g/cm^3	1.81
Tex count, g/1000m	445
Filament diameter, μm	8
Tensile strength, MPa	5.49
Tensile modulus, GPa	294
Elongation, %	1.9

The composites, *i.e.*, moldings, were made by direct thermocompression on a semi-industrial press (Triulzzi, Italy).

The mechanical and thermal properties of the moldings, such as impact resistance (DIN 53453), compression strength (DIN 53454), flexural strength (DIN 53457) and the modulus (DIN 53452), were determined and the heat deflection temperature was analyzed (according to the Marthens method) (DIN 53 462). For all mechanical tests, a universal testing machine (Schenk and Frank, Germany) was used.

A numerical experimental design method, *i.e.*, a full three-factorial experimental design (Table III) was applied for optimization of the processing of the molding compound. The fol-

TABLE III. Plan-matrix for three-factorial experimental design

Characteristics (conditions of experiment)			Experimental design matrix							
X_1 (temperature, °C)	X_2 (fiber length, mm)	X_3 (curing time, min)	X_0	X_1	X_2	X_3	X_1 X_2	X_1 X_3	X_2 X_3	X_1 X_2 X_3
140	25	15	+1	–1	–1	–1	+1	+1	+1	–1
160	25	15	+1	+1	–1	–1	–1	–1	+1	+1
140	50	15	+1	–1	+1	–1	–1	+1	–1	+1
160	50	15	+1	+1	+1	–1	+1	–1	–1	–1
140	25	35	+1	–1	–1	+1	+1	–1	–1	+1
160	25	35	+1	+1	–1	+1	–1	+1	–1	–1
140	50	35	+1	–1	+1	+1	–1	–1	+1	–1
160	50	35	+1	+1	+1	+1	+1	+1	+1	+1

lowing parameters were varied: molding temperature (X_1), fiber length (X_2) and press cycle time (X_3). The base level for the first factor (X_1) was 150 and the interval of variance 10; for the second factor (X_2), the base level was 37.5 and the interval of variance 12.5; for the third factor (X_3), the base level was 25 and the interval of variance 10. This experimental design enables mathematical definitions, in form of regression equations, of the mechanical properties of the moldings as functions of the processing parameters. The regression coefficients were statistically determined by application of the student's criteria and the significance of the regression equations was tested according to Fisher's criteria.[10]

RESULTS AND DISCUSSION

The dependence of the gel time on temperature, in range from 120 to 180 °C, is presented in Fig. 1, from which it can be seen that the gel time of the resin ranged from 500 to 50 s for 120 and 180 °C, respectively. A drastic reduction of the gel time started at temperatures above 140 °C. From the technical point of view, the determination of the gel time is important because it gives an indication of the curing process of the resin and the phase transition from the liquid to the solid state.

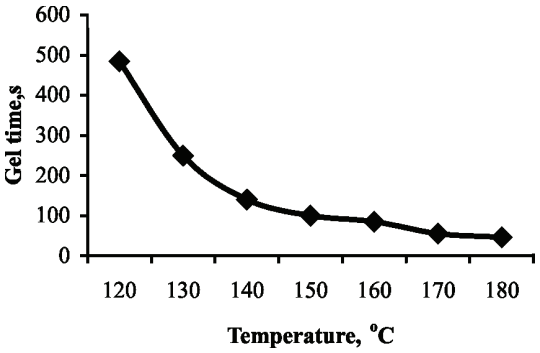

Fig. 1. Temperature dependence of the resin gel time.

Curing of thermosetting resins are highly exothermic processes. This is most critical when thick sections are molded. Addabbo *et al.*[11] studied the curing of a thermoset in a heated mold and showed the existence of a critical thickness below which the cycle time was not dependent on the thickness of the part. Williams *et al.*[12] found that the hottest plane does not always coincide with the centerline and that the cure cycle time is not necessarily proportional to the thickness of the part, as is often asserted. It is important to select the optimal wall temperature so that the mold can be filled without premature gelling, and so that the maximum temperature in the part remains below a ceiling temperature, when degradation or undesirable side reactions may occur. When the cycle time is determined by curing at the wall, it is important not to overestimate the critical conversion needed to eject the part from the mold. The material must reach a critical conversion level at which it is dimensionally stable and can be removed from the mold without losing its shape or blemishing its surface. This is often described as the end of the cure, though there will normally be further reaction ("curing") after this time.

The results of the weight loss of the resin, obtained at a constant heating rate of 20 °C/min in an inert atmosphere, are presented in Fig. 2. From the TG curve, four temperature ranges of weight loss of the resin DX 30 can be noticed. In the first range 0–130 °C, the weight loss was insignificant, 3 %; in the second range 130–230 °C, there was a sharp decline of the curve, *i.e.*, the weight loss of the resin was higher, approximately 15 %, and in the third range 230–400 °C, the weight loss of the resin was again insignificant. At a temperature of 400 °C, the weight loss was approximately 18 %. From 400 to 600 °C there was again a sharp decline of the weight loss curve, *i.e.*, the destruction of the resin rapidly increased. At a temperature of 550 °C, the weight loss of the resin was 33 %.

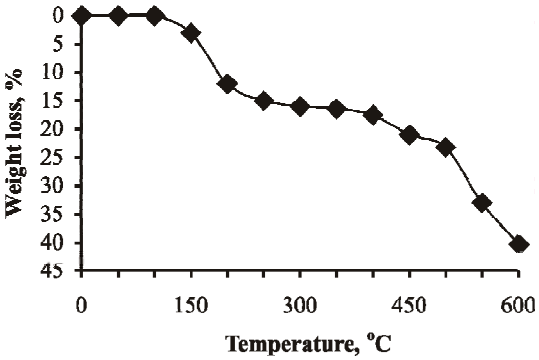

Fig. 2. Thermal degradation (TG) of the resin DX 30.

The preliminary characterization on the resin DX 30 was performed by DSC analysis. The basic temperature transitions: glass transition temperature, t_g, the cure reaction temperature, t_r, and the corresponding effects within these transitions, ΔC_p and $\Delta_r H$, were determined. The onset temperatures of the glass transitions and the curing reactions were also determined. All the obtained values are presented in Table IV.

TABLE IV. DSC results for t_g and t_r of the resin DX 30

t_g, °C	t_g (onset), °C	ΔC_p, J/g K	t_r, °C	t_r (onset), °C	$\Delta_r H$, J/g
73.5	67.7	0.60	189.8	155.4	83.4

According to the DSC results, the curing reactions of the phenolic resin begin at 155 °C. Based on these results, as well as on previous experience, the processing conditions for all samples were determined as follows: molding pressure, p = 75 bar, molding temperature, t = 160 °C and processing cycle time, τ = 20 min.

Under the influence of the heat flux, the resin becomes viscous (vitrification proceeds) and as heating progresses, it begins to degrade, producing a foaming carbon-mass and ultimately a porous carbon char. The char is a thermal insulation; the interior is cooled by the volatile material percolating through it from the decomposing polymer. Thus, a char forming resin acts as a self-regulating ablation radiator, providing thermal protection through cooling and insulation of the interior.[2,3,13,14]

From the molding compounds made with different fiber/matrix ratios (25/75, 45/55, 57/43, 67/33 and 75/25) and with different fiber lengths (25 and 50 mm), test samples were prepared and the basic mechanical and thermal properties of the composites were determined.

Mechanical properties

The analysis of the mechanics of short fiber composites is much more difficult than for continuously aligned fiber composites. There are two reasons for this. Firstly, the stress transfer between the fiber and the matrix is not uniform along the fiber, and there are fiber-end effects that can be neglected in continuous fiber composites but that are important in short fiber composites. Secondly, in short fiber composites, the fibers are never exactly parallel and may even have random orientation.[8,12,15]

Tables V and VI present the impact strength, *an* 10 and *an* 15, respectively, for the test sample-moldings as a function of the content and the length of the carbon fibers.

TABLE V. Impact strength *an* 10 (σ_{10} / kJ m^{-2}) of the moldings; x_{sr} – average value of 5, *SD* – standard deviation and C_v – coefficient of variation

Property	Fiber length: 25 mm				
	Fiber content, %				
	25	45	57	67	75
x_{sr}	105	120	136	122	133
SD	7.90	7.30	4.00	9.60	8.50
C_v	7.50	6.00	2.90	7.80	6.40
	Fiber length: 50 mm				
x_{sr}	128	130	163	125	156
SD	6.90	6.00	4.50	7.90	4.10
Cv	5.40	4.60	2.80	6.30	2.60

TABLE VI. Impact strength *an* 15 (σ_{15} / kJ m^{-2}) of the moldings; x_{sr} – average value of 5, *SD* – standard deviation and C_v – coefficient of variation

Property	Fiber length: 25 mm				
	Fiber content, %				
	25	45	57	67	75
x_{sr}	87.5	98.7	85.1	105	94.2
SD	5.20	9.50	7.80	14.9	7.50
C_v	5.90	9.60	9.20	14.2	8.00
	Fiber length: 50 mm				
x_{sr}	78.3	87.2	116	109	98.0
SD	9.90	5.30	9.20	9.90	7.60
C_v	12.6	6.10	7.90	9.10	7.70

The total impact energy that can be absorbed by the test specimens per unit area was determined. The absorbed energy is spent for the work done against

friction in displacing the fibers relative to the matrix, or the work required to cause elastic debonding is the principal source of this fracture energy. In short--fiber composites, the situation is often slightly clearer because the ends of many fibers must inevitably be nearer to a crack face than half the critical transfer length and these ends will therefore be pulled from the matrix as the composites separates into two or more pieces.[16–20]

The impact strength was higher for the composites with the longer fibers length. A certain deviation was noticed for the impact strength *an* 15 of the composites with fiber contents of 25 mass % and 45 mass % and a fiber length of 50 mm. The higher value for the coefficient of variation (C_v = 12.6) of the first test sample shows that the probable cause for this is the difference in the fiber orientation distribution through the wall thickness of the sample. The composite material with a higher fiber content becomes more rigid, which results in a lower impact strength. The best impact strength exhibited the test sample with 57 mass % fiber content and 50 mm fiber length.

The composites with the shorter fiber length had a higher compression strength, as can be seen inTable VII.

TABLE VII. Compression strength (σ_C / MPa) of the moldings

Property	Fiber length: 25 mm				
	Fiber content, %				
	25	45	57	67	75
x_{sr}	153	159	164	179	143
SD	1.50	0.80	1.40	2.40	5.20
C_v	1.00	0.50	0.90	1.30	3.60
	Fiber length: 50 mm				
x_{sr}	135	128	172	132	141
SD	3.40	6.40	18.5	10.0	6.20
C_v	2.50	5.00	10.8	7.50	4.40

On compression, the matrix is called upon to bear a large fraction of the applied load. Since the reinforcement is not continuous, local shear failure in the matrix initiates a buckling type of rupture as the interface begins to fail and fiber strengthening of the matrix is lost. In composites with poor fiber/matrix bonding, longitudinal splitting occurs but in a well-bonded composite, a substantial proportion of the compression strength may be retained.[13,15]

The highest value for the compression strength is registered for composites with fiber contents of 57–67 mass %, *i.e.*, 164–170 MPa (with fiber length of 25 mm). The deviation of the composite with longer fibers and with a fiber content of 57 mass % is probably the result of non-homogeneity and non-uniformity of the material. A proof for this is the value of the coefficient of variation (C_v = = 10.8), which is higher than the ones for the other composites. In the other com-

posites, the distribution of the fibers was more uniform, which resulted in more uniform compression strengths.

A typical value for the compression strength of phenolic resin/carbon fabric composites is 359 MPa. The obtained values for the compression strength of the BMC-based moldings were half of that of fabric-based composites. Continuous fibers composites show the best mechanical properties, due to the continuous form of the reinforcement and the fiber orientation distribution.[3]

The flexural strength and the modulus of the test moldings as a function of content and length the carbon fibers are presented in Figs. 3 and 4. As is known, the fiber length was selected in accordance with the composite application. The composites with shorter fibers have higher flexural strength and modulus. Generally, for the best mechanical properties, the fiber length should exceed a critical value but if the composite is overloaded, fiber fracture occurs until the fibers degrade to this value. The analysis showed that the fiber length and the aspect ratio should be as large as possible. The dimensions of the short fibers for reinforced composites must be chosen accordingly and steps must be taken during processing to maintain the lengths at adequate levels. The fiber length should not be too long or the fibers becomes entangled, causing problems with dispersion; if it is too short, the stress transfer area is too small and the fibers do not provide effective reinforcement.[8,15]

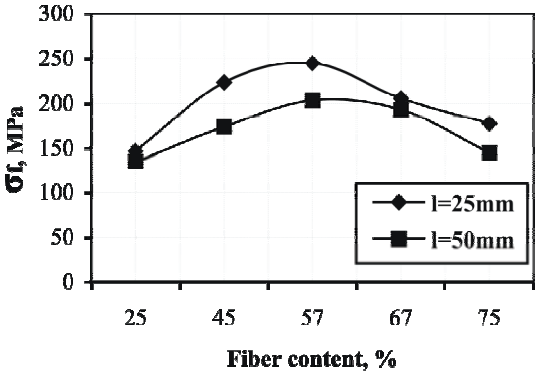

Fig. 3. Flexural strength of the moldings as a function of the fiber content.

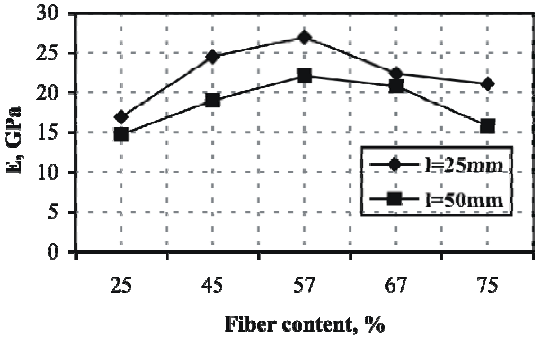

Fig. 4. Flexural modulus of the moldings as a function of the fiber content.

The composites with a fiber content of 57 mass % had the highest values for the flexural strength and the modulus.

Full factorial experimental design

In order to determine the optimal processing parameters and optimal fiber length, full factorial experimental design was applied. In accordance with the plan matrix, eight experiments with the variation of three parameters on two levels were performed. The results showed that the optimal fiber content is 60 mass %.[21] Some test results are presented in Figs 5 and 6.

The impact strength of 10 mm×10 mm test (σ_{10}) moldings *vs*. different fiber lengths at a constant temperature and curing time is presented in Fig. 5.

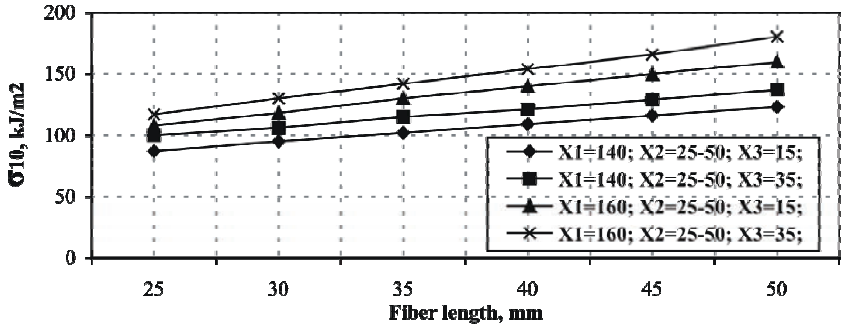

Fig. 5. Impact strength *vs*. fiber length (25–50 mm) at constant temperature and curing time.

Impact strength was higher for the composites with the longer fibers for both types of test moldings (10 mm×10 mm and 15 mm×15 mm). The regression equation (1) shows the individual contribution of the parameters: fiber length, press cycle temperature and press cycle time on the response function, *i.e*., impact strength.

$$y(X) = -32.80 + 0.46X_1 - 1.40X_2 - 0.66X_3 + 0.02X_2X_3 \quad (1)$$

The fiber length had the largest contribution to the impact strength, the contribution of the press cycle temperature was lower and the press cycle time had the lowest contribution. By increasing the fiber length and keeping the press cycle temperature at the upper level, an increase of the impact strength can be achieved at a shorter time.

The flexural strength *vs*. different fiber lengths at a constant temperature and curing time is presented in Fig. 6. An inverse dependence of the flexural strength as a function of the fiber length was found, Eq. (2):

$$y(X) = 58.76 + 1.65X_1 - 3.80X_2 - 0.83X_3 + 0.06X_2X_3 \quad (2)$$

The compression strength for all the tested moldings was also inversely dependant on the fiber length. All the results were in the 147 to 245 MPa range.[22]

From the regression equations, it can be seen that the fiber length had the greatest influence on the mechanical properties of the moldings, next the press cycle temperature and the smallest the press cycle time.

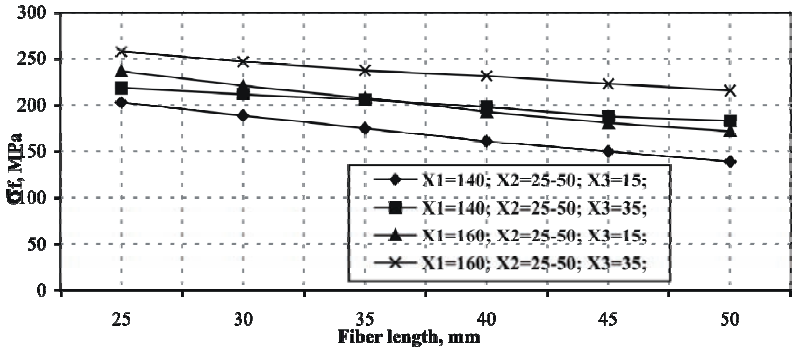

Fig. 6. Flexural strength *vs*. fiber length (25–50mm) at constant temperature and curing time.

Thermal properties

Thermogravimetry of the composites with carbon fiber contents of 25, 45, 57, 67 and 75 mass % and with a fiber length of 25 and 50 mm was performed (Table VIII).

From Table VIII, it can be noticed that the fiber content had a certain influence on the thermal degradation: the composites with the highest fiber content degraded at a higher temperature (the temperature of the excessive thermal degradation occurred at 350 °C, compared to 250 °C for the composite with lowest fiber content). The weight loss of the pure resin was higher compared to that of the fiber-reinforced resins. In addition, the weight loss of the composites with the highest fiber content was lower in comparison with the composites with the lowest fiber content: at 500 °C, the weight loss of the composite with a fiber content of 75 % was 14.6 %, and for the composite with a fiber content of 25 %, it was 22.8 % (see Fig. 7).

TABLE VIII. Weight loss (Δm / %) of the resin and the composites with fiber lengths of 25 and 50 mm

t / °C	Weight loss of Resin DX 30 mg	Fiber content, %							
		25	57	67	75	25	57	67	75
		Composite with l = 25 mm				Composite with l = 50 mm			
0–250	15	9.7	4.4	2.4	1.6	5.4	3.8	2.0	0.9
250–325	1.2	2.4	3.6	2.4	1.4	4.0	3.4	1.6	1.5
325–400	1.3	3.7	5.6	3.2	2.3	3.8	5.3	3.2	2.0
400–500	5.7	7.0	6.6	10.3	9.3	6.2	8.3	10.4	10.2

The heat deflection temperature was measured according to Martens for all moldings and it was found that, in all cases, the value exceed 210 °C, as reported earlier.[23]

The results of the thermal analysis of the composites show that they meet the criteria necessary for high temperature application.

As a result of the investigations, a rocket nozzle was produced and tested under real application conditions. It satisfied all service requirements.

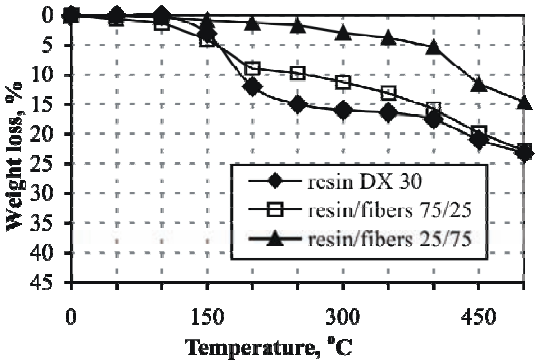

Fig. 7. Thermal decomposition (TG) of the resin DX 30 and composites with 25/75 and 75/25 fiber/matrix ratio.

CONCLUSIONS

The basic mechanical and thermal properties of phenolic resin composites with different fiber contents and fiber lengths were tested. The optimal results were obtained for composites with a carbon fiber content of approx. 60 %. The optimal processing parameters, determined using full factorial experimental design, were found to be: press cycle temperature: 160 °C, press cycle time: 25 min and fiber length: 25 mm.

The composite material based on the ablative phenolic resin and carbon fibers, produced using these processing parameters and a fiber length of 25 mm had the following mechanical properties: flexural strength, 247 MPa; modulus, 27.6 GPa; impact resistance 110 and 91 kJ/m^2 for test moldings of 10 mm×10 mm and 15 mm×15 mm, respectively.

The final composite parts based on this molding compound are recommended for various application in the automotive industry, military (for anti-hail rocket nozzles), leisure, *etc*.

И З В О Д

КОМПОЗИТНИ МАТЕРИЈАЛ НА БАЗИ АБЛАТИВНЕ ФЕНОЛНЕ СМОЛЕ И УГЉЕНИЧНИХ ВЛАКАНА

VINETA SREBRENKOSKA[1], GORDANA BOGOEVA-GACEVA[2] и DIMKO DIMESKI[1]

[1]Faculty of Technology, Goce Delčev University, Krste Misirkov b.b., P.O. Box 201, 2000 Štip and [2]Faculty of Technology and Metallurgy, Sts. Cyril and Methodius University, MK-1000 Skopje, FYR Macedonia

У раду је извршена оптимизација технологије за производњу пресованих композита на бази високотемпературне аблативне фенол–формалдехидне смоле и кратких угљеничних влакана. Окарактерисани су почетни материјали, као и добијени узорци композита са различитом количином и дужином угљеничних влакана. Применом термокомпресије израђени су

узорци, чија су основна механичка и термичка својства испитивана у раду. На бази добијених резултата одређен је оптималан однос влакно–матрица за производњу прес-масе за високо-температурну примену. На основу оптимизације процеса пресовања композитног материјала одређени су параметри процеса адекватни за добијање композита са високим механичким својствима и термичком стабилношћу. За оптимизацију процеса примењена је нумеричка метода планираног експеримента са варирањем три основна фактора: дужина влакна, температура и време пресовања. Механичке карактеристике композита (чврстоћа савијања од 247 MPa, модул од 27,6 GPa, ударна отпорност од 110 (за тест узорка 10mm×10 mm) и 91 kJ/m^2 (за тест узорка 15mm×15mm)) потврђују да је добијени материјал адекватан за примену у аутомобилској, војној и другим индустријама где су неопходне висока температурна издржљивост и задовољавајућа механичка чврстоћа.

(Примљено 27. јула 2007, ревидирано 12. фебруара 2009)

REFERENCES

1. W. Fritz, in *Proceeding of the first seminar on carbon materials*, Belgrade, Vinča, Yugoslavia, (1985), p. 10
2. R. M. Gill, *Carbon fibers in composite materials*, Iliffe Books, London, 1972, p. 42
3. S. M. Lee, *International encyclopedia of composites*, Vol. 1, VCH Publishers, New York, 1990, p. 97
4. A. Knop, W. Scheib, *Chemistry and application of phenolic resins*, Springer-Verlag, Berlin, 1979, p. 53
5. G. Clark, *Composites* **20** (1989) 209
6. J. Harding, L. M. Welsh, *J. Mater. Sci.* **18** (1983) 1810
7. R. L. Gellert, E. P. Pattie, S. D. Woodward, *J. Mater. Sci.* **33** (1998) 1845
8. S. K. De, J. R. White, *Short fiber – polymer composites*, Woodhead Publishers Ltd., Cambridge, 1996, p. 11
9. R. Kruger, in *Proceeding of the conference on composites reinforced fibers*, Novi Sad, Yugoslavia, (1987), p. 12 (in Serbian)
10. S. N. Sautin, Planning of experiments in chemistry and chemical technology, Khimya, Leningrad, 1973, p. 35 (in Russian)
11. H. E. Addabo, A. J. Rojas, R. J. J. Williams, *Polym. Eng. Sci.* **19** (1979) 835
12. R. J. J. Williams, A. J. Rojas, J. H. Marciano, M. M. Ruzo, H. G. Hack, *Polym. Plast. Technol. Eng.* **24** (1985) 243
13. A. X. Schmidt, C. A. Marlies, *Principles of high-polymer theory and practice*, McGraw-Hill, New York, 1948, p. 67
14. R. McCarthy, in *Proceeding of BPF Composites Congress*, Manchester, England, 1992, p. 157
15. M. O. W. Richardson, *Polymer engineering composites*, Applied Science Publishers Ltd., London, 1977, p. 38
16. S. T. Jenq, S. B. Wang, L. T. Sheu, *J. Reinf. Plast. Compos.* **11** (1992) 1127
17. G. A. Cooper, *J. Mater. Sci*. **5** (1970) 645
18. J. L. Helfet, B. Harris, *J. Mater. Sci*. **7** (1972) 494
19. D. Cawthorne, B. Harris, *Composites* **6** (1975) 25
20. G. P. Marshall, L. E. Culver, J. G. Williams, *Plast. Polym.* **75** (1969) 113
21. V. Sebrenkoska, G. Bogoeva Gaceva, D. Dimeski, in *Proceeding of the XVI congress of the chemists and technologists of Macedonia*, Skopje, FYROM, 1999, p. 231

22. V. Sebrenkoska, D. Dimeski, G. Bogoeva Gaceva, in *Proceeding of the conference polymer composites*, Zagreb, Croatia, 2001, p. 31
23. V. Sebrenkoska, G. Bogoeva-Gaceva, D. Dimeski, in *Proceeding of the XVII congress of chemists and technologists of Macedonia*, Skopje, FYROM, 2002, p. 58.

Journal of the Serbian Chemical Society
JSCS@tmf.bg.ac.rs • www.shd.org.rs/JSCS

J. Serb. Chem. Soc. 74 (4) 455–460 (2009)
JSCS–3846

UDC 504.521+665.7:628.516.000.57
Original scientific paper

Bioremediation of soil heavily contaminated with crude oil and its products: composition of the microbial consortium

JELENA S. MILIĆ[1*#], VLADIMIR P. BEŠKOSKI[1#], MILA V. ILIĆ[1#], SAMIRA A. M. ALI[2], GORDANA Đ. GOJGIĆ-CVIJOVIĆ[1#] and MIROSLAV M. VRVIĆ[2#]

[1]*Center of Chemistry, Institute of Chemistry, Technology and Metallurgy, University of Belgrade, Njegoševa 12, Belgrade and* [2]*Faculty of Chemistry, University of Belgrade, Studentski trg 12–16, Belgrade, Serbia*

(Received 23 June, revised 16 July 2008)

Abstract: Bioremediation, a process that utilizes the capability of microorganism to degrade toxic waste, is emerging as a promising technology for the treatment of soil and groundwater contamination. The technology is very effective in dealing with petroleum hydrocarbon contamination. The aim of this study was to examine the composition of the microbial consortium during the *ex situ* experiment of bioremediation of soil heavily contaminated with crude oil and its products from the Oil Refinery Pančevo, Serbia. After a 5.5-month experiment with biostimulation and bioventilation, the concentration of the total petroleum hydrocarbons (TPH) had been reduced from 29.80 to 3.29 g/kg (89 %). In soil, the dominant microorganism population comprised Gram-positive bacteria from actinomycete-*Nocardia* group. The microorganisms which decompose hydrocarbons were the dominant microbial population at the end of the process, with a share of more than 80 % (range 10^7 CFU/g). On the basis of the results, it was concluded that a stable microbial community had been formed after initial fluctuations.

Keywords: bioremediation; microbial consortia; petroleum contamination.

INTRODUCTION

Bioremediation is a modern method in which the natural ability of microorganisms is employed for the reduction of the concentration and/or toxicity of various chemical substances, such as petroleum derivatives, aliphatic and aromatic hydrocarbons, industrial solvents, pesticides and metals.[1]

Some microorganisms can decompose or transform the chemical substances present in petroleum and petroleum derivatives. Hydrocarbons from crude oil represent substrates for microorganisms, hence, when an accidental oil spill occurs,

* Corresponding author. E-mail: jelenamilic@chem.bg.ac.yu
# Serbian Chemical Society member.
doi: 10.2298/JSC0904455M

the number of hydrocarbon degrading microorganisms in the ecosystem increases. A single microorganism can degrade only certain types of petroleum compounds, but a mixed population – microbial community enables a higher level of degradation. Moreover, some substances can be decomposed only by cometabolism. In natural conditions, the presence of microorganisms that use the products of primary degradation is of particular importance. Further decomposition of crude oil is stimulated by the removal of its degradation products.

The speed and efficiency of bioremediation of a soil contaminated with petroleum and petroleum products depends on the number of hydrocarbon-degrading microorganisms in the soil. The most important factors for population growth are temperature, oxygen, pH, content of nitrogen and phosphorus, hydrocarbon class and their effective concentration. The degree and rate of biodegradation are influenced by the type of soil in which the process occurs.[2,3]

The specific metabolic activity of microorganisms in biodegradation experiments could be monitored by molecular biological methods, fatty acid profiling and by classical microbiological methods.[4] The first two methods enable an in detail taxonomical identification and an estimation of the non-cultivatable microorganisms. Despite being time consuming, classical methods are often used not only as a community characterization method but also as a tool for the isolation of microorganisms with the desired characteristics, particularly with substrates of low degradability.

Various authors studied metabolically active microbial communities – consortia during petroleum bioremediation under laboratory condition or as field experiments.[5–8] For example, Groudeva[8] studied the composition of a metabolically active consortium during bioremediation of water and wetlands contaminated with crude oil and heavy metals.

This work represents a continuation of our research in the area of the biodegradation of hydrocarbons in water and sediments on the area of the Pančevo Oil Refinery, Serbia.[9–12] This paper examines the composition of the microbial consortium during the *ex situ* experiment of bioremediation of 150 m^3 of soil heavily contaminated with petroleum and petroleum products from the oil refinery complex. The experiment was performed from May to October 2006.

EXPERIMENTAL

In the complex of the Oil Refinery Pančevo, a 150 m^3 in volume bioremediation pile ("open bioreactor") of a watertight base of soil contaminated with petroleum and petroleum derivatives was made. The natural aeration was stimulated by a system of perforated pipes. Bioremediation was performed by adding organic amendments – poultry manure as an N and P source and sawdust to improve the soil texture. The pile was protected from direct external influences by a "green house".

Every 15 days, six composite samples were prepared by the zigzag technique and used for all determinations.

The number of microorganisms was determined by the method of serial dilution on agar plates incubated on 26 °C. For the total count of bacteria, Nutrient agar was used; for fungi, Malt agar with streptomycin; for Gram-negative bacteria, McConkey agar[13] and for microorganisms which decompose hydrocarbons, mineral base medium[14] with different carbon sources: 2000 ppm diesel fuel, 375 ppm toluene or 200 ppm phenanthrene.[15] Actinomycetes, *Nocardia* and *Pseudomonas* as well as cellulose decomposing bacteria and fungi were determined using selective media.[16,17]

The content of total petroleum hydrocarbons (TPH) in the soil was determined according to DIN EN 14345:2004. Gas chromatography was performed using an Agilent 4890D instrument with an FID detector (column: HP-1MS 30 m×0.25 mm; carrier gas: hydrogen; injector temperature: 250 °C; initial temperature 40 °C, isothermal at 285 °C for 12 min).[18]

RESULTS AND DISCUSSION

The examined soil contaminated with petroleum and petroleum derivatives originated from the Oil Refinery Pančevo, where pollution is high and chronic. The soil initially contained 29.99±1.88 g TPH/kg. Since preliminary experiments (the results are not given) revealed the presence of hydrocarbon degraders in the soil, the growth of microorganisms was stimulated by the addition of N and P sources, aeration and mixing. In this way by application of bioremediation techniques, the concentration of total petroleum hydrocarbons (TPH) was reduced to 3.29 g/kg (89 %) during the five-and-half month experiment. The changes of the TPH as well as the GC chromatogram of the initial and the last sample are shown in Fig. 1.

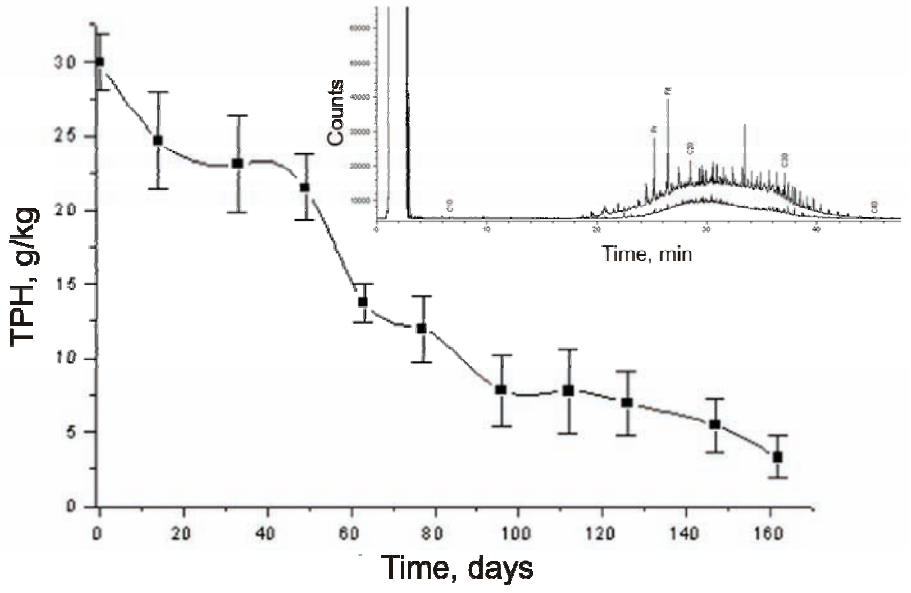

Fig. 1. Time course of the hydrocarbon concentration during the biodegradation process (all results are expressed on the basis of dry weight; mean±*SD*, *n* = 6).

It is noticeable that the highest reduction of TPH occurred in the period from the 49th to the 96th day. Apart from that, it should be pointed out that until the 63rd day, practically 50 % of the hydrocarbons had been decomposed. In initial sample, the hydrocarbons were partially biodegraded so that the part of easily degradable alkane fraction of crude oil was removed, which generally reduces the rate of further degradation.[3,6,12]

As mentioned in the introduction, studies of microbial consortia are of great importance for the best understanding of the biodegradation process. In this study, specific microorganisms groups were chosen on the basis of the general role of microorganisms in the cycling of carbon, nitrogen and phosphorus in soil. In addition, it is well known that the best hydrocarbon degraders are bacteria from the genera *Nocardia*, *Pseudomonas*, *Acinetobacter*, *Flavobacterium*, *Micrococcus*, *Arthrobacter*, *Corynebacterium*, *Achromobacter*, *Rhodococcus*, *Alcaligenes*, *Mycobacterium* and *Bacillus* and the fungi *Rhodotorulla*, *Fusarium*, *Aspergillus*, *Mucor*, *Penicillium*, *Candida* and *Sporobolomyces*.[19]

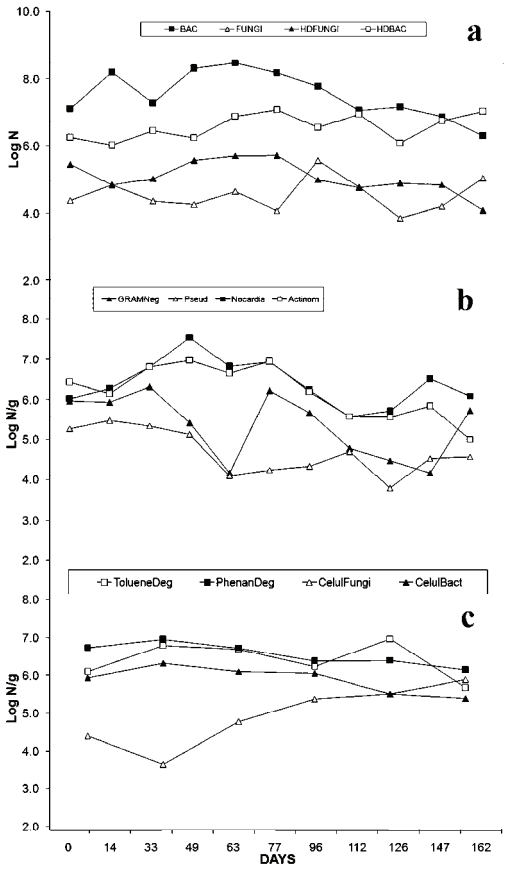

Fig. 2. Changes in the number of microorganisms during the biodegradation process (BAC-total, count of bacteria; FUNGI-total, count of fungi; HDBAC, hydrocarbon degrading bacteria; HDFUNGI, hydrocarbon degrading fungi; GRAM-Neg, Gram-negative bacteria; Pseud, *Pseudomonas*; Nocardia, *Nocardia*; Actinom, *Actinomycete*; ToluneneDeg, toluene degraders; PhenanDeg, phenanthrene degraders; CeluFungi cellulolytic fungi; CeluBac, cellulolytic bacteria).

The changes in the number of microorganisms in specific physiological-biochemical groups are given in Fig. 2. Most of these microorganisms were members of the indigenous microflora and some were introduced into the system with the organic amendments added to the soil in order to stimulate biodegradation.

The highest number of microorganisms was attained between 7–14 weeks of the process. The total number of bacteria in the soil during bioremediation was in range 10^7–10^8 CFU/g dry soil, and yeast and molds 10^4–10^5 CFU/g. The number of hydrocarbon-degrading bacteria was 10^6–10^7 CFU/g, and hydroarbon-degrading fungi 10^5–10^6 CFU/g (Fig. 2a). The number of toluene and pheanthrene degraders was 10^5–10^6 CFU/g (Fig. 2c). The dominant population in the soil comprised Gram-positive bacteria from the actinomycete-*Nocardia* group (10^6–10^7 CFU/g), while the total number of Gram-negative bacteria (10^5–10^6 CFU/g) and members of genus *Pseudomonas* (10^4–10^5 CFU/g) was slightly smaller (Fig. 2b). The number of cellulolytic bacteria was in the range 10^5–10^6 CFU/g, and that of cellulolytic fungi was 10^4–10^5 CFU/g (Fig. 2c).

On the basis of the results presented in Fig. 2, it is apparent that a stable microbial community was formed during the bioremediation experiment.

CONCLUSIONS

The metabolically active microbial community played the key role in the hydrocarbon biodegradation. The maximum number of microorganisms in the consortium was achieved from the 49th to the 96th day of the experiment and simultaneously, the highest rate of hydrocarbon degradation occurred. During the bioremediation experiment, there were no significant changes in the relationships between particular microbial populations, probably because the soil used in the experiment had a high hydrocarbon content and the contamination was aged and chronic.

Acknowledgements. The authors are grateful to the Ministry of Science and Technological Development (project No. 142018). Also, the authors would like to thank the Pančevo Oil Refinery and the Petroleum Industry of Serbia for their support.

И З В О Д

БИОРЕМЕДИЈАЦИЈА ЗЕМЉИШТА ТЕШКО КОНТАМИНИРАНОГ НАФТОМ И НАФТНИМ ДЕРИВАТИМА: САСТАВ КОНЗОРЦИЈУМА МИКРООРГАНИЗАМА

ЈЕЛЕНА С. МИЛИЋ[1], ВЛАДИМИР П. БЕШКОСКИ[1], МИЛА В. ИЛИЋ[1], SAMIRA A. M. ALI[2], ГОРДАНА Ђ. ГОЈГИЋ-ЦВИЈОВИЋ[1] и МИРОСЛАВ М. ВРВИЋ[2]

[1]Центар за хемију, Институт за хемију, технологију и металургију, Универзитет у Београду, Његошева 12, Београд и [2]Хемијски факултет, Универзитет у Београду, Студентски трг 12–16, Београд

Биоремедијација, процес који користи способност микроорганизама да разлажу токсични отпад, представља савремени тренд у пречишћавању загађеног земљишта и подземних вода. Ова технологија је веома ефикасна у уклањању контаминација нафтног загађивача. Циљ овог рада је био карактеризација конзорцијума микроорганизама при *ex citu* биоремедијацији земљишта тешко контаминираног нафтом и њеним дериватима из Рафинерије нафте,

Панчево. После 5,5 месеци експеримента уз биостимулацију и биовентилацију концентрација укупних угљоводоника нафте је смањена са 29,80 на 3,29 g/kg (89 %). Доминантна популација у земљишту укључује Грам-позитивне бактерије из групе актиномицета-*Nocardia*. Микроорганизми који разграђују угљоводонике на крају процеса су били доминантна микробна популација са уделом преко 80 % (ред величине 10^7 CFU/g). На основу ових резултата се може закључити да је, након почетних промена, дошло до формирања стабилне микробне заједнице.

(Примљено 23. јуна, ревидирано 16. јула 2008)

REFERENCES

1. A. Korda, P. Santas, A. Tenente, R. Santas, *Appl. Microbial. Biotechnol.* **48** (1997) 677
2. B. E. Rittmann, P. L. McCarty, *Enviromental Biotechnology: Principles and Applications*, McGraw-Hill, New York, 2001, p. 695
3. J. D. van Hamme, A. Singh, O. P. Ward, *Microbiol. Mol. Biol. Rev.* **67** (2003) 503
4. D. Spiegelman, G. Whissell, C. W. Greer, *Can. J. Microbiol.* **51** (2005) 355
5. H. Li, Y. Zhang, I. Kravchenko, H. Xu, C. Zhang, *J. Environ. Sci.* **19** (2007) 1003
6. R. Margensin, M. Hammerle, D. Tscherko, *Microb. Ecol.* **53** (2007) 259
7. S. J. MacNaughton, J. R. Stephen, A. D. Venosa, G. A. Davis, Y. J. Chang, D. C. White, *Appl. Environ. Microb.* **65** (1999) 3566
8. V. I. Groudeva, S. N. Groudev, A. S. Doycheva, *Int. J. Miner. Process* **62** (2001) 293
9. B. Jovančićević, M. Vrvić, J. Schwarzbauer, H. Wehner, G. Scheeder, D. Vitorović, *Water Air Soil Pollut.* **183** (2007) 225
10. B. Jovančićević, P. Polić, D. Vitorović, G. Scheeder, M. Techner, H. Wehner, *Fresenius Envir. Bull.* **10** (2001) 178
11. B. S. Jovančićević, M. P. Antić, T. M. Solević, M. M. Vrvić, A. Kronimus, J. Schwarzbauer, *Environ. Sci. Pollut. Res.* **12** (2005) 205
12. M. P. Antić, B. S. Jovančićević, M. Ilić, M. M. Vrvić, J. Schwarzbauer, *Environ. Sci. Pollut. Res.* **13** (2006) 320
13. C. H. Collins, P. M. Lyne, J. M. Grange, J. O. Falkinham, *Collins and Lyne's Microbiological methods*, Arnold, London, 2004, p. 45
14. C. Loser, H. Seidel, A. Zehnsdorf, U. Stottmeister, *Appl. Microbiol. Biotechnol.* **49** (1998) 631
15. J. Miličić-Terzić, Y. Lopez-Vidal, M. M. Vrvić, S. Saval, *Bioresource Technol.* **78** (2001) 48
16. E. Rosenberg, D. L. Gutnick, The Prokaryotes, *A Handbook on Habitas, Isolation and Identification of Bacteria*, Vol. 1, M. P. Starr, H. Stolp , H. G. Truper, A. Balows , H. G. Schlegel, Eds., Springer, Berlin, 1981, p. 903
17. I. D. Bossert, L. M. Shor, D. S. Kosson, *Manual of Environmental Microbiology*, 2nd Ed., C. J. Hurst, R. L. Crawford, G. R. Knudsen, M. J. McInerney, L. D. Stetzenbach, Eds., ASM Press, Washington, 2002, p. 934
18. DIN-EN 14345, *Characterization of waste – Determination of hydrocarbon content by gravimetry*, 2004
19. M. T. Balba, N. Al-Awadhi, R. Al-Daher, *J. Microbiol. Methods* **32** (1998) 155.

Journal of the Serbian Chemical Society
JSCS@tmf.bg.ac.rs • www.shd.org.rs/JSCS
J. Serb. Chem. Soc. 74 (4) 461–470 (2009) UDC 551.351.2+539.16:628.518:539.16:539.163
JSCS–3847 *Original scientific paper*

Radioactivity of sand from several renowned public beaches and assessment of the corresponding environmental risks

MIRJANA B. RADENKOVIĆ[1]*, SAEED MASAUD ALSHIKH[2], VELIBOR B. ANDRIĆ[1#] and ŠĆEPAN S. MILJANIĆ[2]

[1]*Vinča Institute of Nuclear Sciences, Radiation and Environmental Protection Department, P.O. Box 522, 11001 Belgrade and* [2]*Faculty of Physical Chemistry, University of Belgrade, P.O. Box 276, 11001 Belgrade, Serbia*

(Received 9 June, revised 17 July 2008)

Abstract: The radiological risk due to the presence of natural and man-made radionuclides in beach sands from several renowned seaside and riverbank public beaches was estimated in this study. The exposure levels to terrestrial radiation of the beaches were determined, as well as hazards due to human use of the analyzed sands in industry and in building constructions. Specific radionuclides concentrations in the sand samples were determined by standard gamma-spectrometry. The corresponding radiation hazards arising due to the use of sand as a building material were estimated by three different radiological hazard indices. The total absorbed gamma dose rate in the air was determined and the corresponding annual effective dose outdoors was estimated. The obtained data are relevant both from human health and environmental monitoring aspects.

Keywords: environmental radioactivity; sand; radiological hazard indices; gamma spectrometry; dose rates.

INTRODUCTION

Natural radioactivity is present in the human environment due to the presence of cosmogenic and primordial radionuclides in the Earth's crust. Cosmogenic radionuclides are produced by the interaction of cosmic-rays with atomic nuclei in the atmosphere, while primordial ones (terrestrial background radiation) were formed by the process of nucleo-synthesis. Only those radionuclides with half-lives comparable to the age of the Earth, *e.g.*, ^{40}K and members of the uranium and thorium series, can still be found today in different geological materials. Gamma radiation from these radionuclides represents the main external source of irradiation of the human body and can be considered as the largest contributor to the external dose absorbed by the population of the world.[1,2]

* Corresponding author. E-mail: mirar@vinca.rs
# Serbian Chemical Society member.
doi: 10.2298/JSC0904461R

Specific levels of terrestrial background radiation mainly depend on the geological and geographical conditions. Higher levels are usually associated with igneous rocks. Weathering and erosion of both igneous and metamorphic rocks in the environment transform rocks into sand deposits, some constituent minerals of which bear natural radionuclides from the uranium and thorium series as well as potassium. The study of the concentrations of radionuclides and their distribution in sands enables the assessment of radiological risk due to external human exposure to gamma radiation outdoors and inhalation of airborne radioactivity emanating from building constructions and dwellings.[3]

The objective of this was to identify and quantify significant gamma-emitting radionuclides in sand samples from several renowned world beaches, regardless their geo-genesis or chemical composition. For this purpose, sand samples were analyzed by high-resolution gamma-radiation spectrometry and the specific activities of ^{226}Ra, ^{232}Th and ^{40}K and ^{137}Cs were determined. In addition, energy-dispersive X-ray fluorescence spectrometry (EDXRFS) was employed for the semi-quantitative elemental analysis of the sands.

Based on radioactivity data, the radiation hazards due to the presence of specified radionuclides in sands commonly used in building constructions were assessed by the following three indices: the radium equivalent activity, Ra_{eq}, the representative level index I_r and the external hazard index H_{ex}.[4–6] Additionally, the absorbed dose rate in air (outdoors) due to the uniform distribution of isotopes from the uranium and thorium series and ^{40}K in the beach soil 1 m above the ground surface was estimated, and the corresponding annual effective dose (mSv yr^{-1}) outdoors calculated as the measure of human exposure to radiation.

EXPERIMENTAL

Sampling and sample preparation

Superficial beach sand samples were collected from the sea coastal sites: Ulcinj City Beach (Ulcinj, Montenegro), Great Beach of Ulcinj (Ulcinj, Montenegro), Patara (Xanthos, Turkey), Tayura (Tripoli, Libya), Tariq-City (Tripoli, Libya), Al Masif Albalady (Tripoli, Libya), Gargaresh (Tripoli, Libya), Qarit-City (Tripoli, Libya), Janzour (Tripoli, Libya), Manhattan Beach (Los Angeles, USA), Santa Monica City Beach (Santa Monica, USA), Great Salt Desert (Salt Lake City, USA) and Copacabana (Rio de Janeiro, Brazil). Some samples were collected from the Lido River Beach (Belgrade, Serbia), located on the sediment Great War Island (Danube River) in Belgrade.

The Great Beach of Ulcinj, Montenegro is located in the southern part of the eastern Adriatic Coast, 5 km from the city of Ulcinj. It is 13 km long and about 60 m wide, having an estimated capacity of about 15000 people. It is completely covered with finest grey sand.

The Patara Beach near Xanthos, Turkey is a 14.2 km long beach, located on the Mediterranean coast in southern Turkey, covered with fine brown sand and backed by swooping dunes.

All the Tripoli, Libya beaches mentioned in this work are parts of the very long Libyan Coast on the Mediterranean See, with sand of similar characteristics.

The Manhattan Beach and the Santa Monica City Beach are two parts of a much longer sandy beach in the Santa Monica Bay. The former is 3.4 km long, while the latter is 5.6 km. Both are located in the Los Angeles area (southern California).

The Copacabana, Brazil is probably the world's most famous and most popular beach. It is four kilometers long and located in the heart of Rio de Janeiro, covered with fine light yellow sand.

The Lido, Belgrade is a beach on the Great War Island, which is a river island, located in the heart of the city of Belgrade (Serbia), at the confluence of the Sava and Danube Rivers. It is covered with fine light gray sand, which can also be found on some other places along the Danube River in this area.

Approximately 2 kg of sand was taken from 50×50 cm^2 surface areas (0–10 cm depth) at each sampling site. Samples from the same location were taken at points distant from each other, about 1.5 to 2 km along the beaches. Samples from all the beaches were morphologically similar with 0.2–1.0 mm diameter grains. After the bulk samples had been homogenized and dried at 110 °C in an oven, about 450 cm^3 was transferred into cylindrical Marinelli beakers, weighed and sealed. After 40 days, the secular radioactive equilibrium between ^{226}Ra, ^{232}Th and their daughter products was attained and the samples were ready for gamma spectrometric counting.

Less than 1 g of each homogenized sample was used without further treatment for non-destructive energy dispersive X-ray fluorescence spectrometric measurements.

Analyses

The activity concentrations of ^{226}Ra, ^{232}Th and ^{40}K in the samples were determined by standard gamma spectrometry using a HP Ge detector (Canberra) with a 23 % relative efficiency and a resolution 1.8 keV for the 1332.5 keV ^{60}Co gamma line. The detector calibration was performed using a certified standard reference soil material (MIX-OMH-SZ, National Office of Measures, Budapest) spiked with ^{22}Na, ^{57}Co, ^{60}Co, ^{89}Y, ^{133}Ba and ^{137}Cs in a cylindrical Marinelli beaker geometry. The background radiation and the samples were counted for about 68000 s. The 295.21 and 351.92 keV ^{214}Pb and 1120.29 keV ^{214}Bi gamma ray lines were used to determine the ^{226}Ra activity concentration. The ^{232}Th activity concentration was determined using the 911.07 and 969.11 keV ^{228}Ac gamma lines. The activities of ^{40}K and ^{137}Cs were determined directly from the 1460.8 and 661.66 keV gamma lines, respectively. The uncertainties are given at the 90 % confidence level.

A more detailed characterization of the sands from the different locations was performed by semi-quantitative EDXRFS spectrometry. The measurements were performed using the Canberra spectrometry system with ^{109}Cd as the excitation source and a Si(Li) detector, with a detection limit of 10 ppm. Since the same measurement time of 60 ks was chosen for all samples, a comparison of the integrated areas of the peaks at wavelengths characteristic for the elements: Cl, K, Ca, Ti, Cr, Mn, Fe, Zn, Br, Rb, Sr, Y and Zr, was possible for samples originating from very different areas of the world.

Gamma irradiation hazard indices and dose rates estimation

Three different indices were calculated, *i.e.*, the radium equivalent activity, Ra_{eq}, the representative level index I_r and the external hazard index H_{ex}. In addition, the absorbed dose rate, D, in the air was estimated.

The radium equivalent activity, Ra_{eq}, defined by Beretka and Mathew (1985),[4] is the most widely used index, which can be calculated according to the equation:

$$Ra_{eq} = c_{Ra} + \frac{10}{7} c_{Th} + \frac{10}{130} c_K \quad (1)$$

where c_{Ra}, c_{Th} and c_K are the activity concentrations of ^{226}Ra, ^{232}Th and ^{40}K in Bq kg^{-1}, respectively. Here, it is assumed that the same dose rate is produced from 370 Bq kg^{-1} ^{226}Ra or 259 Bq kg^{-1} ^{232}Th or 4810 Bq kg^{-1} ^{40}K present in the same matrix.

The representative level index I_r is defined by equation:[5]

$$I_r = \frac{1}{150} c_{Ra} + \frac{1}{100} c_{Th} + \frac{1}{1500} c_K \quad (2)$$

This index value must be less than unity in order to keep the radiation hazard insignificant, *i.e.*, the radiation exposure due to radioactivity from construction materials is limited to 1 mSv yr-1.

The external hazard index H_{ex} is given as:[6]

$$H_{ex} = \frac{1}{370} c_{Ra} + \frac{1}{259} c_{Th} + \frac{1}{4810} c_K \quad (3)$$

The total absorbed dose rate, *D*, in the air (outdoors) due to the uniform distribution of all the ^{226}Ra and ^{232}Th series, and ^{40}K in the beach soil 1 m above the ground surface was estimated by the formula:[7]

$$D = 0.427 c_U + 0.662 c_{Th} + 0.0432 c_K \quad (4)$$

where the constants represent conversion factors (nGy h^{-1} *per* Bq kg^{-1}) calculated by the Monte Carlo technique for radionuclides and c_U is average activity concentration of ^{238}U.

RESULTS AND DISCUSSION

Contents of natural and man-made radionuclides

The obtained values of the activity concentrations (Bq kg^{-1}) determined for the radionuclides ^{226}Ra, ^{232}Th, ^{40}K and ^{137}Cs in the analyzed sand samples are listed in Table I. The presented results of the contents of radionuclides in sand samples, randomly taken from both sea and river beach areas of tourist zone, show low activity concentration of ^{226}Ra and ^{232}Th, originating from the natural radioactive series, as well as naturally occurring ^{40}K. The minimum activity concentration 2.24 Bq kg^{-1} of ^{226}Ra was determined in the sand sample from the Copacabana Beach (Brazil), while the maximum value of 15.9 Bq kg^{-1} was found in the sand from the Great Beach of Ulcinj (Montenegro). The activity concentrations of ^{232}Th were in the range 2.6–17.3, with a minimum value for the Patara Beach (Turkey) and a maximum for the Manhattan Beach (USA). The differences are not so significant and are attributable to the geochemical composition and origin of rock types in a particular area.

The content of ^{40}K depended much more on the location and had the lowest value of 18.9 Bq kg^{-1} for the sand sample from the Copacabana Beach (Brazil) and relatively low values for Tripoli (Libya) and Patara (Turkey) sands. Values up to 696 Bq kg^{-1} may be noticed at the other sites, probably due to the presence of K-feldspar in the mineral matrix of the sand deposits.

TABLE I. Activity concentrations of ^{226}Ra, ^{232}Th, ^{40}K and ^{137}Cs in the sand samples collected in the period from 2004 to 2007

Sampling site		c / Bq kg^{-1}			
		^{226}Ra	^{232}Th	^{40}K	^{137}Cs
Ulcinj, Montenegro	City Beach	7.4 ±1.0	9.0 ± 1.2	192 ± 18	0.43± 0.09
	Great Beach 1	15.9 ± 2.0	14.60 ± 1.9	398 ± 37	1.83 ± 0.30
	Great Beach 2	11.2 ± 1.6	17.2 ± 2.2	412 ± 38	2.16 ± 0.31
	Great Beach 3	8.9 ± 1.2	13.4 ± 1.7	338 ± 31	1.19 ± 0.20
	Great Beach 4	9.6 ± 1.2	11.8 ± 1.5	276 ± 26	2.32 ± 0.29
	Great Beach 5	10.0 ± 1.3	12.4 ± 1.6	314 ± 29	2.49 ± 0.35
	Great Beach 6	10.4 ± 1.3	12.6 ± 1.6	251 ± 24	1.99 ± 0.27
Lido, Danube River, Belgrade, Serbia	1	7.9 ± 1.0	6.41 ± 0.87	299 ± 27	1.41 ± 0.19
	2	7.6 ± 1.0	8.8 ± 1.1	307 ± 28	1.06 ± 0.17
	3	8.4 ± 1.1	9.7 ± 1.2	278 ± 25	0.59 ± 0.12
USA	Manhattan Beach, Los Angeles, CA	5.0 ± 1.1	17.3 ± 2.4	457 ± 44	0.65 ± 0.16
	City Beach, Santa Monica, CA	11.1 ± 1.8	12.5 ± 2.2	696 ± 65	1.40 ± 0.26
	Great Salt Desert, Utah	9.4 ± 1.7	11.2 ± 1.9	230 ± 25	12.8 ± 1.4
Patara Beach, Xanthos, Turkey		10.8 ± 1.2	2.56 ± 0.53	54.5 ± 6.0	<0.3
Tripoli, Libya	Tayura-City Beach	8.5 ± 1.1	4.39 ± 0.73	54.2 ± 5.9	<0.3
	Tariq-City Beach	12.2 ± 1.4	8.4 ± 1.0	82.4 ± 8.4	<0.3
	Al Masif Albalady, Tower	7.24 ± 0.89	5.91 ± 0.82	62.4 ± 6.7	<0.3
	Al Masif Albalady	14.0 ± 1.6	3.42 ± 0.62	77.6 ± 8.0	<0.3
	Gargaresh, City	7.37 ± 0.90	3.08 ± 0.51	27.5 ± 3.3	<0.3
	Qarit-City Beach	7.15 ± 0.87	3.48 ± 0.54	31.0 ± 3.6	<0.3
	Janzour	11.28 ± 1.29	3.70 ± 0.64	80.5 ± 8.2	<0.3
Copacabana, Rio de Janeiro, Brazil		2.24 ± 0.36	6.14 ± 0.75	18.9 ± 2.4	<0.3

These results are in accordance with some previous studies,[8–10] as well as world quoted values for sand minerals: 25 (7–50), 25 (10–50) and 370 (100–700) Bq kg^{-1} for ^{226}Ra, ^{232}Th and ^{40}K, respectively.[11] The unexpectedly low natural radionuclide content found in the Brazilian sand from the Copacabana Beach suggests the presence of light minerals, such as quartz and feldspar, as the source rather than pre-Cambrian period basement rocks deposits.[12]

Main differences in the elemental composition of the analyzed sand samples are shown in Figs. 1 and 2, where the results of X-ray fluorescence spectrometry are arranged into two groups. It can be noticed that sands from the Mediterranean region (Fig. 2) have somewhat higher Ca contents, indicating the carbonate nature of the sediment rocks, while the sands from the American continent have noticeable Zr contents. The somewhat higher values of the Fe concentrations in the sand samples may have been caused by traffic-related pollution of the urban areas where the beaches are located. All other values are of the same order of

magnitude and the differences are insignificant. These results may be considered only as an indication due to the limitations of the method used and limited number of samples.

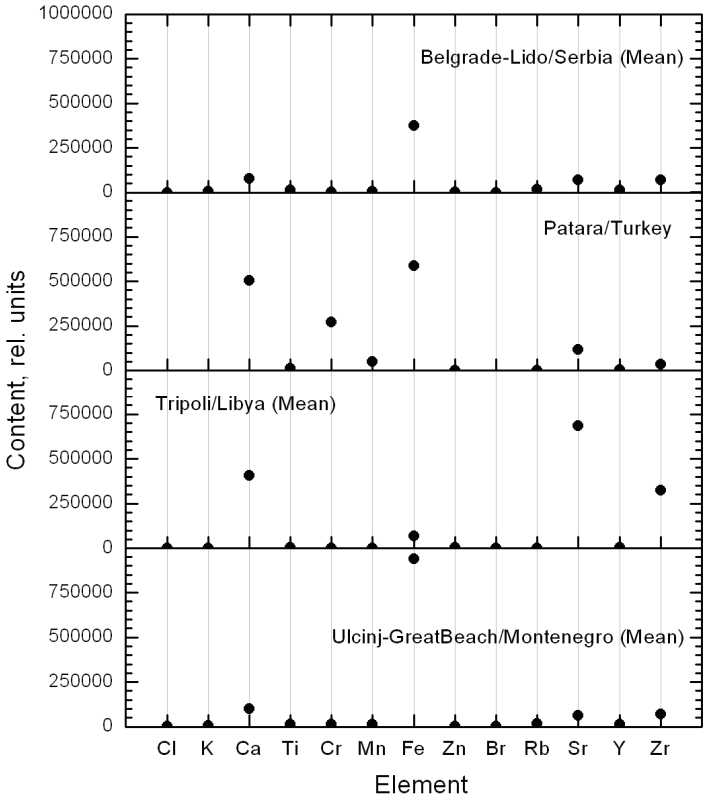

Fig. 1. Contents of some elements in the analyzed sea-and river-sand samples from the Mediterranean region.

The activity concentration of the man-made radionuclide ^{137}Cs was in the range 0.43–2.49 Bq kg^{-1} in the analyzed sand samples, with a maximum value of 12.8 Bq kg^{-1} measured in the Great Salt Desert, Utah, USA, sample radioactive cesium, a fission product with a half-life of 30.2 yr, is mostly present in the environment due to the Chernobyl nuclear accident in 1986, but it may be assumed that nuclear probes performed during sixties in this part of the world (in the neighboring state of New Mexico) also contributed. The activity concentration of ^{137}Cs becomes lower if compared with some previous results[13,14] for location sites in Serbia and Montenegro, mostly due to the selective migration and geochemical fractionation of cesium in sediments. In general, the ^{137}Cs contents were very low in all samples, especially in the Turkish and Libyan sands, where they were below the minimal detectable value.

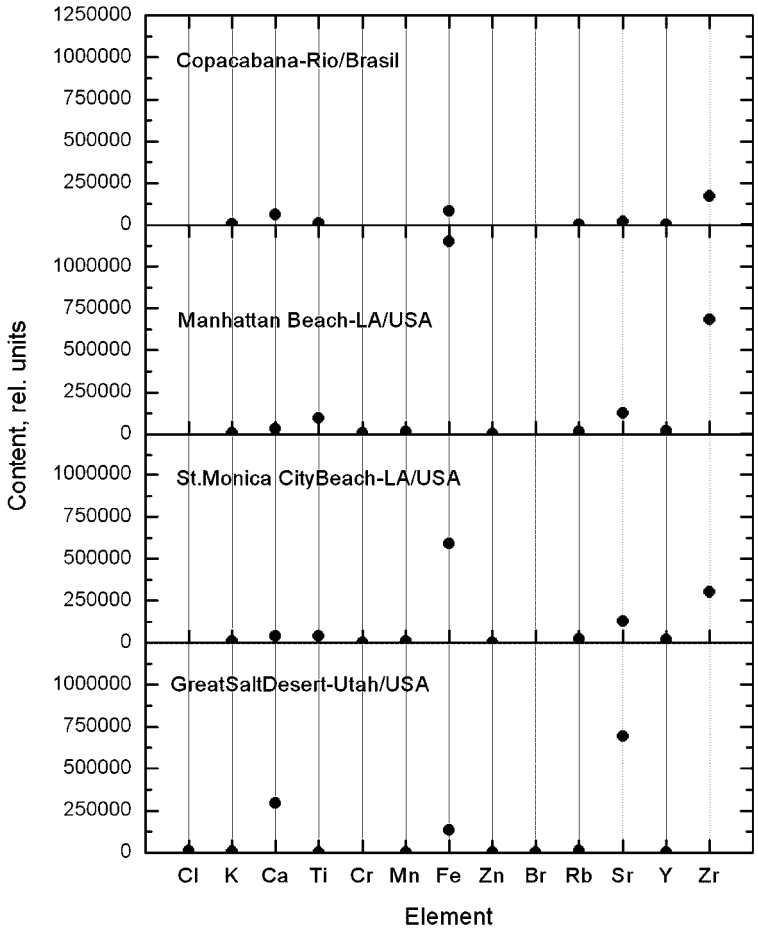

Fig. 2. Contents of some elements in the analyzed sea-sand samples from the American Continent region.

Gamma irradiation hazard indices and dose rates

As river- and sea-beach sand minerals are used in industry and in building constructions, the gamma-ray radiation hazards due to the specified radionuclides were assessed by three indices, *i.e.*, the radium equivalent activity, Ra_{eq}, the representative level index, I_r, and the external hazard index, H_{ex}. The results obtained for the sands studied in this work are presented in Table II.

The presented results show that the Ra_{eq} index for the sand samples had values in the range 12.5 (Rio de Janeiro, Brazil) to 82.5 Bq kg^{-1} (Santa Monica, CA, USA), compared with the population-weighted average value of global primordial radiation of 59 nGy h^{-1}.[2] This index is related to the external gamma dose and internal dose due to radon and its daughter products and allows a comparison of the activities and radiological effects of sediment samples containing

different concentrations of radionuclides. The calculated values of I_r were within 9.0–66 % of the 1 Bq kg^{-1} limit value.

TABLE II. Gamma radiation hazard indices for the analyzed sands: radium equivalent activity, Ra_{eq}, representative level index, I_r, external hazard index, H_{ex}, and the corresponding absorbed dose, D, and annual effective dose, E

Sampling site		Ra_{eq} Bq kg^{-1}	I_r Bq kg^{-1}	H_{ex} Bq kg^{-1}	D nGy h^{-1}	E mSv yr^{-1}
Ulcinj, Montenegro	City Beach	35.1	0.27	0.18	17.4	0.041
	Great Beach 1	67.4	0.52	0.09	33.7	0.021
	Great Beach 2	67.5	0.52	0.18	33.9	0.041
	Great Beach 3	54.1	0.42	0.15	27.3	0.033
	Great Beach 4	47.7	0.37	0.13	23.8	0.029
	Great Beach 5	51.9	0.40	0.14	26.1	0.032
	Great Beach 6	47.7	0.36	0.13	23.6	0.029
Lido, Danube River, Belgrade, Serbia	1	40.0	0.32	0.11	20.6	0.025
	2	43.7	0.34	0.12	22.3	0.027
	3	43.7	0.34	0.12	22.0	0.027
USA	Manhattan Beach, Los Angeles, CA	64.9	0.51	0.18	33.4	0.041
	City Beach, Santa Monica, CA	82.5	0.66	0.22	43.1	0.053
	Great Salt Desert, Utah	43.2	0.33	0.12	21.4	0.026
Patara Beach, Xanthos, Turkey		18.7	0.13	0.05	8.7	0.011
Tripoli, Libya	Tayura-City Beach	19.0	0.14	0.05	8.9	0.011
	Tariq-City Beach	30.5	0.22	0.08	14.3	0.018
	Al Masif Albalady, Tower	20.5	0.15	0.06	9.7	0.012
	Al Masif Albalady	24.9	0.18	0.07	11.6	0.014
	Gargaresh, City	13.9	0.10	0.04	6.4	0.008
	Qarit-City Beach	14.5	0.10	0.04	6.7	0.008
	Janzour	22.8	0.17	0.06	10.7	0.013
Copacabana, Rio de Janeiro, Brazil		12.5	0.09	0.03	5.8	0.007

All gamma-ray absorbed dose rates, D, presented in Table II are within the range 5.8–43.1 nGy h^{-1}, *i.e.*, less than the world average of 55 nGy h^{-1}.[11] Finally, in order to obtain a rough estimate for the annual effective dose outdoors, the conversion coefficient from the absorbed dose in air to the effective dose and the outdoors occupancy factor had to be taken into account. As in the UNSCEAR reports (1993, 2000), a conversion coefficient of 0.7 Sv Gy^{-1} from the absorbed dose in air to the effective dose received by adults and an outdoor occupancy factor of 0.2 were used. The annual effective dose E (mSv yr^{-1}) outdoors was then calculated using the following formula:

$$E = D \times 24\ \text{h} \times 365.25\ \text{d} \times 0.2 \times 0.7 \times 10^{-3} \quad (5)$$

The obtained E values for all the analyzed sands were lower than the world-wide outdoors annual effective dose average of 0.07 mSv yr^{-1},[2] and also below the value of 1.0 mSv yr^{-1}, recommended by the International Commission on Radiological Protection[15] as the maximum allowed annual dose for the public.

CONCLUSIONS

This study showed that the analyzed sand samples from different world beaches had various radionuclide contents within the average world quoted values. The corresponding gamma radiation hazard indices and annual effective dose were below those of the limits considered acceptable.

Acknowledgements. The authors gratefully acknowledge the financial support of the Ministry of Science of the Republic of Serbia through Projects No. 142050 and 142067.

ИЗВОД

РАДИОАКТИВНОСТ ПЕСКА СА НЕКОЛИКО ПОЗНАТИХ ЈАВНИХ ПЛАЖА И ПРОЦЕНА ОДГОВАРАЈУЋИХ РИЗИКА ПО ЖИВОТНУ СРЕДИНУ

МИРЈАНА Б. РАДЕНКОВИЋ[1], SAEED MASAUD ALSHIKH[2], ВЕЛИБОР Б. АНДРИЋ[1] И ШЋЕПАН С. МИЉАНИЋ[2]

[1]Институт за нуклеарне науке "Винча", Лабораторија за радиолошку заштиту и заштиту животне средине, п.пр. 522, 11001 Београд и [2]Универзитет у Београду, Факултет за физичку хемију, п.пр. 276, 11001 Београд

У раду су приказани резултати процене радиолошке опасности која је последица присуства природних и произведених радионуклида у песку са неколико познатих морских и речних јавних плажа. Одређени су нивои изложености људи зрачењу из песка на плажама као и опасност услед коришћења анализираних песака у индустрији и грађевинарству. Концентрације значајнијих радионуклида у узорцима су одређене стандардном гама-спектрометријом. Радиолошка опасност услед коришћења песка као грађевинског материјала процењена је на основу три индикатора радиолошког ризика. Одређена је укупна апсорбована доза гама зрачења у ваздуху и процењене су одговарајуће годишње ефективне дозе услед боравка на плажама. Добијени резултати су битни са аспекта заштите људског здравља као и мониторинга животне средине.

(Примљено 9. јуна, ревидирано 17. јула 2008)

REFERENCES

1. United Nations Scientific Committee on the Effects of Atomic Radiation, UNSCEAR, *Sources, Effects and Risks of Ionizing Radiation*, United Nations, New York, 1993
2. United Nations Scientific Committee on the Effects of Atomic Radiation, UNSCEAR, *Sources and Effects of Ionizing Radiation*, United Nations, New York, 2000
3. M. N. Alam, M. I. Chowdhury, M. Kamal, S. Ghose, M. N. Islam, M. N. Mustafa, M. M. H. Miah, M. M. Ansary, *J. Environ. Radioact.* **46** (1999) 243
4. J. Beretka, P. J. Mathew, *Health Phys.* **48** (1985) 87
5. Nuclear Energy Agency Organization for Economic Cooperation and Development, NEA-OECD, *Exposure to Radiation from Natural Radioactivity in Building Materials*, Report by the NEA Group of Experts, OECD, Paris, 1979

6. R. Veiga, N. Sanches, R. M. Anjos, K. Macario, J. Bastos, M. Iguatemy, J. G. Aguiar, A. M. A. Santos, B. Mosquera, C. Carvalho, M. Baptista Filho, N. K. Umisedo, *Radiat. Meas.* **41** (2006) 189
7. United Nations Scientific Committee on the Effects of Atomic Radiation, UNSCEAR, *Sources and Effects of Ionizing Radiation*, United Nations, New York, 1988
8. I. Bikit, J. Slivka M. Vesković, E. Varga, N. Žikić-Todorović, D. Mrdja, S. Forkapić, *Radiat. Meas.* **41** (2006) 477
9. A. M. El-Arabi, *J. Environ. Radioact.* **81** (2005) 11
10. Y. Orgun, N. Altinsoy, S. Y. Sahin, Y. Gungor, A. H. Gultekin, G. Karahan, Z. Karacik, *Appl. Radiat. Isot.* **65** (2007) 739
11. United Nations Scientific Committee on the Effects of Atomic Radiation, UNSCEAR, *Sources and Effects of Ionizing Radiation*, United Nations, New York, 1998
12. R. M. Anjos, R. Veiga, C. Carvalho, K. D. Macario, P. R. S Gomes, *Nucl. Phys. A* **787** (2007) 642
13. S. Lulić, *Radioactivity of the Danube River*, Annual Report, Rudjer Bosković Institute, Zagreb, 1990 (in Croatian)
14. P. Vukotić, G. I. Borisov, V. V. Kuzmič, N. Antović, S. Dapčević, V. V. Uvarov, V. M. Kulakov, *J. Radioanal. Nucl. Chem.* **235** (1998) 151
15. The International Commission on Radiological Protection, *ICRP Recommendations of the ICRP, Publication 60*, Pergamon Press, Oxford, UK, 1990.

Journal of the Serbian Chemical Society
JSCS@tmf.bg.ac.rs • www.shd.org.rs/JSCS

J. Serb. Chem. Soc. 74 (4) 471–476 (2009)

UDC 543+061.3(4)
EuCheMS news

DIVISION OF ANALYTICAL CHEMISTRY
EUROPEAN ASSOCIATION FOR CHEMICAL AND MOLECULAR SCIENCES

EUCHEMS NEWS

European analytical column No. 37 from the Division of Analytical Chemistry (DAC) of the European Association for Chemical and Molecular Sciences (EuCheMS)

(January 2009)

BO KARLBERG[1], MANFRED GRASSERBAUER[2] and JENS E. T. ANDERSEN[3]*

[1]*Department of Analytical Chemistry, Stockholm University, SE-10691 Stockholm, Sweden,* [2]*Vienna University of Technology, Department of Chemistry, Getreidemarkt 9, A-1060 Wien, Austria and* [3]*Department of Chemistry, Technical University of Denmark, Building 207, DK-2800 Lyngby, Denmark*

INTRODUCTORY COMMENTS FROM THE CHAIRMAN OF DAC

The European Analytical Column has again a somewhat different format. We have once more invited a guest columnist to give their views on various matters related to Analytical Chemistry in Europe. This year we have invited Professor Manfred Grasserbauer of the Vienna University of Technology to present some of the current challenges for European analytical chemistry. During the period 2002–2007 Professor Grasserbauer was Director of the Institute for Environment and Sustainability, Joint Research Centre of the European Commission, Ispra. There is no doubt that many challenges exist at the present time for all of us representing a major branch of chemistry, namely analytical chemistry.

The global financial crisis is affecting all branches of chemistry but analytical chemistry in particular since our discipline by tradition has many close links to industry. We notice already now a decreased industrial commitment with respect to new research projects and sponsoring of conferences. It is therefore important that we strengthen our efforts and that we keep our presence at analytical chemistry meetings and conferences unchanged.

Recent activities of DAC and details regarding the major analytical-chemistry event this year in Europe, Euroanalysis XV in Innsbruck, are also reported.

* Corresponding author. E-mail: jeta@dac-euchems.org

THE PERSONAL VIEWS OF MANFRED GRASSERBAUER ON "THE EUROPEAN UNION POLICY FOR SUSTAINABLE DEVELOPMENT – SOME CHALLENGES FOR ANALYTICAL CHEMISTRY"

During the "Anthropocene"[1] human beings have had a profound impact on our planet: up to now half of the land surface has been transformed by humans. In the past 3 centuries the population on earth increased 10-fold to 6 billion and industrial production increased 40-fold in the last 100 years.

These developments lead to a "Europe of Today" characterized by economic wealth, cultural richness and social security, but also caused significant problems in Europe and globally, particularly environmental pollution, excessive urbanisation, global warming and over-exploitation of natural resources.

This evolution eventually led to the present Policy Framework for the European Union where Sustainable Development is a key objective for all European Community Policies and thus one of the Guiding Principles for the European Union.

The present key issues for Sustainable Development are the management of natural resources, climate change and clean energy, and global poverty and development cooperation. The issue of sustainable management of natural sources concerns primarily air, water, soil and natural ecosystems like forests.

Clean air for Europe

Air pollution has been a major concern in Europe since the mid-sixties and has been addressed in a series of policy initiatives and legislation for the limitation of emissions from industry, energy production and transport dating back at the European level as early as 1970 with regular updates and revisions. Nevertheless recent health studies demonstrate that – even if major improvements in the quality of ambient air have been achieved – significant parts of the population still suffer from summer (ozone) or winter smog (particulate matter) and respiratory diseases are very common. Nowadays European hot spots for air pollution can be predominantly found in urban areas and regions with a very high traffic density. Road transport and shipping are responsible for a major part of the emissions of CO_2, particulate matter, SO_2, NO_x and VOCs (forming ozone) in many regions. The key challenge is to develope a more sustainable transport system in Europe based on an integrated approach for the assessment of the environmental impact of transport aiming at the identification of a mix of different transport modes which is energy efficient, cost effective and environmentally friendly.

Analytical sciences play a major role in this context and faces many challenges, like improving the quality of relevant data by linking routine air quality monitoring to metrological measurement systems or harmonising/standardising PM2.5 (fine particles of dimensions less than 2.5 micron) monitoring, establishing reliable methods for source apportionment of particulate matter, developing "on-board" emission diagnostic devices for heavy duty vehicles. Furthermore, the combination of monitoring and modeling for regional and hemispherical transport of pol-

lutants, assessment of non-local contributions to a particular emission situation as well as establishment of reliable models must be further advanced. The development of space based monitoring systems, *e.g.* within the frame of Copernicus project, and calibration/validation through *in-situ* measurements is another task which will require a massive contribution from Analytics and will represent a major contribution to a future Spatial Environmental Information System (SEIS).

Water quality and quantity

As far as the natural resource, water, is concerned the European problems are primarily that 20 % of the surface water bodies are still seriously threatened by pollution (*e.g.* by nitrate and pesticides), that 30.000 km^2 of European freshwaters are affected by acidification and that the ecological status of inland waters is often poor. European seas are significantly affected by eutrophication. In addition, there is a wide-spread over-consumption of water, particularly in the South of Europe. Water scarcity affects now already 100 million people in Europe and a dramatic increase is predicted for Southern Europe as a consequence of global warming.

Several initiatives of the European Commission address these issues, in particular the Water Framework Directive of 2000 and the Marine Thematic Strategy of 2005.

The challenges for Analytical Sciences relate to the development of methods and their harmonisation/standardisation for priority pollutants, emerging pollutants and ecological quality parameters of lake, river and coastal waters. Furthermore, new cost effective monitoring strategies based on "learning networks", dedicated sensor networks, space based monitoring systems (particularly for eutrophication assessment) an effective combination of monitoring and modeling for input, transport and effects of pollutants should be developed. The establishment of the SEIS element "Water Quality and Quantity" based on the "WISE" Water Information System for Europe is a further priority.

Climate change

Climate Change provides the probably biggest challenge for Europe and the whole world. Green House Gas emissions have strongly enhanced the natural warming having led to an overall increase of the global mean temperature by 0.78±0.18 °C and a sea level rise by 15 cm over the past century. Under baseline scenarios CO_2 emissions will further increase (by 70 % in industrialized countries and by 250 % by countries in development till 2050) leading to a temperature increase of more than 2 degrees by 2050 and ca. 4 degrees by 2100 according to the IPCC report of 2007. The contribution of various countries to the Green House gas emissions differ widely, also on a *per capita* basis: annual emissions are less than 1 ton per inhabitant for developing countries and India, ca. 4 tons for China, nearly 10 tons for the European Union and nearly 20 tons for the

USA. Approximately 75 % of GHG emissions are from consumption of fossil fuel and biomass.

We have become aware of many different effects of global warming, like the strong retreat of Alpine glaciers, the reduction of the Arctic ice shield by 40 % since 1970, a warming of the Mediterranean Sea by 2–3 °C during the last 25 years.

The European Union has reacted to global warming by introducing the European Climate Change Programs I and II. These include ratification of the Kyoto Protocol in 1997 and the proposal of an integrated climate and energy policy in 2006 aiming at a 20 % reduction target for GHG emissions, a 20 % increase of the efficiency of energy consumption and a 20 % share of renewable energies by 2020, and a massive efforts to arrive at a global agreement for mitigation of global warming.

The EU policy to combat climate change requires massive efforts to develop new clean and sustainable technologies and we need to aim at a "Third Industrial Evolution" (Hans Joachim Schellnhuber, Climate Advisor to President Barroso and Chancellor Merkel). Analytical Sciences have a particularly important role in assessing the "Green House Gas Problem" and monitoring global change. The quality assurance systems for emission inventories need to be further developed, by *e.g*. reducing uncertainties in the flux of Green House Gases in the domain agriculture, forestry and land use, new assessment systems based on a combination of monitoring and modeling for emission and transport of Green House Gases and air pollutants need to be established. Of particular importance is the development of space based monitoring systems which need to be calibrated and validated through *in-situ* measurements for the assessment of the global concentrations of climate effective gases and aerosols and the study of climate change impacts.

Global poverty and development cooperation

In respect to the priority theme, Global Poverty and Development Cooperation, the main issues are on the one hand, that changes outside Europe are exerting pressures on the European Union through air pollution, GHG emissions of other countries etc., but on the other hand, that Europe is also exporting pressure on the environment by consumption of global resources: its ecological foot print is 3 times as much as its "fair earth share" and is not in line with the "One Planet Living" concept.

The EU has made many important initiatives to foster development cooperation, such as fully endorsing the Doha Development Agenda of the WTO Member States of 2001, the Cotonou agreement of 2000 with Africa, Caribbean and Pacific States, and it is strongly supporting to achieve the UN Millennium Development Goals.

The principles of Sustainable Development have been introduced in all relevant policies, like External Relations, Trade, Security and Development Cooperation.

The environmental pressures on the ecosystems in areas outside Europe are increasing at a dramatic speed. In the rapidly growing economies, we encounter massive land spoilisation, water and air pollution in and around new mega-cities.

The "Less Developed Economies" are stricken by different problems: lack of essential infrastructure and services (2 billion people without energy services, like access to electricity), shortage of agricultural land, food and water (globally only 12 % of land surface is usable for agriculture and overall only 2.5 % is high value farmland, 1 billion people are without access to safe drinking water), widespread diseases and poverty (in Sub-Saharan Africa 50 % of the people live on less than 1 Euro/day, there are millions of potential migrants).

Africa has been identified as a Priority Partner of the European Union. 3 billion Euros are provided annually as development aid to support infrastructure development, the sustainable use of natural resources, and food security.

Important tasks for Analytical Sciences include the provision of environmental monitoring systems and knowledge/know-how to the rapidly developing economies and the developing countries, furthermore the development of globally operating space based observation systems with calibration/validation through *in-situ* measurements for monitoring of pollution of air and water, the exploitation of natural resources, the assessment of climate change impacts, and the monitoring of agricultural productivity and, last but not least, the establishment of data and observation systems for environmental health.

The overall major challenge for the European Union, as for other highly industrialized and wealthy societies, is without doubt to develop a functioning an interdependent global system where the presently 6.7 billion people (and 10 billion in 2050) from 1000 nations and 200 countries can live together peacefully. Key questions will relate to environmental quality, the sustainable management of natural resources, combating climate change and achieving a better equilibrium in the distribution of resources. New technologies and an integrated thinking will be the key to progress. Analytical Sciences as a key discipline for providing reliable and useful information will play an important role in this evolution.

INFORMATION FROM THE **EU**CHE**MS** DIVISION OF ANALYTICAL CHEMISTRY

Great achievements this year for EuCheMS! DAC welcomes the Division of Inorganic Chemistry and the Division of Organic Chemistry as new Divisions of EuCheMS. This move certainly strengthens the EuCheMS as a whole, and DAC is looking forward to collaborations maintaining a high level of activity. Most likely, the new Divisions are going to organize conferences of their own but before a series of successive events is established; DAC encourages delegates and members to participate in Euroanalysis XV, 6-10 September 2009 in Innsbruck, Austria. The head-line title of the conference is "The Impact of Analytical Chemistry on Quality of Life".

The expansion of EuCheMS led by the former Chairman Giovanni Natile and by the new Chairman Luis Oro calls for appointment of liaison persons to participate in planning of events and optimizing resources in times where they might be limited. The DAC liaison to other organizations operates well with exchanges of newsletters and minutes of meetings. The Delegates are urged to supply information to the Secretary for distribution in EuCheMS Newsletter, CITAC Newsletter and Eurachem Newsletter. The EuCheMS Newsletter and the associated Brussels News Update both available at the EuCheMS homepage (www.euchems.org) should be circulated by Delegates nationwide.

The DAC Annual Meeting 2008 was held in Turin, Italy, on Tuesday, 09 September 2008. The Meeting was hosted by Luigia Sabbatini of the Italian Chemical Society and by Maria Careri of the Italian Division of Analytical Chemistry and took place at the Lingotto Congress Centre. Our Italian colleagues made a great effort to organize the Annual Meeting and to ensure a prominent position of analytical chemistry at the EuCheMS 2nd European Chemistry Congress; two half-day sessions of analytical chemistry, a school of analytical chemistry, short courses, seminars and workshops. Many thanks are due to the organizers who also published[2] a tribute to P. G. Zambonin who has contributed for many years to analytical chemistry and to the work of the DAC.

The quality label "Organized in Cooperation with DAC" was awarded to five international meetings and conferences on analytical chemistry in 2008. A best-poster award worth 200 €, introduced by Springer Publishers was given to young scientists at Analysdagarna in Gothenburg, Sweden. This very prominent courtesy generously announced by Steffen Pauli (Steffen.Pauli@springer.com) of Springer will also be awarded at forthcoming meetings that have obtained the DAC designation. The guidelines (Appendix II of the DAC Statutes) prescribe, that a DAC Delegate addresses the participants with information on the Division, and the designation also imply that the Delegate reports in writing to the following Annual Meeting. A report template may be downloaded from the DAC site (www.dac-euchems.org).

The Study Group of Education headed by Reiner Salzer has created a number of templates for case studies, which may be downloaded from the DAC site. The Members, Delegates and Guest are encouraged to contribute case studies to teaching at all university levels by using the templates. The Study Group Education intends to collect a series of case studies that may be used by the teacher to demonstrate fundamental principles of analytical chemistry using real-life measurements.

REFERENCES

1. P. J. Crutzen, E. F. Stoermer, *Global Change Newsletter* **41** (2000) 17
2. E. Desimoni, F. Palmisano, L. Sabbatini, *Anal. Bioanal. Chem.* **389** (2007) 2051.